



HAL
open science

Biomass derivatives in heterogeneous catalysis : adsorption, reactivity and support from first principles

Romain Reocreux

► **To cite this version:**

Romain Reocreux. Biomass derivatives in heterogeneous catalysis : adsorption, reactivity and support from first principles. Catalysis. Université de Lyon, 2017. English. NNT : 2017LYSEN019 . tel-01839221

HAL Id: tel-01839221

<https://theses.hal.science/tel-01839221>

Submitted on 14 Jul 2018

HAL is a multi-disciplinary open access archive for the deposit and dissemination of scientific research documents, whether they are published or not. The documents may come from teaching and research institutions in France or abroad, or from public or private research centers.

L'archive ouverte pluridisciplinaire **HAL**, est destinée au dépôt et à la diffusion de documents scientifiques de niveau recherche, publiés ou non, émanant des établissements d'enseignement et de recherche français ou étrangers, des laboratoires publics ou privés.



Numéro National de Thèse : 2017LYSEN019

THÈSE de DOCTORAT de L'UNIVERSITÉ DE LYON

opérée par

l'École Normale Supérieure de Lyon

École Doctorale N° 206

École Doctorale de Chimie de Lyon

Spécialité : Chimie Théorique

Discipline : Chimie

Soutenue publiquement le 13/07/2017, par :

Romain RÉOCREUX

Biomass derivatives in heterogeneous catalysis : adsorption, reactivity and support from first principles

Dérivés de la biomasse en catalyse hétérogène :

adsorption, réactivité et support depuis les premiers principes

Devant le jury composé de :

Núria LÓPEZ-ALONSO	Professeure Institut Català d'Investigació Química (ICIQ)	Rapporteure
Jean-Sébastien FILHOL	Professeur Institut Charles Gerhardt, Université de Montpellier	Rapporteur
Alessandra Elsje QUADRELLI	Directrice de Recherche CNRS C2P2, CPE Lyon	Examinatrice
Romuald POTEAU	Professeur LPCNO, Université Paul Sabatier	Examinateur
Philippe SAUTET	Professeur CBE, University of California Los Angeles	Directeur de thèse
Carine MICHEL	Chargée de Recherche CNRS Laboratoire de Chimie, ENS de Lyon	Co-encadrante de thèse
Lionel PERRIN	Directeur de Recherche CNRS ICBMS, Université de Lyon	Membre Invité

Contents

1	Exploring vast phase-spaces while doing heterogeneous catalysis	17
I	Lignin derivatives on Pt(111)	39
2	Lignin: structure and valorization	41
3	Controlling the Adsorption of Aromatic Compounds on Pt(111) with Oxygenate Substituents: From DFT to Simple Molecular Descriptors	45
	Réocreux R., Huynh M., Michel C., Sautet P. <i>J. Phys. Chem. Lett.</i> , 2016 , <i>7</i> , 2074-2079	
4	Decomposition Mechanism of Anisole on Pt(111): Combining Single-Crystal Experiments and First-Principles Calculations	47
	Réocreux R., Hamou C. A. O., Michel C., Giorgi J., Sautet P. <i>ACS Catal.</i> , 2016 , <i>6</i> , 8166-8178	
5	Adsorption and Decomposition of a Lignin β-O-4 Linkage Model, 2-Phenoxyethanol, on Pt(111): Combination of Experiments and First-Principles Calculations	49
	Hamou C. A. O., Réocreux R., Sautet P., Michel C., Giorgi J. <i>J. Phys. Chem. C</i> , 2017 , <i>121</i> , 9889-9900	
II	γ-Al₂O₃ at the interface with liquid water	51
6	γ-Al₂O₃ model surfaces	53

CONTENTS

7	Structuration of water at the γ-Al₂O₃ (110) interface: an <i>Ab Initio</i> Molecular Dynamics perspective	63
8	Insights from <i>Ab Initio</i> Molecular Dynamics on the Early Stage Mechanism of γ-Al₂O₃ decomposition in neutral liquid water	85
9	Adsorption of Ethanol and Propane-1,3-diol on γ-Al₂O₃ at the Interface with Water	101

Remerciements

Je tiens tout d'abord à adresser mes plus vifs remerciements à mon encadrante, Dre Carine Michel, et mon directeur de thèse, Pr Philippe Sautet. Vous m'avez donné la chance d'embrasser d'audacieux projets tout en me laissant une très grande liberté scientifique. Suggestions plus qu'instructions, collaboration plus que direction, c'est ainsi que *cette* thèse a rapidement pu devenir l'expression de *mon* projet, fièrement empreint de vos deux approches certes semblables mais aussi complémentaires à de nombreux égards. Travailler avec toi Philippe a été une réelle leçon d'anticipation. Ne présenter que des résultats pour lesquels on a pris le soin d'avoir au moins un ou deux coups d'avance, voilà ce que je retiens de nos réunions et discussions. Cela m'a poussé à développer un souci du détail et à m'efforcer de toujours aller voir plus loin que le bout de mon nez (ou du fichier d'*output* devrais-je plutôt dire). Un gigantesque merci à toi Carine ! Merci pour ton enseignement de la technique, ton incitation à la créativité et au sens de l'initiative, ta patience et ton écoute, ton incroyable sens de la gestion des ressources humaines. Tu as su me pousser pour que je sois capable d'attaquer des problèmes différents et de complexité croissante. Tu dis parfois que j'ai fait deux thèses tant les deux parties de mon manuscrit peuvent paraître distinctes. Mais je n'aurais probablement pas pu faire la deuxième partie si tu n'avais pas été là pour me sortir de ma zone de confort, tout en sachant évaluer jusqu'où tu pouvais pousser. Bref, merci pour tout. C'était, c'est et ce sera toujours un réel plaisir de travailler avec toi.

Je tiens aussi à remercier le jury de ma thèse. Merci Pre Núria López-Alonso et Pr Jean-Sébastien Filhol pour avoir accepté d'être les rapporteur-e-s de ce manuscrit. Merci encore à vous et aussi aux autres membres du jury, Pr Romuald Poteau et Dr Lionel Perrin ainsi que la Présidente Dre Alessandra Elsje Quadrelli, pour votre temps et la

riche discussion scientifique qui a suivi la soutenance.

Je remercie également Pr Tom Baker, Pr Javier Girogi et Aghiles Ould Hamou de l'Université d'Ottawa. Sans vous, une partie de ce travail n'aurait jamais pu prendre une telle envergure. Au-delà d'une aventure scientifique, cette collaboration théorie/expérience institutionnalisée par le Laboratoire International Associé FunCat (Fundamental Catalysis) a aussi été une merveilleuse aventure humaine. Je profite de ce paragraphe ottavien pour remercier Flora Marguerite qui a rendu mes voyages si faciles, ainsi que Minh Huynh et Mark Slodki, les deux stagiaires canadiens que j'ai co-encadrés, qui ont fourni un travail formidable et participé à certains développements de cette thèse. Pour clore ce paragraphe sur les collaborations internationales, je remercie profondément Dre Marcella Iannuzzi et Dre Dorothea Golze pour le temps que vous m'avez accordé lors de mes visites zurichoises à me former à l'art de la dynamique moléculaire *ab initio*. Plus qu'un enseignement technique, vous m'avez appris à *regarder* la chimie à une échelle plus large que celle de l'atome ou de la molécule unique. Cela peut paraître d'une nécessité évidente, mais ça demande un vrai effort, notamment en terme d'analyse de simulations numériques. Merci de m'en avoir donné les outils.

Merci aussi à Dre Dorothee Laurenti, Dr Pascal Raybaud et Pre Anne Millet pour avoir participé à mes comités de suivi de thèse et pour les conseils que vous m'y avez donnés. Merci à Dr David Loffreda, Dr Tangui Le Bahers, Dr Stephan Steinmann, Dr Tao Jiang, Dr Vincent Krakoviack, Pre Élise Dumont et Pr Paul Fleurat-Lessard pour avoir répondu à mes questions, pour en avoir soulevées d'autres, pour m'avoir aidé sur l'analyse de mes simulations, la physique statistique, l'intégration thermodynamique et autres enthalpies libres qu'elles soient standard ou non.

Merci aux directeurs de département (Dr Philippe Maurin puis Dr Cyrille Monnerieu) et aux responsables de la préparation à l'agrégation (Pr Paul Fleurat-Lessard puis Dr Martin Vérot) pour la confiance que vous m'avez accordée dans la réalisation des TP et cours magistraux au sein du département de chimie. Ça a été un réel épanouissement ! Merci aussi à l'équipe technique pour avoir rendu la préparation des TP aussi facile.

Merci à toutes les occupant-e-s du bureau : Sarah, Enza, Chris, Antton, Ayad, Laureline. Que ç'ait été à l'époque de la Crazy Room, de la Finalisation ou de la Rédaction, vous avez toutes contribué à une super ambiance au travail ! Merci à Mathilde (Maïac), Manue et Thomas, les voisin-e-s de bureau, et les expérimenteurices

Margaux, Maxime, Mathieu, Corentin, Anh-Thi pour ces nombreux afterworks. Merci aussi à Jean-Christophe, Delphine, Laure, Christian, Yann, Christophe, Sandrine et Bastien pour m'avoir accepté dans votre couloir-café et pour tous ces moments conviviaux passés avec vous et Mathilde (Manioc) entre un matin et un après-midi de thèse. Oh non, je ne vous oublie pas Maëlle, Laure-Lise et Sara ! Mais en tant que Josettes vous méritez quelques phrases à part. Vous avez été de géniales compagnes d'aventures (qu'il convient de ne pas énoncer ici) avec qui j'ai pu partager les nombreux sentiments si pluriels que procure une thèse. Et tellement plus encore !

Merci à toi Gladys. Pour m'avoir hébergé pendant mes visites doctorales à l'Université de Zürich. Pour avoir pris la température pendant ces trois ans. Pour avoir écouté mes doutes. Pour m'avoir mis une claque quand j'en avais besoin. Pour m'aider à faire des choix. La précieuse boussole que tu es, a été d'une aide cruciale dans les moments importants de ma vie ces dernières années. Que ça continue ainsi ! Merci aussi à mes colocataires, et en particulier Pierrick et Éloïse, pour votre soutien pendant la rédaction, les périodes de questionnement sur l'avenir et les recherches de postdocs.

Je remercie DéMesurément Théo, Ulysse, Sonia, Manue, Thomas, Marylou, Thibaut, Jean-Loup, Léo, Jérémy, Léa et plus tard Manon, Anissa, Audrey, Rémi et toutes les autres comparses du laboratoire junior DéMesures. Un petit *espace sauf* d'émulation créative extraordinaire au milieu de la troisième année de thèse. Une bouffée d'air(e). Un germe de *tout est possible*. L'impulsion qui permet de dépasser ses propres limites, quelles qu'elles soient. Mais aussi une petite loge où l'on s'apprend à vulgariser et communiquer la science avec de nouveaux outils, avec de nouvelles personnes, avec de nouvelles institutions.

Merci enfin à mes amis de Lyon et de Saint-Chamond ainsi qu'à ma famille pour leurs perpétuels soutien et encouragement. J'applaudis mes parents autant que je les remercie. Ils ont réussi à nous donner, à mes frères et moi, les outils pour tenter d'échapper, même partiellement, au déterminisme social. *Vous serez ouvriers si vous le voulez. Mais en attendant, faites des études ! Et des études qui vous plaisent. On s'occupe du reste.*

Merci pour tout.

“Die Grenzen meiner Sprache bedeuten die Grenzen meiner Welt.”

Logisch-Philosophische Abhandlung, Ludwig Wittgenstein

Résumé

L'abandon progressif des ressources fossiles s'accompagne de l'exploitation croissante de la biomasse. Cette transition nécessite de développer de nouveaux procédés notamment en catalyse hétérogène. Les chimistes se heurtent alors à deux défis majeurs : (i) désoxygéner la biomasse (cellulose/lignine) pour revenir à la chimie maîtrisée des grands intermédiaires (ii) rendre les catalyseurs résistants à l'eau, omniprésente en biomasse.

En collaboration avec des expérimentateurs de l'Université d'Ottawa, nous nous sommes d'abord intéressés à la désoxygénation d'aromatiques de type lignine. Les calculs *ab initio* (DFT) nous ont permis de dresser les caractéristiques d'adsorption de ces composés sur Pt(111) en termes de descripteurs moléculaires simples. Nous avons ensuite étudié le mécanisme de décomposition de l'anisole et du 2-phénoxyéthanol, molécules modèles. Nos études ont montré l'importance de l'hydrogène et des fragments carbonés sur la réaction de désoxygénation de ces composés.

En parallèle nous nous sommes intéressés à la stabilité, dans l'eau, d'un des supports catalytiques majeurs : l'alumine- γ . Ce sujet clé pose des défis considérables en modélisation, puisqu'il nécessite d'utiliser des méthodes de dynamiques moléculaires *ab initio*. Celles-ci nous ont permis de caractériser la structuration de l'eau au contact de l'alumine et l'importance de la solvataion sur les aluminols de surface. À l'aide de méthodes d'événements rares (dynamique contrainte, métadynamique) nous avons enfin abordé la réactivité d'alcools et de l'eau avec l'alumine hydratée. Ces simulations ont permis d'identifier les premières étapes d'hydratation et de mieux comprendre comment les limiter.

Abstract

Moving away from fossil resources is currently being accompanied by the increasing exploitation of biomass. This shift requires the development of new processes, in particular in heterogeneous catalysis. Chemists are now facing two major challenges: (i) deoxygenate biomass (cellulose/lignin) to produce platform intermediates with a well-known chemistry (ii) make catalysts resistant to water, ubiquitous within the context of biomass.

Within a collaboration with experimentalists at the University of Ottawa, we have first studied the deoxygenation of lignin-like aromatics. From an *ab initio* (DFT) inspection, we have characterized and described the adsorption of such aromatic oxygenates on Pt(111) with simple molecular descriptors. We have then investigated the decomposition mechanism of anisole and 2-phenoxyethanol. For these two model compounds, we have showed the significance of hydrogen and carbonaceous species to have the deoxygenation reaction proceed properly.

Meanwhile, we have examined the stability, in water, of γ -alumina, a major support in heterogeneous catalysis. The necessity to perform *ab initio* molecular dynamics simulations makes the modeling of such a system particularly challenging computationally. The simulations have nevertheless enabled us to characterize the structuration of liquid water in contact with alumina and the significance of solvation on surface aluminol groups. Using rare-event methods (constrained dynamics, metadynamics) we have eventually been able to probe the reactivity of alcohols and water with hydrated alumina. We have then identified the first steps of hydration and gained insights on how to limit them.

Introduction

As human activities intensify, so does the global population’s awareness of their environmental impact. Earth is indeed experiencing growing difficulties to “buffer” human activities, which importantly rely on petroleum chemistry to produce materials and energy. Consequently, petroleum resources, accumulated for hundreds of millions of years from biomass sedimentation, have been over-exploited and are now on the brink to depletion. To make the matter worse, petroleum combustion is associated with emissions of carbon dioxide in far larger amounts than what Earth can absorb back, thus having dramatic consequences on the climate.

In an effort to modify our activities and have them meet the requirement of sustainable development, it has been proposed to replace petroleum, admittedly partially, by biomass as new feedstock for the production of carbon-based materials and energy.¹ The main goal is to bypass the millions-of-year-long production of petroleum from biomass with processes that efficiently yield relevant industrial intermediates (benzene, toluene and xylene – the so-called BTX platform – ethylene, *etc.*), and this directly from biomass. Catalysis, of course, holds a central place in this context of accelerated biomass conversion.

The transition from petroleum to biomass chemistry is however not trivial. Indeed, compared to petroleum, biomass has a larger oxygen-content and its transformation is often related to water (as a product or a solvent).¹ Designing water-resistant deoxygenation catalysts is hence the main challenge that chemists face to make the transition possible. In heterogeneous catalysis, this implies to reinvent and optimize complex systems involving a catalyst and a support in a given medium. In the present work we propose to perform first principle calculations on such challenging systems to attempt

rationalizing their necessary optimization.

The optimization of catalysts brings us back to Sabatier principle.² It states that the interaction between the substrate and the catalyst should be neither too weak, nor too strong to maximize the activity of the catalyst. This can be rationalized by studying energy profiles. Let's consider the reaction $\mathbf{A} \rightarrow \mathbf{B}$ that proceeds through the adsorbed states \mathbf{A}^* and \mathbf{B}^* , and the transition state \mathbf{TS} . Three profiles are given in Figure 1 for three different catalysts. All three show the same activation barrier for the step $\mathbf{A}^* \rightarrow \mathbf{B}^*$, but they do not interact the same way with substrates \mathbf{A} and \mathbf{B} . In the bad interaction limit (Figure 1a), the overall barrier corresponds to the sum of the adsorption energy and the activation energy of process $\mathbf{A}^* \rightarrow \mathbf{B}^*$. The associated activity is not expected to be optimal since we can find catalysts that diminish the energetic contribution of the adsorption step. In the strong interaction limit (Figure 1c), $\mathbf{A} \rightarrow \mathbf{A}^*$ and $\mathbf{A}^* \rightarrow \mathbf{B}^*$ are very easy steps compared to the huge desorption energy of $\mathbf{B}^* \rightarrow \mathbf{B}$ that the system has to provide in order to recover the product and a clean catalyst. Again, the activity is expected to be low. It is only when the profile looks rather flat (neither too strong nor too weak interactions) and also inclined downwards that the catalyst shows optimal activity (Figure 1b). The characterization of such an energy profile is therefore important to understand the modulation of reactivity from one catalyst to another.

The link between the thermodynamics of adsorption and the catalytic activity has been intensively investigated experimentally. It is often represented by the mean of a volcano-plot. For example, Rootsart and Sachtler³ studied a large range of catalysts for the decomposition of formic acid into a metal formate. They determined the temperature T_r at which the reaction reaches a given rate (6.3 s^{-1} in their work) and then plotted it against the heat of formation of the metal formate. The higher T_r , the less active the corresponding catalyst. As showed in Figure 2, the best catalysts are the ones that show moderate affinity to formate (320 kJ/mol on a range going approximatively from 250 to 450 kJ/mol), namely platinum and iridium. This constitutes a quantitative experimental evidence of Sabatier principle.

With the development of computational catalysis in the late 90s, such screenings have become possible computationally.⁴ The improved accuracy of density functional theory (DFT) has indeed allowed computational chemists to determine the relative stability of intermediates and transition states in heterogeneous catalysis, and get a detailed picture

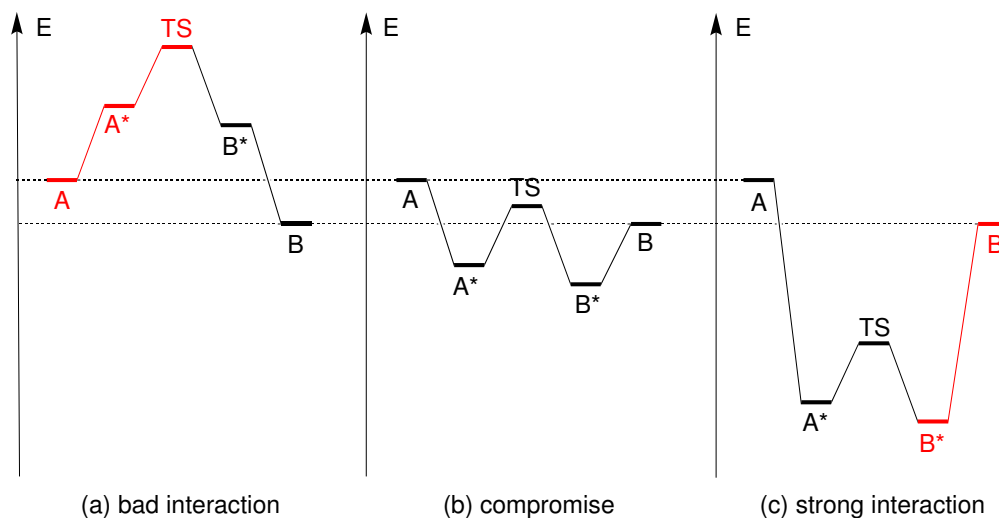


Figure 1: Energy profiles of the reaction $A \rightarrow B$. A^* , B^* and TS stand for the adsorbed states of A and B and the transition state for the elementary step $A^* \rightarrow B^*$. The barrier of the latter is considered constant, representing the influence of the interaction of A and B with the surface catalyst.

of the energy profiles. Their careful analysis can provide theoretical volcano-plots like the one given in Figure 3 showing the activity (given by the evaluation of the overall activation energies) of the production of methane from carbon monoxide and hydrogen. The best catalysts were found to be rhodium, ruthenium, nickel, cobalt and a nickel/iron alloy (Ni_3Fe).⁵ This approach offers the prospect of a rational computational design of catalysts.^{6,7}

It relies on the determination of the energy of selected points on the energy profile (basically intermediates and transition states) and is qualified as static. But for systems that show intrinsic flexibility and fluctuations (like solvents for example) or for which the nature of the products is not really known, other methods have been developed over the last two decades. These so-qualified dynamical approaches model the dynamics of molecules at a given temperature. In practice, the system is prepared in a particular state, for example the reactant, and the ensemble of its molecules (solvent, surface, etc.) are allowed to move and even react during the time of the numerical simulation. The details concerning both the static and dynamical approaches are given in the first chapter of this work. Both types of methods have been used during this thesis in the context of biomass conversion. Computationally, the goal of the present work is therefore not to develop new methods but rather bring existing methods to an increased level of

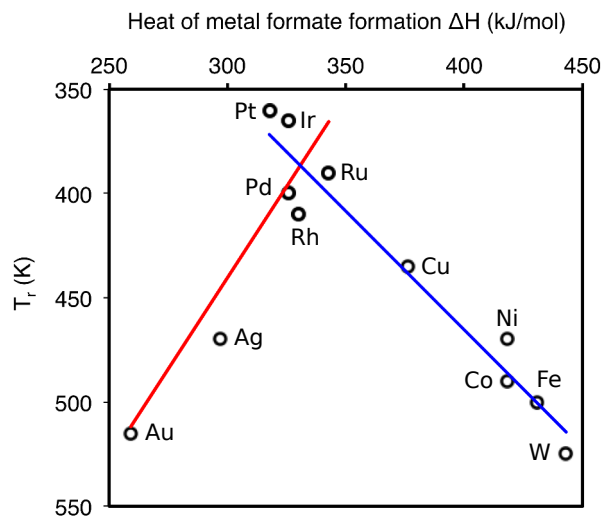


Figure 2: Volcano-plot for formic acid decomposition as a function of the heat of formation ΔH of formate. T_r is the temperature at which a rate of 6.3 s^{-1} is reached for a given catalyst. Replotted from data published by Rootsart and Sachtler.³

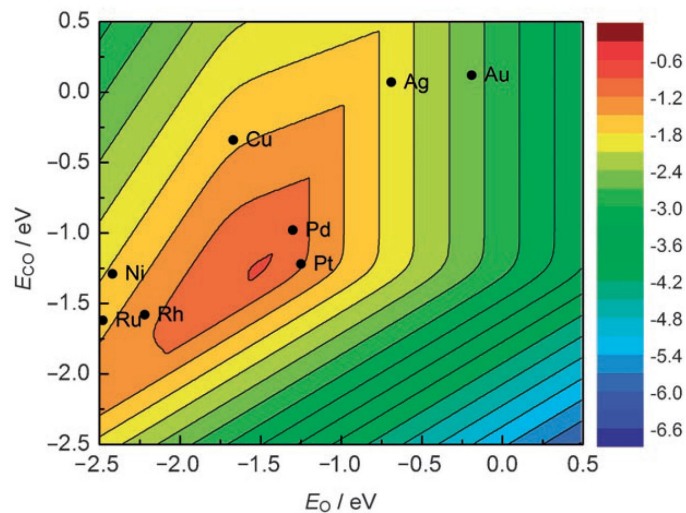


Figure 3: 2D volcano plot obtained from first principles calculations for the reaction $\text{CO} + \frac{1}{2} \text{O}_2 \rightarrow \text{CO}_2$. It represents the activity (the color scale gives the effective activation energy in eV) of catalysts as a function of oxygen and carbon monoxide binding energies to the surface. From Falsig *et al.*,⁵ Copyright ©2000 by John Wiley Sons, Inc. Reprinted by permission of John Wiley & Sons, Inc.

system complexity, one of the main challenge of realistic computational heterogeneous catalysis.⁴ Two families of challenging systems have been considered.

In the first part we have focused on derivatives of lignin. This polymer has recently raised the chemists' interest since it is the most abundant aromatic polymer in biomass.⁸ The processes that allow for its depolymerization mainly yield aromatic oxygenates, which have to be depolymerized to obtain molecules of the BTX platform. Using static methods, we have first studied how lignin derivatives interact with platinum, an important heterogeneous catalyst. We have then investigated, in close collaboration with experimentalists, vast reaction networks of complex lignin derived compounds that exhibit many functional groups, namely anisole and 2-phenoxyethanol.

In the second part, we have studied the influence of water (ubiquitous in biomass) on γ -alumina (γ -Al₂O₃), a major support in heterogeneous catalysis. Using dynamical methods, we have first scrutinized the structuration of water at the interface with γ -Al₂O₃. We have then considered the reactivity of γ -Al₂O₃ with pure water and solutions of alcohols. γ -Al₂O₃ is indeed unstable in water but seems to be stabilized by such organics.⁹ Also, the atomic-scale understanding of this effect could allow for the optimization of γ -Al₂O₃ as a support for biomass conversion purposes.

Bibliography

- [1] Sanderson, K. *Nature* **2011**, *474*, S12–S14.
- [2] Masel, R. I. *Principles of Adsorption and Reaction on Solid Surfaces*; John Wiley & Sons, Inc., 1996.
- [3] Rootsart, W. J. M.; Sachtler, W. M. H. *Zeitschrift für Phys. Chemie Neue Folge* **1960**, *26*, 16–26.
- [4] López, N.; Almora-Barrios, N.; Carchini, G.; Błoński, P.; Bellarosa, L.; García-Muelas, R.; Novell-Leruth, G.; García-Mota, M. *Catal. Sci. Technol.* **2012**, *2*, 2405.
- [5] Falsig, H.; Hvolbæk, B.; Kristensen, I. S.; Jiang, T.; Bligaard, T.; Christensen, C. H.; Nørskov, J. K. *Angew. Chemie Int. Ed.* **2008**, *47*, 4835–4839.
- [6] Nørskov, J. K.; Bligaard, T.; Rossmeisl, J.; Christensen, C. H. *Nat. Chem.* **2009**, *1*, 37–46.
- [7] Nørskov, J. K.; Abild-Pedersen, F.; Studt, F.; Bligaard, T. *Proc. Natl. Acad. Sci.* **2011**, *108*, 937–943.
- [8] Zakzeski, J.; Bruijninx, P. C. A.; Jongerius, A. L.; Weckhuysen, B. M. *Chem. Rev.* **2010**, *110*, 3552–3599.
- [9] Ravenelle, R. M.; Copeland, J. R.; Van Pelt, A. H.; Crittenden, J. C.; Sievers, C. *Top. Catal.* **2012**, *55*, 162–174.

Chapter 1

Exploring vast phase-spaces while doing heterogeneous catalysis

Introduction

The phase-space corresponds to the ensemble of variables needed for the description of the state of each particle in a given system. Among many possible choices, the ensemble of atomic coordinates and velocities often constitutes a natural representation of the whole phase space. Although this concept rather belongs to the physicists' jargon, chemists have developed many tools to describe, at least partially, phase spaces. The sequence of the different states encountered along a reaction can be represented drawing a mechanism with - admittedly idealized and codified - key structures: reactants, products, reaction intermediates and transition states. These structures are actually associated with particular points of the system's (free) energy surface plotted against atomic coordinates, the resulting landscape of which indeed shows valleys (minima for reactants, products and intermediates) and saddles (1st order saddle-point for transition states only).

More O'Ferrall Jencks diagrams, for instance, provide a nice representation of (free) energy variations as a function of selected phase-space coordinates. Figure 1.1 gives such a diagram for the β -elimination reaction $\text{HRX} + \text{B}^- \rightarrow \text{R} + \text{BH} + \text{X}^-$ (B and X are a base and a leaving group respectively, and R can be a $-\text{CH}_2\text{CH}_2-$ unit). The diagonal corresponds to the concerted step that goes through a unique transition state: the so-called E2 mechanism. The two other mechanisms, namely E1 and E1cB, are also

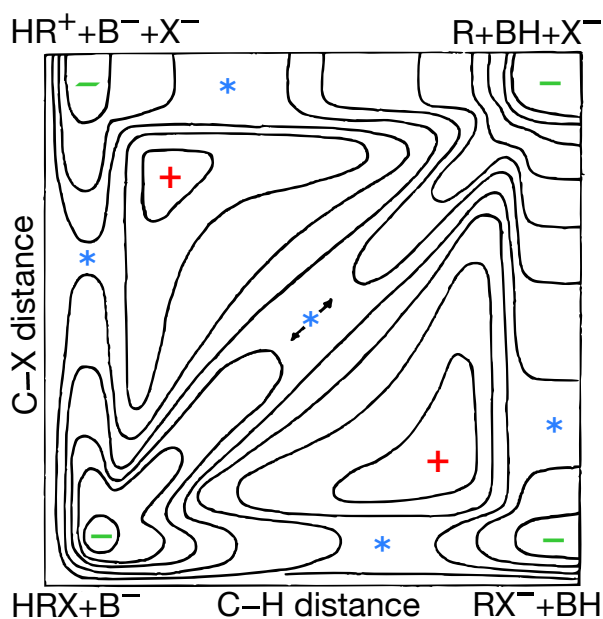


Figure 1.1: More O'Ferrall Jencks diagram of the β -elimination $\text{HRX} + \text{B}^- \rightarrow \text{R} + \text{BH} + \text{X}^-$. R, X and B represent a CH_2CH_2 unit, a leaving group, and a base respectively. It gives an isovalue free energy diagram plotted versus the C-H and C-X distance. Pluses, minuses and asterisks indicate maxima, minima and 1st order saddle points respectively. Adapted from More O'Ferrall¹ with permission of the Royal Chemical Society.

represented and go through the minima located at the top-left and bottom-right corner for the E1 and E1cB mechanisms respectively. The curvilinear abscissa of the path of least (free) energy going from one minimum to another is called the reaction coordinate. It is the most synthetic combination of phase space coordinates that enables the description of the reaction at the atomic scale. That is why we often represent the (free) energy profile only as a function of the reaction coordinate (which implies that all the other phase space coordinates are averaged along the path). It gives a simple representation of the relative stability of the different species and the barrier to overcome in order to have the reaction proceed. The reading of this profile is extremely informative and allows controlling the reaction under given experimental conditions. The question is really how we can build these diagrams.

The earlier mechanistic investigations, which are still of current relevance, rely on kinetic studies under various experimental conditions. By changing the initial concentrations, the pH, the ionic strength, the pressure, by substituting atoms with isotopes, *etc.* it is indeed possible to get information on the molecularity of the rate determining steps,

the charge of particular intermediates, the change in the atomic connectivities, and also the (free) energy barriers to overcome.² With the help of spectroscopies, we can go even further and get structural information on reaction intermediates,³⁻⁵ and even transition states on surfaces.⁶ In spite of the development of new spectroscopies, the increase of the complexity of reactions that involve a huge network of intermediates makes the entire mechanistic picture out of reach. By prescind from the experimental conditions and technical limitations, computational chemistry provides a complementary perspective to mechanistic investigations. Almost all imaginable intermediates can be modeled, all elementary steps be postulated. The energy can be decomposed into various types of contributions and very different experimental conditions can be taken into account. However, the investigation of the phase space becomes almost abyssal and guidance from experimentalists becomes a precious help.⁷⁻⁹

Put your hiking shoes on (there is going to be some hills and valleys) and let's have a small tour within the methods available in computational heterogeneous catalysis to investigate reaction mechanisms.

Investigations based on the electronics of molecules and materials.

When representing an energy profile, we actually plot the total potential energy of the system. We can then consider the entropy and plot a free energy profile. The goal of this section is to show how we can get these diagrams from first principles. We shall first consider that the potential energy surface approximately corresponds to the electronic energy calculated from first principles within the Born-Oppenheimer approximation. By the end of this section, we shall see what corrections need to be added to the electronic energy in order to picture the actual potential energy and the free energy.

How to calculate the electronic energy?

In the realm of computational catalysis, Density Functional Theory (DFT) stands among the most popular methods for the evaluation of the electronic energy.¹⁰ It originates back from the work of Thomas¹¹ and Fermi^{12,13} who have been able, in 1927, to first write the electronic energy as a functional of the electron density. Assuming that inhomogeneous electron densities can be approximated as the sum of a locally homogeneous electron gas

with same density, the Local Density Approximation (LDA)¹⁴ has provided a reasonable description of solids and surfaces, in particular metals.^{15–17} Further improvements have been reported and classified on the so-called *Jacob’s ladder* of DFT by Perdew.¹⁸ To account for density inhomogeneity, functionals of both the density and its gradient have been developed in the 90s. The so-called Generalized Gradient Approximation (GGA) functionals like PW91¹⁹ and PBE²⁰ represent a considerable improvement over LDA. Offering a better estimation of reaction energies, in particular adsorption energies of small molecules, the introduction of GGA has literally opened the field of computational catalysis. Following the success of this first-order gradient correction to LDA, higher order terms of the gradient have been considered without really improved accuracy.²¹ Being exact in the Hartree-Fock (HF) approach, the addition of a certain amount HF exchange has allowed improving further more the accuracy of so-called hybrid functionals. B3LYP²² on the one hand and PBE0^{23,24} and HSE03²⁵ on the other hand achieve indeed high accuracy for molecules and non-metallic solids, respectively. However they do not improve any better the description of surface metallic sorbate interactions. It is only within the Random Phase Approximation (RPA) approach,²⁶ on top of the *Jacob’s ladder* of DFT, that very accurate adsorption energies can be obtained from first principle. Unlike the other DFT approximations presented here, correlation interactions (in particular long range correlation from which London interactions arise) are indeed accurately taken into account at the RPA level. However this approach is computationally extremely expensive and, consequently, other schemes have been proposed to evaluate these weak van der Waals interactions. They are mainly built as corrections to GGA functionals (even if other functionals can be used as well), which stand out to be the best compromise for the description of surface sorbate interactions. These schemes have been classified, by Klimeš *et al.*, on a *stairway to heaven* in analogy with the *Jacob’s ladder*.²⁷ At the bottom of the stairway, simple semi-classical C_6r^{-6} corrections are found, with in particular the most widely used Grimme’s D2 approach.²⁸ Within this approach, the C_6 coefficients only depend on the nature of the interacting atoms. Making them dependent on the local environment of each atom constitutes an important improvement and brings us to the second step of the stairway. That includes for example the atomic volume dependent vdW(TS),²⁹ the density dependent dDsC,^{30,31} and the coordination number dependent Grimme’s D3 approaches.³² The third step consists of long-range density functionals that actually add a non-local correlation energy to local functionals

(like standard GGAs).^{33,34} These methods have recently received particular attention in the context of unsaturated organics adsorption on metal surfaces. They have appeared to reasonably account for dispersion, especially with aromatics.^{35,36} To move up to the next step of the *stairway to heaven*, we need to go beyond the pairwise additive scheme. And the aforementioned computationally demanding RPA is an example of such an approach.

Picture the potential energy surface

We have just mentioned how DFT is able to determine, more or less accurately, the electronic energy of a system for all geometries, including the vast continuum of the displacement of all atoms. However, there is no need to survey the entire potential energy surface. Only minima (which correspond to reactants, products and reaction intermediates) and first order saddle points (which correspond to transition states) are relevant in order to calculate the reaction and activation energies. Minima are located using conjugated gradient algorithms. As for first order saddle points, the task is a bit more complicated since they consist in minima in all the directions but one, the actual reaction coordinate, which is not very well known before doing the calculation. In computational catalysis, the problem is tackled using different kinds of algorithms. Starting from the geometric interpolation of n substructures between the reactant and the product, the n geometries are optimized together with nudged elastic band algorithms^{37,38} so that their position, in the atomic coordinates space, gets closer to the actual reaction coordinate to be determined. With the help of quasi-Newton or dimer algorithms,³⁹⁻⁴¹ the saddle point can finally be properly located, providing both the electronic energy and the structure of the transition state. To assess its first order saddle point property, an extra frequency calculation is required. Hence, transition state search is rather expensive computationally and also extremely user-time demanding since it requires playing with different algorithms.

Structure and energy relationships

As the effort to compute both the energy and the geometry of transition states is particularly demanding compared to the location of minima, computational chemists have started, over the last decade, recycling old theories that had proven their reliability.^{42,43} The problem of catching transition states is indeed not new. In 1955, Hammond⁴⁴ pro-

posed to compare the structure and stability of transition states to the closest (in terms of both energy and reaction coordinate) intermediate. This postulate actually originates from previous works by Bell,⁴⁵ Evans and Polanyi⁴⁶ who have proposed linear relationships between activation and reaction parameters for Brønsted acidic reactions.⁴⁷ The groups of Vlachos,^{48,49} Mavrikakis⁵⁰ and Greeley⁵¹ have extensively reintroduced the idea for the computation screening of heterogeneous catalysts, in particular in the field of biomass conversion. Both reaction energies and activation barriers are calculated over a set of well chosen elementary steps in order to determine, from first principles, the linear relationships between the activation barrier and the reaction energy. Once the parameters are evaluated and the accuracy of the relationship assessed statistically, it can be used for various, if not any, similar reactions. They have allowed screening several catalysts very efficiently, by shunting transition states searches, for various reactions such as alcohol activations (and in particular C–O vs. C–C activations)⁵⁰ and aromatic deoxygenation.⁴⁹

Other relationships exist and correlate minima energies with both electronic and geometric descriptors. For instance, linear-scaling relationships correlate the energy of reaction intermediate with that of the atom that directly interacts with the metal surface.^{52–54} The parameters of the correlation are shown to depend on coordination numbers. This restrains the DFT study to a couple of atoms (C, N, O mainly) at a couple of adsorption sites. When several atoms are involved in the interaction with the surface, group additivity relationships can be used.^{55,56} The evaluation of adsorption energies using descriptors (d-band centre, orbital energies, electrophilicities, ...) goes beyond the simple problem of efficient phase-space sampling.^{57–61} It provides to all chemists, experimentalists and theoreticians, tools for the rational design of catalysts.^{62,63}

The use of different linear relationships can be very complementary and help gaining insight on the parameters that trigger the electronic energy. However, albeit important and necessary, the electronic energy alone is not enough to clarify all the reactivity aspects.

From electronic energies to reaction kinetics

Although the total potential energy is often assimilated to the electronic energy, it is not strictly speaking true. The potential energy of the nuclei has also to be included. The classical vision of the Born-Oppenheimer approximation (and in particular how

it is implemented most routinely) indeed keeps the position of the nuclei fixed upon electronic optimization. Their position is therefore well-defined as well as their velocity, which is zero. This violates Heisenberg's uncertainty principle: nuclei oscillate around their equilibrium position even at 0 K. To correct for that, we need to add the so-called Zero Point Energy (ZPE) correction. Most of the time, it is calculated from a frequency calculation within the harmonic approximation using Equation 1.1:⁶⁴

$$\text{ZPE} = \sum_i \frac{\hbar\omega_i}{2} \quad (1.1)$$

with \hbar and ω_i the reduced Planck constant and the wavenumber of eigen vibrational mode i respectively.

The next step is to account for entropy in order to estimate Helmholtz or Gibbs free energies. The entropy can be decomposed into three terms: translational, rotational and vibrational contributions (neglecting the electronic one). They can be evaluated using the partition functions^{2,64,65} within the harmonic oscillator Z_{vib} (Equation 1.2), rigid rotator Z_{rot} (Equation 1.3) and particle-in-a-box Z_{trans} (Equation 1.4) approximations. They take as inputs the harmonic wavenumber ω_i , the symmetry number σ , the rotational constants B_i and the dimensions L_i of the space in which the particle is allowed to translate (2 are needed for a mobile sorbate, 3 for a gas phase molecule). k_B and T are the Boltzmann constant and the absolute temperature respectively.

$$Z_{vib} = \prod_i \left[1 - \exp\left(-\frac{\hbar\omega_i}{k_B T}\right) \right]^{-1} \quad (1.2)$$

$$Z_{rot} \simeq \frac{\sqrt{\pi}}{\sigma} \prod_i \sqrt{\frac{k_B T}{B_i}} \quad (1.3)$$

$$Z_{trans} \simeq \prod_i \frac{L_i}{\Lambda} \quad (1.4)$$

with

$$\Lambda = \frac{h}{\sqrt{2\pi m k_B T}} \quad (1.5)$$

From partition functions, we can determine both the free energy or entropy using Equations 1.6 and 1.7.

$$F = -RT \ln(Z) \quad (1.6)$$

$$S = -\frac{\partial F}{\partial T} \quad (1.7)$$

Using these equations is quite straightforward for gas phase molecules. For adsorbed species they have to be used more carefully. In particular, strongly chemisorbed species do not translate, and then, there is no translational entropy to be taken into account. Physisorbed species or weakly bound sorbates translate on the surface only, and the product in Z_{trans} has to be reduced to the two directions perpendicular to the surface. Rotational modes can be hindered or can be accounted as vibrational modes (calculated from finite difference quantum calculations). Finally, although it is probably the smallest contribution, the evaluation of vibrational entropy is probably the most critical and the theoretical evaluation can be far from experimental values.⁶⁶ Harmonic Z_{vib} is indeed dominated by the softest modes (see the lower mode limit given in Equation 1.8), which are particularly anharmonic and are intrinsically very numerous in heterogeneous catalysis, in particular the catalyst phonons.

$$\left[1 - \exp\left(-\frac{\hbar\omega_i}{k_B T}\right)\right]^{-1} \sim \frac{k_B T}{\hbar\omega_i} \quad \text{for } \hbar\omega_i \ll k_B T \quad (1.8)$$

Some have first proposed to use gas phase entropies, subtracting the translational contribution.⁶⁷ Others have treated all the degrees of freedom (including rotation and translation of sorbates) harmonically regardless of the wavenumber values and get nice results that fit with experiments.^{8,9,64} Steinmann *et al.* have proposed to limit the evaluation of Z_{vib} to large enough wavenumbers (using a cut-off of 50 cm^{-1}).⁶⁸ This arbitrary cut-off, used for all intermediate structures and transition states, does not keep the number of modes constant from one structure to another. Also, modes close to the cut-off can indeed be above or below the cut-off from one structure to another. Since the entropy is a measurement of the volume of the phase space, the cut-off method, albeit practical, is not the best way for the evaluation of entropy. We have recently proposed⁶⁹ to freeze part of the solid for the frequency calculation (and thus limit the number of phonons) and remove specifically identified phonon modes. This constitutes an improvement of the cut-off method, keeping the volume of the phase space constant. There are however no perfect schemes and, above all, no standard for the evaluation of entropy from static calculations in heterogeneous catalysis.⁶⁴ The recent work of Sprowl *et al.*, who have compared different schemes, might however unify and standardize entropic evaluations in heterogeneous catalysis.^{70,71}

Even if the evaluation of entropy is not perfect, the step-by-step addition of the different terms allow analyzing the role of experimental conditions like the area or the volume in which the particles are allowed translating: they are directly linked to the coverage or the partial pressure of the different species.

How to compare theory and experiments? The example of Temperature Programmed Desorption.

Temperature Programmed Desorption (TPD) is an experimental method that measures how strong a given compound interacts or reacts on a surface. As a surface science experiment, the surface samples can be chosen to exhibit a well-defined structure and the whole experiment takes place in a Ultra High Vacuum (UHV) chamber with a pressure of about 10^{-10} bar. A well-defined surface and void : a perfect system for theoreticians to model, isn't it?

The experiment starts at about 110 K with a compound deposited on the surface. A temperature ramp β (~ 5 K/s usually) is then applied. As soon as the sample is hot enough to have molecules desorb, they are detected by the mass spectrometer placed just above the surface sample. Desorption temperatures T_d are therefore measured with this technique. The desorption kinetics can be modeled using an Arrhenius like Polanyi-Wigner kinetics (see Equation 1.9) that relates the time derivative of coverage θ as a function of the pre-exponential factor ν , the activation energy $\Delta_d^\ddagger E$, the rate order n , temperature T and the gas constant R .⁷² The measurement of the desorption temperature peak enables the determination of the activation energy $\Delta_d^\ddagger E$ using Redhead Equation 1.10.^{72,73}

$$-\frac{d\theta}{dt} = \nu \exp\left(-\frac{\Delta_d^\ddagger E}{RT}\right) \theta^n \quad (1.9)$$

$$\Delta_d^\ddagger E = RT_d \ln\left(\frac{\nu RT_d^2 n \theta^{n-1}}{\beta \Delta_d^\ddagger E}\right) \quad (1.10)$$

The microscopic interpretation of $\Delta_d^\ddagger E$ is not so straightforward, since desorption processes can follow different paths as shown in Figure 1.2. For a molecule that does not undergo any decomposition reactions on the surface, $\Delta_d^\ddagger E$ is the activation energy of desorption (see Figure 1.2a). Since molecular adsorption is usually not activated, $\Delta_d^\ddagger E$ can be interpreted as a reaction energy of desorption (see Figure 1.2b). If the fragment

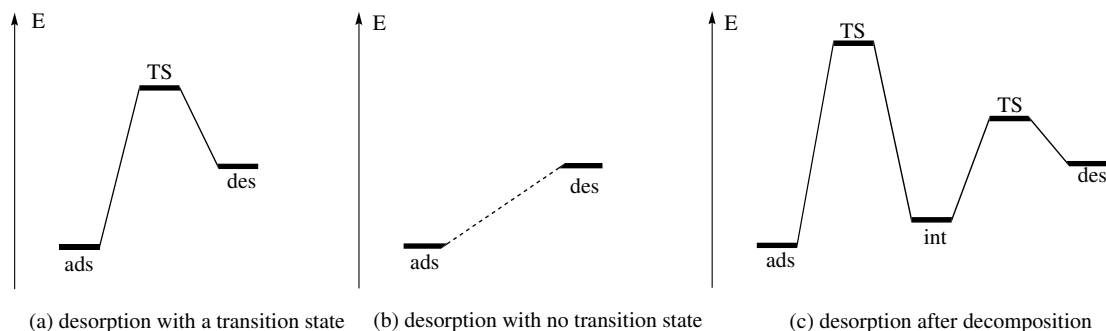


Figure 1.2: Three different energy profiles of desorption. *ads*, *int*, *des* and *TS* stand for adsorbed reactant, adsorbed intermediate, transition state and desorbed product respectively. The vertical axis reports variations of the potential energy.

detected in the mass spectrometer is a product of decomposition (see Figure 1.2c), $\Delta_d^\ddagger E$ can be interpreted as the desorption energy, the activation energy of desorption or even as the activation energy of the decomposition process on the surface, depending on which is the rate determining step. In the latter case, the temperature of desorption is usually higher than the one that could be measured during a TPD experiment with the product only. The activated decomposition can indeed delay the formation of the actual product.

Besides the issue of interpretation, the choice of the pre-factor is also critical in the evaluation of the energy $\Delta_d^\ddagger E$. Traditionally a value of 10^{13} s^{-1} is used. Using an Eyring-derived approach, Campbell and co-workers⁶⁶ have recently showed that higher accuracy can be achieved using entropy to estimate the pre-factor ν . The so-obtained energies can be compared with DFT calculations to support the interpretation of the experimental data. With a proper kinetic modeling, DFT can also be used to simulate TPD spectra and assess coverage effects and reactivity.^{74–80} However most of the studies aim at comparing experimental and theoretical energies and spectra. When large reaction networks are involved, this approach blurs the details of each elementary step.

Another approach consists in investigating directly the whole reaction network at the DFT level and then see how it corroborates with experimental TPD data. We could determine the desorption temperature for each reaction route, but we can do better and follow the variation of the free energy of activation of different processes over the whole temperature range scanned during the experiment. Within the harmonic approximation we can indeed determine activation barriers as explained in the previous section. The only problem arises when steps with no transition state on the electronic energy surface,

like phenol desorption from Pt(111), are involved. In the lines of Campbell and coworkers,⁸¹ we have proposed to decompose the activation free energy of desorption $\Delta_d^\ddagger F$ as a function of the desorption energy $\Delta_d E$ and an entropic term ΔS_{2D} .⁶⁹

$$\Delta_d^\ddagger F = \Delta_d E - T\Delta S_{2D} \quad (1.11)$$

ΔS_{2D} is evaluated using the vibrational and rotational entropy of gas phase molecules and the translational entropy of a 2D gas. This *desorbing transition state* models the increase of both energy and entropy upon desorption. To completely bridge DFT and TPD we finally need to determine the temperature from which a process has a low enough free energy of activation to proceed sufficiently rapidly. If the 1% conversion time, for example, is smaller than the typical TPD time scale T/β (see Equations 1.12 and 1.13), we can consider the reaction being rapid enough. From Eyring's equation for a first order process (molecular desorption or decomposition of one molecule), we can define $\Delta^\ddagger F_0$, the activation free energy above which the reaction is too slow to happen. This approach has recently shown success interpreting the TPD of anisole on Pt(111).

$$\tau_{1\%} = -\frac{\ln(0.99)h}{k_B T} \exp\left(+\frac{\Delta^\ddagger F}{RT}\right) \quad (1.12)$$

$$\tau_{1\%} < \frac{T}{\beta} \quad \Rightarrow \quad \Delta^\ddagger F < \Delta^\ddagger F_0 = RT \ln\left(\frac{k_B T^2}{-\ln(0.99)\beta h}\right) \quad (1.13)$$

This is how we recently compared DFT with TPD data concerning the reaction network of anisole, a biomass model, on Pt(111). This has allowed us to provide an important description of the decomposition network, reciprocally supported by both theory and experiment.⁶⁹

The approach presented here considers entropy as a vertical correction to the electronic energy surface. The structures are indeed not optimized taking directly entropy into account. We are compelled to introduce tricks like the desorbing transition state and work at low enough coverages to avoid considering conformational entropy, which is particularly difficult to evaluate for flexible systems such as biomass derivatives. When the system shows intrinsic flexibility or fluctuation we need to go beyond a fumbling approach of the phase space sampling.

Investigation based on the direct sampling of the phase space.

When systems with intrinsic fluctuations are studied (for example a fluid⁸² or a flexible structure like polymers⁸³) molecular dynamics (MD) provides a much better picture than that described in the previous section. The goal is to model, at a given temperature, the dynamics of molecules (translation, rotation and vibration) over a long enough time scale. The time scale mostly depends on the system studied and the method applied. Classical MDs provide simulations of the order of hundreds of microseconds but cannot describe changes in the connectivity of atoms (water without Grotthuss mechanism for example). The *ab initio* MDs (AIMD) can be used to analyze slightly activated bond formations and cleavages. However, the accessible simulation times are much shorter, namely a few dozen of picoseconds.

Born-Oppenheimer molecular dynamics.

Within the Born-Oppenheimer approximation, the dynamics of nuclei is ruled by the Newton-like equation of motion indicated in Equation 1.14, where the electronic energy $E_e(\{\vec{R}_i\})$ at time t with nuclei of mass M_i at \vec{R}_i plays the role of a potential energy.⁸⁴

$$M_i \times \frac{d^2 \vec{R}_i}{dt^2} = -\vec{\nabla}_i E_e(\{\vec{R}_i\}) \quad (1.14)$$

Hence, the accuracy of the numerical integration depends on the accuracy of the electronic energy evaluation and the integration algorithm with time-step dt . When hydrogen atoms are involved, molecular dynamics simulations are often performed using $dt = 0.5$ fs. For water/oxides systems with about 10^3 atoms, simulation times generally achieve a few dozen of picoseconds. For a first-order reaction with an activation barrier of 20 kJ/mol, half of the reactants are converted in about 300 ps, which is already about 10 times bigger than the typical simulation times we can achieve today for such systems. Simulating activated reactions is therefore really difficult. Literature on water/oxides interfaces modeled with AIMD indeed shows examples of almost unactivated processes (like the Grotthuss mechanism) but not activated processes.^{82,85-93} To go beyond the limitations of simple AIMD simulations we need to use *rare events* methods. These are specifically dedicated to the modeling of such processes.

Thermodynamic integration

Among *rare events* methods, thermodynamic integration (TI)^{94–96} has been reported for the determination of pKas^{86,88,97,98} in the context of water/oxides interfaces and the nucleation of solids from aqueous solutions.⁹⁹ In this specific case, the system is forced to follow a certain reaction coordinate that depends on the bonds lengths involved in the proton transfer or the cation/anion interaction in the ionic solid formation. We can also imagine constraints like the height of a sorbate from a surface, in order to model adsorption/desorption processes.

To evaluate the free energy difference between the reactant and the product (or the transition state), several simulations are inserted with intermediate values of the constraint. For each simulation (a few dozen of picoseconds), the time average of the derivative of the free energy F with respect to the constraint η , namely $\langle dF/d\eta \rangle$, is determined by the mean of Lagrangian multipliers. It is then integrated between states A and B to estimate the free energy variation between the two states (see Equation 1.15)

$$\Delta F_{A \rightarrow B} = - \int_A^B \left\langle \frac{dF}{d\eta} \right\rangle d\eta \quad (1.15)$$

To soften a bit the constraint, we can allow the system to move close to the constraint using a parabolic bias within the Umbrella Sampling (US) scheme.^{100–102} However, both US and TI require the multiplication of the number of simulations between the reactant and the product to reach accuracy. Moreover the reaction coordinate has to be known prior to the simulation, which makes these methods only suitable for simple reactions. The method could be extended to complex reaction coordinates, but that would imply a many dimensions scanning of the free energy profile and make the computational cost explode.

Metadynamics

Unlike the above-mentioned *rare events* methods, metadynamics (MtD) does not require a perfect knowledge of the reaction coordinate prior to simulation.^{103–106} It relies on the choice of collective variables (CVs) on which the reaction coordinate can depend. They can be seen as a restriction of the full phase-space. They only have to be functions of the atomic coordinates and can be distances, angles, dihedrals, heights, *etc.* They can even be more complex functions like coordination numbers (that roughly equals the

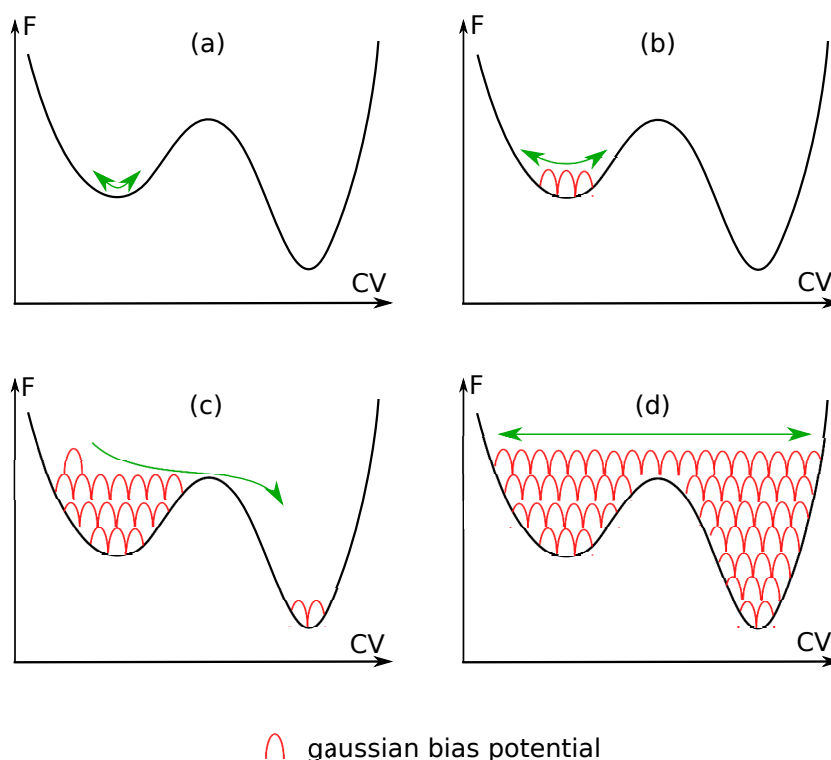


Figure 1.3: Representation of the principle of metadynamics at four different instants of the dynamics. Here we consider a one-dimension sampling along one CV. During the simulation, repulsive gaussians are added to have the the system visit a larger and larger phase-space. The green arrow represents the amplitude of phase-space sampling.

number of bonds around a given atom of an ensemble of atoms) or symmetry function (like the Steinhardt parameters).¹⁰⁷ Unlike US and TI where the system is forced to stay at several non-equilibrium positions, MtD offers the possibility to run only one simulation, starting with one equilibrated position in the phase-space (see Figure 1.3a). To help the system escape the initial potential well (that of the reactant) to other wells (intermediates and product) and sample the phase-space described by the CVs, a certain amount of free energy is regularly added during the run of the dynamics. This so-called bias potential has the form of gaussians with height h and width σ_i in the direction of the CV_i . It is a bit like trying to make a rubber ducky go out of a bathtub by filling it with water. As soon as enough gaussians have been added, the system starts to sample other wells (see Figure 1.3c). When the whole restricted phase-space described by the CVs has been sampled, the sum of the unknown free energy profile $F(\{CV_i\})$ with added gaussians g_j converges approximatively to a constant C (see Equation 1.16 and Figure

1.3d). Since only free energies differences are relevant, the constant disappears when calculating activation or reaction free energies. The sum of gaussians corresponds thus to a “cast” of the unknown free energy profile.

$$F(\{CV_i\}) + \sum_j g_j(\{CV_i\}) \simeq C \quad (1.16)$$

However, the relation given in Equation 1.16 is all the more exact that the size of the gaussians is small. But, if we start with small gaussians, the simulation can take forever to converge. To improve MtD, well-tempered MtD has been introduced.¹⁰⁸ It uses gaussians, the height of which decreases as a function of the number of previously added gaussians at the same position in the CV space. Other improvements include multiple walkers MtD,¹⁰⁹ with parallel MtD simulations that add gaussians at multiples positions in the CV space, and parallel tempering,¹¹⁰ that regularly exchanges the configuration of the actual MtD with a higher temperature simulation. The last two methods aim at providing an improved sampling of the CV space.

Conclusion

Dynamical approaches can appear as very attractive, since they provide a proper sampling of the phase-space including the evaluation of entropy. However they remain extremely expensive computationally, notably in heterogeneous catalysis. That is why literature shows very few occurrences of *ab initio* studies of metal/liquid interfaces.^{111,112} Chemical reactions are more frequently considered with computationally cheaper systems (like ionic solids, silica, alumina, *etc.*) but they remain limited to a few elementary steps like proton transfers (pKa, Grotthuss mechanism)^{82,88,98} and Lewis pair association (precipitation of calcium oxalate).⁹⁹

Static approaches remain today among the most efficient methods for the investigation of large reaction networks. When solvent effects are important, in particular in the field of electrocatalysis, polarizable continuum models are still widely used.¹¹³

Besides these two methods, we can however cite Monte Carlo methods for the study of systems with intrinsic fluctuations and/or flexibility. In lieu of using molecular dynamics to sample phase-spaces, large number of configurations are generated with a Monte Carlo algorithm. They have been used, for instance, in the determination of TPD spectra.⁷⁸ A detailed description of such schemes goes however beyond the scope of this thesis.

Bibliography

- [1] O’Ferrall, R. A. M. *J. Chem. Soc. B* **1970**, 274–277.
- [2] Laidler, K. *Chemical Kinetics*; Harper and Row, 1987.
- [3] Stepanov, A. G.; Zamaraev, K. I.; Thomas, J. M. *Catal. Letters* **1992**, *13*, 407–422.
- [4] Shi, D.; Vohs, J. M. *ACS Catal.* **2015**, *5*, 2177–2183.
- [5] Berruyer, P.; Lelli, M.; Conley, M. P.; Silverio, D. L.; Widdifield, C. M.; Siddiqi, G.; Gajan, D.; Lesage, A.; Copéret, C.; Emsley, L. *J. Am. Chem. Soc.* **2017**, *139*, 849–855.
- [6] Ostrom, H. et al. *Science (80-.)*. **2015**, *347*, 978–982.
- [7] Sieffert, N.; Réocreux, R.; Lorusso, P.; Cole-Hamilton, D. J.; Bühl, M. *Chem. - A Eur. J.* **2014**, *20*, 4141–4155.
- [8] Larmier, K.; Chizallet, C.; Cadran, N.; Maury, S.; Abboud, J.; Lamic-Humblot, A.-F.; Marceau, E.; Lauron-Pernot, H. *ACS Catal.* **2015**, *5*, 4423–4437.
- [9] Larmier, K.; Nicolle, A.; Chizallet, C.; Cadran, N.; Maury, S.; Lamic-Humblot, A.-F.; Marceau, E.; Lauron-Pernot, H. *ACS Catal.* **2016**, *6*, 1905–1920.
- [10] López, N.; Almora-Barrios, N.; Carchini, G.; Błoński, P.; Bellarosa, L.; García-Muelas, R.; Novell-Leruth, G.; García-Mota, M. *Catal. Sci. Technol.* **2012**, *2*, 2405.
- [11] Thomas, L. H. *Math. Proc. Cambridge Philos. Soc.* **1927**, *23*, 542.
- [12] Fermi, E. *Zeitschrift für Phys.* **1926**, *36*, 902–912.
- [13] Fermi, E. *Zeitschrift für Phys.* **1928**, *48*, 73–79.
- [14] Kohn, W.; Sham, L. J. *Phys. Rev.* **1965**, *137*, A1697–A1705.
- [15] Kurth, S.; Perdew, J. P.; Blaha, P. *Int. J. Quantum Chem.* **1999**, *75*, 889–909.
- [16] Silva, J. L. F. D.; Stampfl, C.; Scheffler, M. *Phys. Rev. Lett.* **2003**, *90*, 066104.
- [17] Rosa, A. L.; Neugebauer, J. *Phys. Rev. B* **2006**, *73*, 205346.
- [18] Perdew, J. P.; Schmidt, K. *AIP Conf. Proc.* **2001**, *577*, 1–20.

-
- [19] Perdew, J. P.; Chevary, J. A.; Vosko, S. H.; Jackson, K. A.; Pederson, M. R.; Singh, D. J.; Fiolhais, C. *Phys. Rev. B* **1992**, *46*, 6671–6687.
- [20] Perdew, J. P.; Burke, K.; Ernzerhof, M. *Phys. Rev. Lett.* **1996**, *77*, 3865–3868.
- [21] Perdew, J. P.; Kurth, S.; Zupan, A.; Blaha, P. *Phys. Rev. Lett.* **1999**, *82*, 2544–2547.
- [22] Stephens, P. J.; Devlin, F. J.; Chabalowski, C. F.; Frisch, M. J. *J. Phys. Chem.* **1994**, *98*, 11623–11627.
- [23] Adamo, C.; Barone, V. *J. Chem. Phys.* **1999**, *110*, 6158.
- [24] Adamo, C.; Cossi, M.; Barone, V. *J. Mol. Struct.* **1999**, *493*, 145–157.
- [25] Heyd, J.; Scuseria, G. E.; Ernzerhof, M. *J. Chem. Phys.* **2003**, *118*, 8207–8215.
- [26] Harl, J.; Kresse, G. *Phys. Rev. Lett.* **2009**, *103*, 056401.
- [27] Klimeš, J.; Michaelides, A. *J. Chem. Phys.* **2012**, *137*, 120901–120913.
- [28] Grimme, S. *J. Comput. Chem.* **2006**, *27*, 1787–1799.
- [29] Tkatchenko, A.; Distasio, R. A.; Car, R.; Scheffler, M. *Phys. Rev. Lett.* **2012**, *108*, 1–5.
- [30] Steinmann, S. N.; Corminboeuf, C. *J. Chem. Theory Comput.* **2011**, *7*, 3567–3577.
- [31] Steinmann, S. N.; Corminboeuf, C. *J. Chem. Phys.* **2011**, *134*, 044117.
- [32] Grimme, S.; Antony, J.; Ehrlich, S.; Krieg, H. *J. Chem. Phys.* **2010**, *132*, 154104.
- [33] Dion, M.; Rydberg, H.; Schröder, E.; Langreth, D. C.; Lundqvist, B. I. *Phys. Rev. Lett.* **2004**, *92*, 246401.
- [34] Dion, M.; Rydberg, H.; Schröder, E.; Langreth, D. C.; Lundqvist, B. I. *Phys. Rev. Lett.* **2004**, *92*, 246401.
- [35] Yildirim, H.; Greber, T.; Kara, A. *J. Phys. Chem. C* **2013**, *117*, 20572–20583.
- [36] Gautier, S.; Steinmann, S. N.; Michel, C.; Fleurat-Lessard, P.; Sautet, P. *Phys. Chem. Chem. Phys.* **2015**, *17*, 28921–28930.
- [37] Henkelman, G.; Uberuaga, B. P.; Jonsson, H. *J. Chem. Phys.* **2000**, *113*, 9901.

BIBLIOGRAPHY

- [38] Sheppard, D.; Terrell, R.; Henkelman, G. *J. Chem. Phys.* **2008**, *128*, 134106.
- [39] Henkelman, G.; Jonsson, H. *J. Chem. Phys.* **1999**, *111*, 7010.
- [40] Heyden, A.; Bell, A. T.; Keil, F. J. *J. Chem. Phys.* **2005**, *123*, 224101.
- [41] Kastner, J.; Sherwood, P. *J. Chem. Phys.* **2008**, *128*, 014106.
- [42] Cheng, J.; Hu, P.; Ellis, P.; French, S.; Kelly, G.; Lok, C. M. *J. Phys. Chem. C* **2008**, *112*, 1308–1311.
- [43] Santen, R. a. V.; Neurock, M.; Shetty, S. G. *Chem. Rev.* **2010**, *110*, 2005–2048.
- [44] Hammond, G. S. *J. Am. Chem. Soc.* **1955**, *77*, 334–338.
- [45] Bell, R. P. *Proc. R. Soc. London. Ser. A, Math. Phys. Sci.* **1935**, *154*, 414–429.
- [46] Evans, M. G.; Polanyi, M. *Trans. Faraday Soc.* **1938**, *34*, 11–24.
- [47] Brønsted, J. N. *Chem. Rev.* **1927**, 231–338.
- [48] Sutton, J. E.; Vlachos, D. G. *ACS Catal.* **2012**, *2*, 1624–1634.
- [49] Lee, K.; Gu, G. H.; Mullen, C. A.; Boateng, A. A.; Vlachos, D. G. *ChemSusChem* **2015**, *8*, 315–322.
- [50] Ferrin, P.; Simonetti, D.; Kandoi, S.; Kunkes, E.; Dumesic, J. A.; Nørskov, J. K.; Mavrikakis, M. *J. Am. Chem. Soc.* **2009**, *131*, 5809–5815.
- [51] Liu, B.; Greeley, J. *J. Phys. Chem. C* **2011**, *115*, 19702–19709.
- [52] Abild-Pedersen, F.; Greeley, J.; Studt, F.; Rossmeisl, J.; Munter, T. R.; Moses, P. G.; Skúlason, E.; Bligaard, T.; Nørskov, J. K. *Phys. Rev. Lett.* **2007**, *99*, 016105.
- [53] Calle-Vallejo, F.; Loffreda, D.; Koper, M. T. M.; Sautet, P. *Nat. Chem.* **2015**, *7*, 403–410.
- [54] Calle-Vallejo, F.; Tymoczko, J.; Colic, V.; Vu, Q. H.; Pohl, M. D.; Morgenstern, K.; Loffreda, D.; Sautet, P.; Schuhmann, W.; Bandarenka, A. S. *Science (80-.)*. **2015**, *350*, 185–189.

-
- [55] Chen, Y.; Saliccioli, M.; Vlachos, D. G. *J. Phys. Chem. C* **2011**, *115*, 18707–18720.
- [56] Gu, G. H.; Vlachos, D. G. *J. Phys. Chem. C* **2016**, *120*, 19234–19241.
- [57] Hammer, B.; Nørskov, J. *Surf. Sci.* **1995**, *343*, 211–220.
- [58] Geerlings, P.; De Proft, F.; Langenaeker, W. *Chem. Rev.* **2003**, *103*, 1793–1874.
- [59] Kokalj, A. *Chem. Phys.* **2012**, *393*, 1–12.
- [60] Obot, I.; Macdonald, D.; Gasem, Z. *Corros. Sci.* **2015**, *99*, 1–30.
- [61] del Rosal, I.; Mercy, M.; Gerber, I. C.; Poteau, R. *ACS Nano* **2013**, *7*, 9823–9835.
- [62] Nørskov, J. K.; Bligaard, T.; Rossmeisl, J.; Christensen, C. H. *Nat. Chem.* **2009**, *1*, 37–46.
- [63] Cusinato, L.; del Rosal, I.; Poteau, R. *Dalt. Trans.* **2017**, *46*, 378–395.
- [64] Saliccioli, M.; Vlachos, D. G. *ACS Catal.* **2011**, *1*, 1246–1256.
- [65] Atkins, P.; Paula, J. D. *Chemistry (Easton)*; 2010.
- [66] Campbell, C. T.; Árnadóttir, L.; J. R. V. Sellers, *Zeitschrift für Phys. Chemie* **2013**, *227*, 1435–1454.
- [67] Saliccioli, M.; Chen, Y.; Vlachos, D. G. *Ind. Eng. Chem. Res.* **2011**, *50*, 28–40.
- [68] Steinmann, S. N.; Michel, C.; Schwiedernoch, R.; Filhol, J.-S.; Sautet, P. *ChemPhysChem* **2015**, *16*, 2307–2311.
- [69] Réocreux, R.; Ould Hamou, C. A.; Michel, C.; Giorgi, J. B.; Sautet, P. *ACS Catal.* **2016**, *6*, 8166–8178.
- [70] Sprowl, L. H.; Campbell, C. T.; Árnadóttir, L. *J. Phys. Chem. C* **2016**, *120*, 9719–9731.
- [71] Sprowl, L. H.; Campbell, C. T.; Árnadóttir, L. *J. Phys. Chem. C* **2017**, *120*.
- [72] Masel, R. I. *Principles of Adsorption and Reaction on Solid Surfaces*; John Wiley & Sons, Inc., 1996.
- [73] Redhead, P. *Vacuum* **1962**, *12*, 203–211.

BIBLIOGRAPHY

- [74] Mei, D.; Ge, Q.; Neurock, M.; Kieken, L.; Lerou, J. *Mol. Phys.* **2004**, *102*, 361–369.
- [75] Calaza, F.; Stacchiola, D.; Neurock, M.; Tysoe, W. T. *Surf. Sci.* **2005**, *598*, 263–275.
- [76] Wang, H.; Male, J.; Wang, Y. *ACS Catal.* **2013**, *3*, 1047–1070.
- [77] Mullen, G. M.; Zhang, L.; Evans, E. J.; Yan, T.; Henkelman, G.; Mullins, C. B. *J. Am. Chem. Soc.* **2014**, *136*, 6489–6498.
- [78] Pogodin, S.; López, N. *ACS Catal.* **2014**, *4*, 2328–2332.
- [79] Robinson, A. M.; Mark, L.; Rasmussen, M.; Hensley, J. E.; Medlin, J. *J. Phys. Chem. C* **2016**, *in review*.
- [80] enozan, S.; Ustunel, H.; Karatok, M.; Vovk, E. I.; Shah, A. A.; Ozensoy, E.; Tofoli, D. *Top. Catal.* **2016**, *59*, 1383–1393.
- [81] Gottfried, J. M.; Vestergaard, E. K.; Bera, P.; Campbell, C. T. *J. Phys. Chem. B* **2006**, *110*, 17539–17545.
- [82] Ma, S.-Y.; Liu, L.-M.; Wang, S.-Q. *J. Phys. Chem. C* **2016**, *120*, 5398–5409.
- [83] Boero, M.; Parrinello, M.; Hüffer, S.; Weiss, H. *J. Am. Chem. Soc.* **2000**, *122*, 501–509.
- [84] Tuckerman, M. E. *J. Phys. Condens. Matter* **2002**, *14*, R1297–R1355.
- [85] Cimas, Á.; Tielens, F.; Sulpizi, M.; Gaigneot, M.-P.; Costa, D. *J. Phys. Condens. Matter* **2014**, *26*, 244106.
- [86] Gaigneot, M.-P.; Sprik, M.; Sulpizi, M. *J. Phys. Condens. Matter* **2012**, *24*, 124106.
- [87] Pfeiffer-Laplaud, M.; Gaigneot, M.-P. *J. Phys. Chem. C* **2016**, *120*, 14034–14047.
- [88] Pfeiffer-Laplaud, M.; Gaigneot, M.-P.; Sulpizi, M. *J. Phys. Chem. Lett.* **2016**, *7*, 3229–3234.
- [89] Machesky, M. L.; Predota, M.; Wesolowski, D. J.; Vlcek, L.; Cummings, P. T.; Rosenqvist, J.; Ridley, M. K.; Kubicki, J. D.; Bandura, A. V.; Kumar, N.; Sofo, J. O. *Langmuir* **2008**, *24*, 12331–12339.

-
- [90] Mattioli, G.; Filippone, F.; Caminiti, R.; Bonapasta, A. A. *J. Phys. Chem. C* **2008**, *112*, 13579–13586.
- [91] Tilocca, A.; Selloni, A. *J. Phys. Chem. C* **2012**, *116*, 9114–9121.
- [92] Hass, K. C.; Schneider, W. F.; Curioni, A.; Andreoni, W. *Science (80-.)*. **1998**, *282*, 265–268.
- [93] Hass, K. C.; Schneider, W. F.; Curioni, A.; Andreoni, W. *J. Phys. Chem. B* **2000**, *104*, 5527–5540.
- [94] Ciccotti, G.; Ferrario, M. *J. Mol. Liq.* **2000**, *89*, 1–18.
- [95] Darve, E.; Pohorille, A. *J. Chem. Phys.* **2001**, *115*, 9169–9183.
- [96] Gullingsrud, J. R.; Braun, R.; Schulten, K. *J. Comput. Phys.* **1999**, *151*, 190–211.
- [97] Tazi, S.; Rotenberg, B.; Salanne, M.; Sprik, M.; Sulpizi, M. *Geochim. Cosmochim. Acta* **2012**, *94*, 1–11.
- [98] Pfeiffer-Laplaud, M.; Costa, D.; Tielens, F.; Gaigeot, M.-P.; Sulpizi, M. *J. Phys. Chem. C* **2015**, *119*, 27354–27362.
- [99] Parvaneh, L. S.; Donadio, D.; Sulpizi, M. *J. Phys. Chem. C* **2016**, *120*, 4410–4417.
- [100] Patey, G. N.; Valleau, J. P. *J. Chem. Phys.* **1975**, *63*, 2334–2339.
- [101] Torrie, G.; Valleau, J. *J. Comput. Phys.* **1977**, *23*, 187–199.
- [102] Mezei, M. *J. Comput. Phys.* **1987**, *68*, 237–248.
- [103] Laio, A.; Parrinello, M. *Proc. Natl. Acad. Sci.* **2002**, *99*, 12562–12566.
- [104] Micheletti, C.; Laio, A.; Parrinello, M. *Phys. Rev. Lett.* **2004**, *92*, 170601.
- [105] Iannuzzi, M.; Laio, A.; Parrinello, M. *Phys. Rev. Lett.* **2003**, *90*, 238302.
- [106] Bussi, G.; Laio, A.; Parrinello, M. *Phys. Rev. Lett.* **2006**, *96*, 090601.
- [107] Laio, A.; Gervasio, F. L. *Reports Prog. Phys.* **2008**, *71*, 126601.
- [108] Barducci, A.; Bussi, G.; Parrinello, M. *Phys. Rev. Lett.* **2008**, *100*, 020603.

BIBLIOGRAPHY

- [109] Raiteri, P.; Laio, A.; Gervasio, F. L.; Micheletti, C.; Parrinello, M. *J. Phys. Chem. B* **2006**, *110*, 3533–3539.
- [110] Bussi, G.; Gervasio, F. L.; Laio, A.; Parrinello, M. *J. Am. Chem. Soc.* **2006**, *128*, 13435–13441.
- [111] Herron, J. A.; Morikawa, Y.; Mavrikakis, M. *Proc. Natl. Acad. Sci.* **2016**, *113*, E4937–E4945.
- [112] Bellarosa, L.; García-Muelas, R.; Revilla-López, G.; López, N. *ACS Cent. Sci.* **2016**, *2*, 109–116.
- [113] Steinmann, S. N.; Michel, C.; Schwiedernoch, R.; Filhol, J.-S.; Sautet, P. *ChemPhysChem* **2015**, *16*, 2307–2311.

Part I

Lignin derivatives on Pt(111)

Chapter 2

Lignin: structure and valorization

Lignin is Nature's most abundant aromatic polymer and represents approximately 35 % of biomass.^{1,2} Unlike cellulose, which represents about 40% of biomass, lignin is not particularly valorized and is a major product of the paper industry.¹ However its structure (see Figure 2.1), which is based on the three alcohol monomers represented in Figure 2.2 (coumaryl, coniferyl and sinapyl alcohols, also called monolignols), shows many aromatic moieties. Lignin valorization into the high-valuable benzene-toluene-xylene (BTX) platform therefore requires its depolymerization and deoxygenation.¹⁻³

The idea of depolymerizing lignin is however not new and was originally introduced by Pepper *et al.*^{4,5} in the context of analytical chemistry for the determination of lignin composition. Using late transition metals (Ni, Pd, Ru, Rh), they were able to extract different types of aromatic units under hydrogenolysis conditions (with a pressure of hydrogen of about 30 bars). More recently, noble metals (Ru, Pd, Pt) have been intensively investigated for the hydrodeoxygenation (HDO) reaction in the context of biomass valorization.⁶⁻⁹ Other catalysts,¹⁰⁻¹² developed for the hydrodesulfurization (HDS) of oil fractions, have also been tested for the HDO of lignin.* Among these heterogeneous catalysts, Pt shows the higher conversions, although it appears to be very bad at deoxygenating aromatics, even under high pressures of hydrogen (100 bars).⁹

Within this context, we have decided to study 2-phenoxyethanol (2-PE) on a platinum catalyst. We have chosen 2-PE because it mimics the environment of a β -O-4 linkage, the most abundant linkage between two monomers in lignin. To investigate its interaction and reactivity from a very fundamental point-of-view, we have joined forces

* well, oxygen and sulfur are both chalcogens, aren't they?

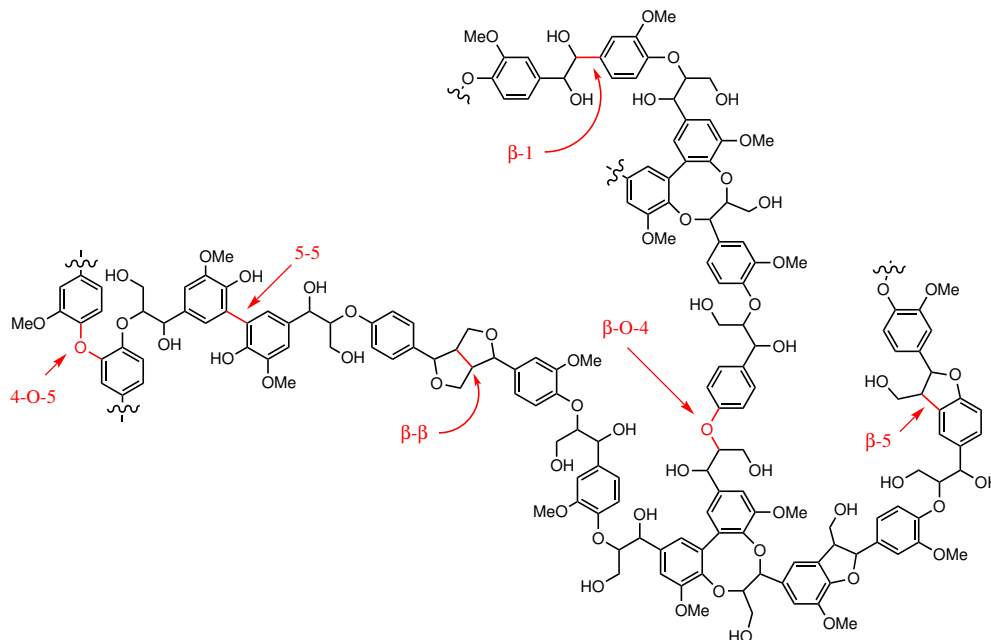


Figure 2.1: Representative structure of lignin with its characteristic linkages highlighted in red.¹

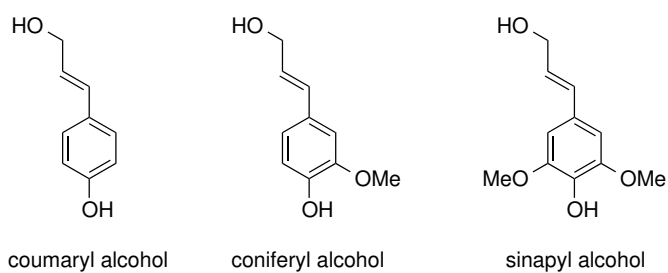


Figure 2.2: Alcohol monomers of lignin.

with surface science experimentalists, studying, both of us, 2-PE on Pt(111) under vacuum conditions. This system has rapidly appeared to be very complex. That is why we have first focused, computationally only, on a set of aromatic oxygenates on Pt(111) in order to understand and rationalize their adsorption in terms of simple molecular descriptors, as reported in **Chapter 3**. We have then extensively studied, combining theory and experiments, the reaction networks of anisole and 2-PE, as reported in **Chapter 4** and **Chapter 5**. This has allowed us to address the role of hydrogen in the HDO performed on platinum. We have also demonstrated the necessity of having a reductant in the system to make platinum suitable as a catalyst of the deoxygenation of aromatics. Recently, similar conclusions have been reported in the literature.¹³

Bibliography

- [1] Zakzeski, J.; Bruijninx, P. C. A.; Jongerius, A. L.; Weckhuysen, B. M. *Chem. Rev.* **2010**, *110*, 3552–3599.
- [2] Ragauskas, A. J. et al. *Science (80-.)*. **2014**, *344*, 1246843.
- [3] Sanderson, K. *Nature* **2011**, *474*, S12–S14.
- [4] Pepper, J. M.; Lee, Y. W. *Can. J. Chem.* **1969**, *47*, 723–727.
- [5] Pepper, J. M.; Fleming, R. W. *Can. J. Chem.* **1978**, *56*, 896–898.
- [6] Lin, Y.-C.; Li, C.-L.; Wan, H.-P.; Lee, H.-T.; Liu, C.-F. *Energy & Fuels* **2011**, *25*, 890–896.
- [7] Nimmanwudipong, T.; Runnebaum, R. C.; Ebeler, S. E.; Block, D. E.; Gates, B. C. *Catal. Letters* **2012**, *142*, 151–160.
- [8] Zhu, X.; Lobban, L. L.; Mallinson, R. G.; Resasco, D. E. *J. Catal.* **2011**, *281*, 21–29.
- [9] Wildschut, J.; Mahfud, F. H.; Venderbosch, R. H.; Heeres, H. J. *Ind. Eng. Chem. Res.* **2009**, *48*, 10324–10334.
- [10] Laurent, E.; Delmon, B. *Ind. Eng. Chem. Res.* **1993**, *32*, 2516–2524.
- [11] Laurent, E.; Delmon, B. *Appl. Catal. A Gen.* **1994**, *109*, 77–96.

BIBLIOGRAPHY

[12] Romero, Y.; Richard, F.; Brunet, S. *Appl. Catal. B Environ.* **2010**, *98*, 213–223.

[13] Shi, D.; Arroyo-Ramírez, L.; Vohs, J. M. *J. Catal.* **2016**, *340*, 219–226.

Chapter 3

Controlling the Adsorption of Aromatic Compounds on Pt(111) with Oxygenate Substituents: From DFT to Simple Molecular Descriptors

Réocreux R., Huynh M., Michel C., Sautet P. *J. Phys. Chem. Lett.*, **2016**, 7, 2074-2079

Article and Supporting Information available at:

<https://doi.org/10.1021/acs.jpcllett.6b00612>

Chapter 4

Decomposition Mechanism of Anisole on Pt(111): Combining Single-Crystal Experiments and First-Principles Calculations

Réocreux R., Hamou C. A. O., Michel C., Giorgi J., Sautet P. *ACS Catal.*, **2016**, *6*, 8166-8178

Article and Supporting Information available at:

<https://doi.org/10.1021/acscatal.6b02253>

I performed all the DFT calculations (but XPS predictions) and kinetic analysis (experimental & theoretical). Hamou C. A. O. performed all the experiments and related analysis.

Chapter 5

Adsorption and Decomposition of a Lignin β -O-4 Linkage Model, 2-Phenoxyethanol, on Pt(111): Combination of Experiments and First-Principles Calculations

Hamou C. A. O., Réocreux R., Sautet P., Michel C., Giorgi J. *J. Phys. Chem. C*, **2017**, *121*, 9889-9900

Article and Supporting Information available at:

<https://doi.org/10.1021/acs.jpcc.7b01099>

I performed all the DFT calculations (but XPS predictions) and kinetic analysis (experimental & theoretical). Hamou C. A. O. performed all the experiments and related analysis.

Part II

$\gamma\text{-Al}_2\text{O}_3$ at the interface with liquid water

Chapter 6

γ -Al₂O₃ model surfaces

γ -Al₂O₃ is one of the most popular support in heterogeneous catalysis.^{1,2} It is indeed a solid with a large specific area (ca 200-250 m²/g) that shows Lewis basic sites, on which one can strongly adsorb catalysts such as metal particles³⁻⁸ or metal complexes.^{9,10} It can also adsorb Lewis bases on its coordinative unsaturated sites in particular the under-coordinated aluminum cations. Moreover, like amorphous silica, another important support, Brønsted basicity and acidity also arise from the aluminol (OH) groups that are produced upon partial surface hydration. Each of these properties can be crucial to assist the reactions that take place on the actual catalyst.⁸⁻¹² They have been extensively investigated using a large variety of spectroscopies (IR,¹³⁻²¹ NMR,^{17,18,20-24} TEM,^{16,20-26} XRD,²⁰⁻²⁸ XPS,²⁹ ...). However these experimental data mainly give a global statistic picture of the structure of γ -Al₂O₃ rather than the atomistic viewpoint required for the modulation and the optimization of its chemical properties. γ -Al₂O₃ is indeed not a simple solid surface with a very well defined structure. In spite of that, a working model is needed to have a picture, perhaps idealized, of surface γ -Al₂O₃.

With the development of GGA functionals in the 90s,^{30,31} DFT has enabled chemists to model oxides provided that their cohesion does not mainly rely on weak van der Waals interactions. Carefully comparing with available experimental data, Krokidis *et al.*³² first proposed in 2001 a structure for bulk γ -Al₂O₃ based on DFT calculations. They built a perfect crystal bulk structure by modeling the synthesis of γ -Al₂O₃ from boehmite AlOOH, a topotactic* condensation (dehydration) process during which boehmite layers

*the reactant and product lattices are related one to another with well defined transformations concerning the crystallographic orientations

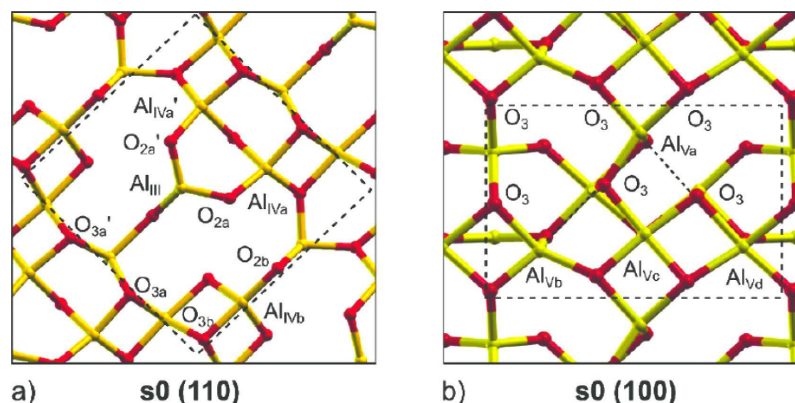


Figure 6.1: Completely dehydrated (110) and (100) surfaces of γ -Al₂O₃. **s0** stands for *surface with 0 chemisorbed water molecules*. Yellow balls are Al cations and red balls are O anions. Reprinted with permission from Wischert *et al.*³⁵ Copyright 2012 American Chemical Society.

collapse to form γ -Al₂O₃. The resulting unit cell of bulk γ -Al₂O₃ can be described with a fcc sublattice of oxygen atoms, the tetrahedral and octahedral interstices of which are populated with aluminum cations. A large number of cation distributions were simulated to determine that, in the most stable structure, 25% of the cations occupy tetrahedral sites (about 20 to 30 % experimentally), the actual model. Interestingly enough, DFT calculations showed that the aluminum atoms are not restricted to occupy spinel sites only, unlike the earlier postulated defective spinel[†] model by Lippens. Albeit quite controversial,^{33,34} Krokidis non-spinel model has appeared to be consistent with x-ray diffraction patterns and experimentally determined geometrical features, even if it remains a perfect crystal model that does not depict the actual poor crystallinity of γ -Al₂O₃.

Building on the work reported by Krokidis *et al.*,³² Digne and coworkers were the first to propose, in 2006, realistic surface models for different crystallographic orientations, in particular the most stable (100) surface and the predominant (110) surface.^{36?} The (100) surface is represented in Figure 6.1b. It only displays four pentacoordinated Al cations, labelled Al_V. Statistically more important (about 75% of all exposed surfaces), the (110) surface exhibits more under-coordinated sites with three tetracoordinated Al cations, labelled Al_{IV}, and one tricoordinated Al cation, labelled Al_{III}, for a surface area

[†]To satisfy stoichiometry, some cation sites in the M₃O₄ spinel structure (M designates a metal cation) remain unoccupied.

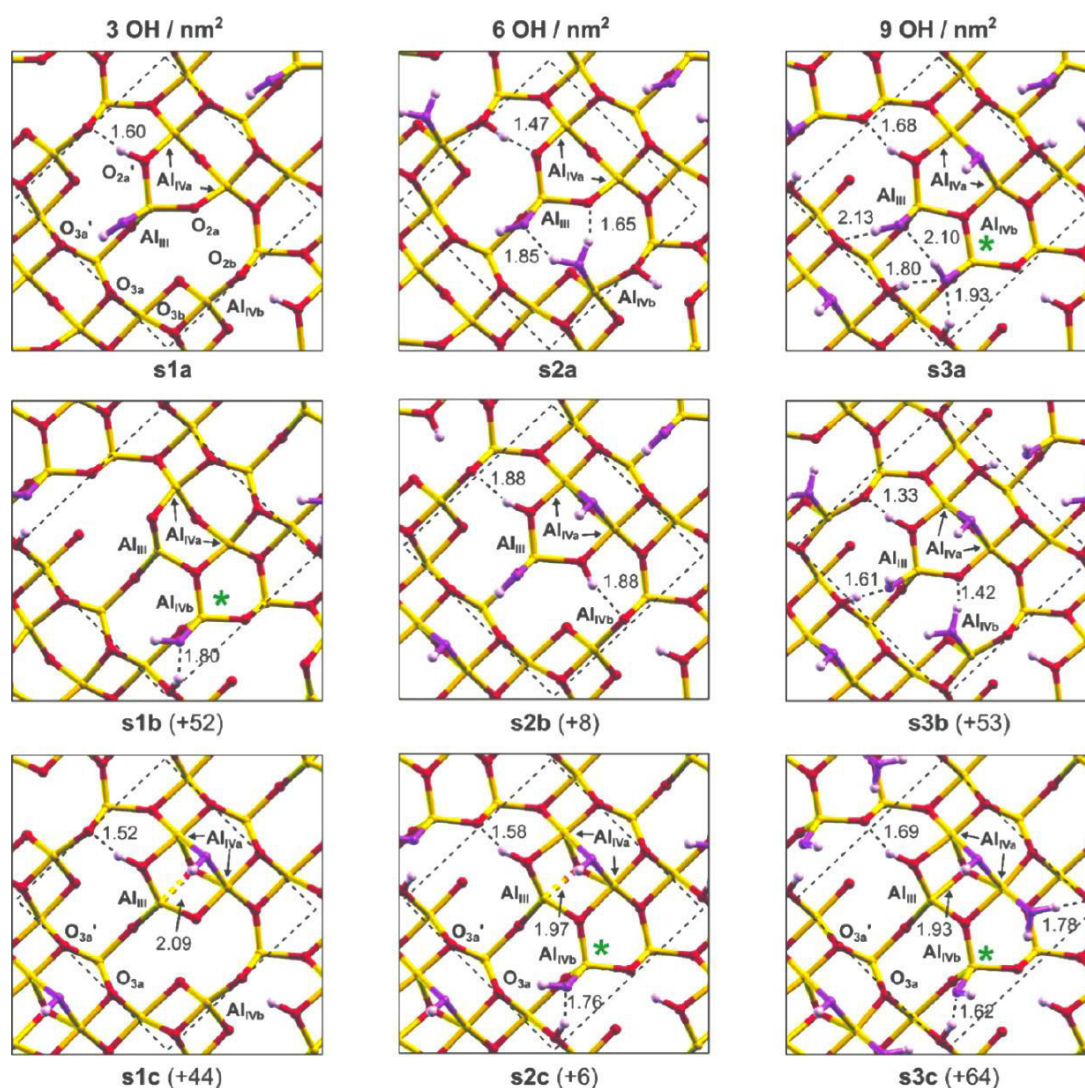


Figure 6.2: Structure variation of γ -Al₂O₃ (110) surface upon hydration. For each OH coverages, three structures **a**, **b** and **c** are considered. **s_i** indicates the number of water molecules *i* adsorbed on the primitive surface. The first row gives the most stable structures. The numbers in parenthesis give the energy relative to the first structures in kJ/mol. Yellow balls are Al cations, red balls are O anions coming from the surface itself, and purple balls are O atoms. Reprinted with permission from Wischert *et al.*³⁵ Copyright 2012 American Chemical Society.

of about 16 Å (see Figure 6.1a). The strong under-coordination of the (110) surface is responsible for its strong affinity with various compounds, including water. These two models have been able to picture the very first steps of γ -Al₂O₃ hydration, the energetics of which agrees with microcalorimetric experiments.³⁷ Moreover the simulated infrared spectroscopy of the resulting aluminols, in agreement with the experimental spectra, have allowed to assign to each band a particular OH group with its specific geometry and binding mode to the surface.

In 2012, Wischert and coworkers further improved the model (110) surface with a more careful study of the impact of hydration on the mobility of aluminum cations, and in particular the so-labelled Al_{IVb} in Figures 6.1 and 6.2. The main structures studied are given in Figure 6.2 and are labelled **sia**, **sib** and **sic** with **s** standing for *surface* and **i** the number of water molecules added on **s0** (110) (see Figure 6.1). The most stable structures, given in the first row, are of particular interest. The first water molecule adsorption is dissociative and occurs at the Al_{III} site, the most under-coordinated cation. The second water molecule adsorbs molecularly at the Al_{IVb} site but other structures, the energy of which is less than 10 kJ/mol uphill, show likely dissociation at the bridging Al_{IVb} site (**s2b**, +8 kJ/mol) and even the migration of Al_{IVb} to another position on the surface (see green starred atom on **s2c**, +6 kJ/mol). With the adsorption of a third water molecule, this migration appears to give a particularly stable surface **s3a** that rules out the other considered structures, at least 50 kJ/mol less stable. On **s3a**, there are two coordinative unsaturated sites left (one on each Al_{IVa}) that might adsorb two water molecules, probably undissociatively as surface **s3c** suggests.

Over the last decade, Digne and Wischert's models have gained success in computational catalysis. They have pointed out the significance of the tricoordinated Al cations (on the (110) surface) in the activation of small non-polar molecules (H₂, N₂ and CH₄)^{35,38,39} and that of pentacoordinated Al cations (on the (100) surface) in the dehydration of alcohols to olefins.^{40,41} Besides its intrinsic catalytic activity, support effects of γ -Al₂O₃ have also been inspected computationally for a couple of single sites catalysts like zirconocenes⁹ and rhenium complexes.¹⁰ The first models of metallic nanoclusters/nanoparticles supported on γ -Al₂O₃ have also been reported in the literature.³⁻⁸

However, this success is not restricted to computational catalysis. Many experimental characterizations of γ -Al₂O₃ refer to this model, in particular with the recent growing interest for the mechanism of γ -Al₂O₃ decomposition in liquid water.^{20,21,24,26} γ -Al₂O₃

is indeed unstable in water and transforms into hydroxides and/or (oxo)hydroxides which makes the supported nanoparticles, used in catalysis, sinter, yielding to catalyst deactivation. However biomass compounds (polyols and lignin) seem to slow down the decomposition, making γ -Al₂O₃ possibly suitable for biomass conversion purposes. In spite of recent experimental studies, the exact mechanism of γ -Al₂O₃ decomposition is still known and the precise role of protecting alcohols to be determined.

To better understand, at the atomic scale, this decomposition in liquid water, we have first performed *ab initio* molecular dynamics simulating the interface between liquid water and the predominant (110) surface of γ -Al₂O₃. **Chapter 1** reports the impact of γ -Al₂O₃ on the structuration of water and the interaction of water with the aluminol groups arising from hydration. Using metadynamics, we have then attempted to model the early stage mechanism of this decomposition and showed, in **Chapter 2**, the particular role of tetrahedral aluminum cations. In **Chapter 3**, we have finally considered the adsorption of alcohols on γ -Al₂O₃ to determine the free energy profile of desorption and assess the role of polyols in the inhibition of the decomposition.

Towards γ -Al₂O₃/water interfaces : where should we start from?

The starting point of this study is surface **s3a** proposed by Wischert *et al.* (see Figure 6.2):³⁵ it has appeared as a good compromise between the description of the aluminum network (taking into account migrations) and the water coverage. However, in order to reach the optimal water coverage determined by Digne *et al.*⁷ at room temperature and atmospheric pressure, two extra water molecules have been adsorbed, undissociatively, on the last two coordinative unsaturated sites, which have not been reported to cleave water (see surface **s3c** in Figure 6.2). The obtained model surface, which would be labelled **s5** using Wischert's notation, is given in Figure 6.3 in a ball and stick representation. For simplicity, skeletal representations will also be used in this Part.

We have also introduced another notation for the labelling in the aluminum centres. Unlike Digne, we need fixed notations to be able to track the evolution of the coordination sphere of the different centres. However Wischert's fixed notation refers to completely dehydrated alumina, too different from the conditions we are interested in. In the lines of Copeland *et al.*,¹⁸ we have kept the arabic numerals for octahedral aluminum atoms

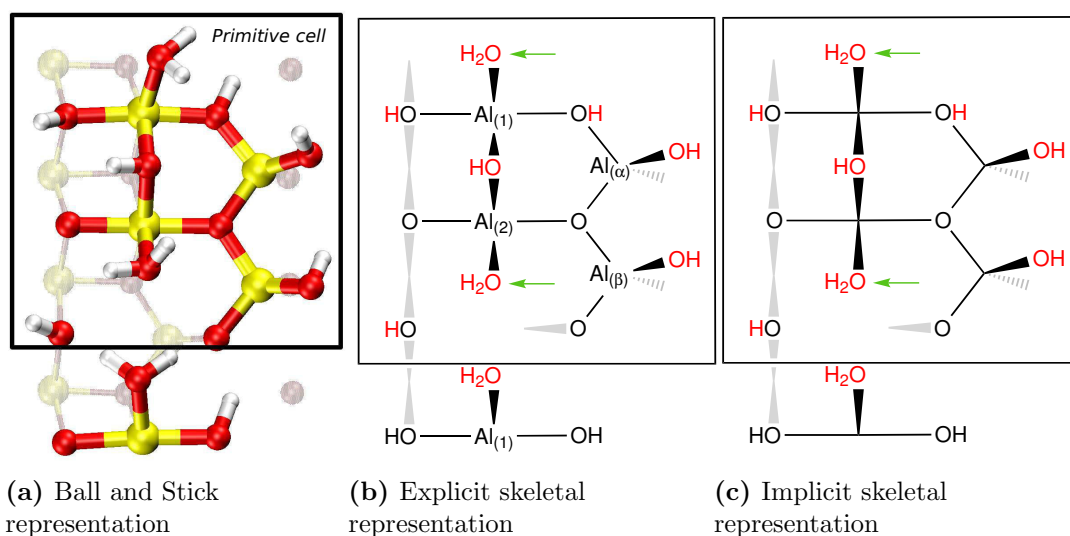


Figure 6.3: Three different representations of the initial (110) surface **s5** used in the present work. (a) Ball and stick representation with yellow balls for Al, red balls for O and white balls for H, (b) explicit skeletal representation with the labelling of the Al atoms used in the present work, (c) implicit skeletal representation (the Al atoms are not represented but are found at the intersection of at least two bounds). In (b) and (c), green arrows point out the two extra water molecules added on surface **s3a** (see Figure 6.2), red atoms come from the chemisorption of water on pristine γ - Al_2O_3 and are therefore not considered to belong to γ - Al_2O_3 . In (a), (b) and (c) the square represents the limits of the surface primitive cell.

the present work	Digne [?]	Wischert ³⁵	Copeland ¹⁸
Al ₍₁₎	Al _{VI}	Al _{IVa}	Al1
Al ₍₂₎	Al _{VI}	Al _{IVa}	Al2
Al _(α)	Al _{IV}	Al _{III}	-
Al _(β)	Al _{IV}	Al _{IVb}	-

Table 6.1: Correspondance between the different notations available in the literature concerning the labelling of the surface Al atoms of γ -Al₂O₃ on the (110) surface

and introduced greek letters for tetrahedral aluminum atoms of our **s5** surface. Table 6.1 gives the correspondance between the different notations.

Finally, as an arbitrary convention, γ -Al₂O₃ only refers to the ensemble of atoms that originates from bulk γ -Al₂O₃. Adsorbed O_xH_y (x=0,1 and y=1,2) fragments coming from water (see red atoms in Figures 6.3b and 6.3c) are still designated as chemisorbed water even if strong bonds with γ -Al₂O₃ are involved.

Bibliography

- [1] Euzen, P.; Raybaud, P.; Krokidis, X.; Toulhoat, H.; Le Loarer, J.-L.; Jolivet, J.-P.; Froidefond, C. *Handb. Porous Solids*; 2002; Vol. 3; pp 1591–1677.
- [2] Trueba, M.; Trasatti, S. P. *Eur. J. Inorg. Chem.* **2005**, 3393–3403.
- [3] Hu, C. H.; Chizallet, C.; Mager-Maury, C.; Corral-Valero, M.; Sautet, P.; Toulhoat, H.; Raybaud, P. *J. Catal.* **2010**, *274*, 99–110.
- [4] Mager-Maury, C.; Bonnard, G.; Chizallet, C.; Sautet, P.; Raybaud, P. *ChemCatChem* **2011**, *3*, 200–207.
- [5] Mager-Maury, C.; Chizallet, C.; Sautet, P.; Raybaud, P. *ACS Catal.* **2012**, *2*, 1346–1357.
- [6] Raybaud, P.; Chizallet, C.; Mager-Maury, C.; Digne, M.; Toulhoat, H.; Sautet, P. *J. Catal.* **2013**, *308*, 328–340.
- [7] Gorczyca, A.; Moizan, V.; Chizallet, C.; Proux, O.; Del Net, W.; Lahera, E.; Hazemann, J.-L.; Raybaud, P.; Joly, Y. *Angew. Chemie Int. Ed.* **2014**, *53*, 12426–12429.
- [8] Silaghi, M.-C.; Comas-Vives, A.; Copéret, C. *ACS Catal.* **2016**, *6*, 4501–4505.

BIBLIOGRAPHY

- [9] Motta, A.; Fragala, I. L.; Marks, T. J. *J. Am. Chem. Soc.* **2008**, *130*, 16533–16546.
- [10] Valla, M.; Wischert, R.; Comas-Vives, A.; Conley, M. P.; Verel, R.; Copéret, C.; Sautet, P. *J. Am. Chem. Soc.* **2016**, *138*, 6774–6785.
- [11] Bui, V. N.; Laurenti, D.; Delichère, P.; Geantet, C. *Appl. Catal. B Environ.* **2011**, *101*, 246–255.
- [12] Wang, H.; Feng, M.; Yang, B. *Green Chem.* **2017**,
- [13] Knözinger, H.; Ratnasamy, P. *Catal. Rev.* **1978**, *17*, 31–70.
- [14] Morterra, C.; Magnacca, G. *Catal. Today* **1996**, *27*, 497–532.
- [15] Tsyganenko, A. A.; Mardilovich, P. P. *J. Chem. Soc. Faraday Trans.* **1996**, *92*, 4843.
- [16] Paglia, G.; Buckley, C. E.; Udovic, T. J.; Rohl, A. L.; Jones, F.; Maitland, C. F.; Connolly, J. *Chem. Mater.* **2004**, *16*, 1914–1923.
- [17] Pecharromán, C.; Sobrados, I.; Iglesias, J. E.; González-Carreño, T.; Sanz, J. *J. Phys. Chem. B* **1999**, *103*, 6160–6170.
- [18] Copeland, J. R.; Shi, X.-R.; Sholl, D. S.; Sievers, C. *Langmuir* **2013**, *29*, 581–593.
- [19] Copeland, J. R.; Santillan, I. A.; Schimming, S. M.; Ewbank, J. L.; Sievers, C. *J. Phys. Chem. C* **2013**, *117*, 21413–21425.
- [20] Abi Aad, J.; Courty, P.; Decottignies, D.; Michau, M.; Diehl, F.; Carrier, X.; Marceau, E. *ChemCatChem* **2017**, *9*, 2106–2117.
- [21] Ravenelle, R. M.; Copeland, J. R.; Van Pelt, A. H.; Crittenden, J. C.; Sievers, C. *Top. Catal.* **2012**, *55*, 162–174.
- [22] Paglia, G.; Buckley, C. E.; Rohl, A. L.; Hart, R. D.; Winter, K.; Studer, A. J.; Hunter, B. A.; Hanna, J. V. *Chem. Mater.* **2004**, *16*, 220–236.
- [23] Ravenelle, R. M.; Copeland, J. R.; Kim, W.-G.; Crittenden, J. C.; Sievers, C. *Am. Chem. Soc. Catal.* **2011**, *1*, 552–561.
- [24] Jongerius, A. L.; Copeland, J. R.; Foo, G. S.; Hofmann, J. P.; Bruijninx, P. C. A.; Sievers, C.; Weckhuysen, B. M. *ACS Catal.* **2013**, *3*, 464–473.

- [25] Carrier, X.; Marceau, E.; Lambert, J. F.; Che, M. *J. Colloid Interface Sci.* **2007**, *308*, 429–437.
- [26] Abi Aad, J.; Casale, S.; Michau, M.; Courty, P.; Diehl, F.; Marceau, E.; Carrier, X. *ChemCatChem* **2017**, *9*, 2186–2194.
- [27] González-Peña, V.; Díaz, I.; Márquez-Alvarez, C.; Sastre, E.; Pérez-Pariente, J. *Microporous Mesoporous Mater.* **2001**, *44-45*, 203–210.
- [28] Ren, T.-Z.; Yuan, Z.-Y.; Su, B.-L. *Langmuir* **2004**, *20*, 1531–1534.
- [29] Bhattacharya, A.; Pyke, D.; Walker, G.; Werrett, C. *Appl. Surf. Sci.* **1997**, *108*, 465–470.
- [30] Perdew, J. P.; Wang, Y. *Phys. Rev. B* **1992**, *45*, 244–249.
- [31] Perdew, J. P.; Burke, K.; Ernzerhof, M. *Phys. Rev. Lett.* **1996**, *77*, 3865–3868.
- [32] Krokidis, X.; Raybaud, P.; Gobichon, A.-E.; Rebours, B.; Euzen, P.; Toulhoat, H. *J. Phys. Chem. B* **2001**, *105*, 5121–5130.
- [33] Sun, M.; Nelson, A. E.; Adjaye, J. *J. Phys. Chem. B* **2006**, *110*, 2310–2317.
- [34] Digne, M.; Raybaud, P.; Sautet, P.; Rebours, B.; Toulhoat, H. *J. Phys. Chem. B* **2006**, *110*, 20719–20720.
- [35] Wischert, R.; Laurent, P.; Copéret, C.; Delbecq, F.; Sautet, P. *J. Am. Chem. Soc.* **2012**, *134*, 14430–14449.
- [36] Digne, M.; Sautet, P.; Raybaud, P.; Euzen, P.; Toulhoat, H. *J. Catal.* **2004**, *226*, 54–68.
- [37] Castro, R. H. R.; Quach, D. V. *J. Phys. Chem. C* **2012**, *116*, 24726–24733.
- [38] Joubert, J.; Salameh, A.; Krakoviack, V.; Delbecq, F.; Sautet, P.; Copéret, C.; Basset, J. M. *J. Phys. Chem. B* **2006**, *110*, 23944–50.
- [39] Wischert, R.; Copéret, C.; Delbecq, F.; Sautet, P. *Angew. Chemie Int. Ed.* **2011**, *50*, 3202–3205.
- [40] Larmier, K.; Chizallet, C.; Cadran, N.; Maury, S.; Abboud, J.; Lamic-Humblot, A.-F.; Marceau, E.; Lauron-Pernot, H. *ACS Catal.* **2015**, *5*, 4423–4437.

BIBLIOGRAPHY

- [41] Larmier, K.; Nicolle, A.; Chizallet, C.; Cadran, N.; Maury, S.; Lamic-Humblot, A.-F.; Marceau, E.; Lauron-Pernot, H. *ACS Catal.* **2016**, *6*, 1905–1920.

Chapter 7

Structuration of water at the γ -Al₂O₃ (110) interface: an *Ab Initio* Molecular Dynamics perspective

Introduction

Because of the propensity of water to adsorb on a vast variety of surfaces (metals, oxides, minerals, ...), interfaces involving liquid water and a solid are ubiquitous. In fluid physics, tribology, geochemistry, electrochemistry, corrosion, chromatography, heterogeneous catalysis, *etc.* interfaces indeed play a very central and key role since they are, by definition, the regions between two phases where different physics or chemistry happens, compared to bulk materials. Beyond extremely idealized simple 2D borders between two phases, they rather consist in 3D regions the thickness of which depends on both the chemical nature of the two phases in contact and also the characteristic length of the phenomena of interest (from about 1 Å for an adsorbate bound chemically to the solid surface to a couple of nanometers for electric double layers). Such an equivocal definition of a system that is ambivalent by nature makes the experimental characterization of liquid water / solid interfaces challenging. Moreover, interfaces constitute a rather small region of an entire system to probe.

Referencing all the experimental techniques available is far beyond the scope of the

present work, and Zaera has recently provided an important review on the subject.¹ Among numerous spectroscopic methods, vibrational spectroscopies (Second Harmonic Generation, Vibrational Sum Frequency Generation, Polarization Modulation Infra-Red Reflection Absorption Spectroscopy, Attenuated Total Internal Reflection Infra-Red) have been developed to probe the structure of water (possible dissociation, hydrogen bonds network, pH effects ...) and adsorbates on various surfaces.²⁻⁸ X-Ray absorption spectroscopies have also been able to follow the evolution of both the solid and the liquid phases under given experimental conditions.⁹ The recent development of surface sensitive NMR techniques using radical molecular probes in frozen solvents has opened the opportunity to obtain completely resolved experimental structures at the interfaces.^{10,11}

Along with the development of interface sensitive experimental methods, molecular dynamics simulations have been of great support over the last decades to get a molecular level understanding of the liquid water / solid interfaces. Classical molecular dynamics (MD) has been applied to many systems involving metal surfaces,¹²⁻²³ oxides²⁴⁻⁴⁵ and minerals.⁴⁶⁻⁵⁴ Although classical MD is able to picture many important characteristics of liquids at interfaces (*e.g.* diffusivity and viscosity,^{37,47} zeta potential,³⁶ ...), it relies on the parametrization of force fields, mostly unreactive and not optimized for interfacial systems. To go beyond those limitations, *ab initio* molecular dynamics (AIMD) can be performed. Because of their computational cost, only a few systems involving a liquid water/metal interface have been reported.⁵⁵⁻⁶⁰ However they have shed light on the reactivity of water molecules under aqueous conditions on different metals (Ru, Pd, Pt)⁶⁰ and revealed the role of the interface in the solvation of adsorbed species under electrochemical conditions.⁵⁹

Albeit computationally less expensive, the study of liquid water/oxides interfaces happens to be also very challenging. The protonation level, the surface density of hydroxyl groups (silanol, aluminol, ...) and their local geometries, the possible ion migrations upon surface hydration, etc. indeed make the actual chemical nature of the oxide surface difficult to describe at the atomic level and is, moreover, highly dependent on the experimental conditions. However *ab initio* simulations are particularly well suited to account for weakly activated processes (like the Grotthuss mechanism) and describe the dynamical chemistry of such systems. *Ab initio* simulations have for example been reported in the literature to describe allotropes of SiO₂. They have in particular evidenced the structuration of water in contact with the solid and linked it to

vibrational spectroscopic signatures.^{61–63} The role of electrolytes on the electric double layer at the water/quartz has also been reported.⁶⁴ Finally, rare events simulations at the DFT level have been able to determine the pKa of different silanol groups in this interfacial medium.^{61,63,65} Such studies are also available for other oxides like TiO₂^{66–68} and minerals^{69–75} proposing, in particular, the modeling of solid precipitation.⁷⁴ Among this large literature on AIMD simulation for liquid water/solid interfaces, alumina has also received considerable attention because of its broad technological significance (α -Al₂O₃ in material science, γ -Al₂O₃ in heterogeneous catalysis). Hass *et al.*^{76,77} have in particular showed the chemical flexibility of the (0001) surface of α -Al₂O₃ arising from a slightly activated Grutthuss mechanism and a reorganization of the Al-O that involves the oxygen atoms of both the liquid and solid phases. More recently efforts have been made to describe the influence of α -Al₂O₃ on the structuration of the whole interface of water as well as the spectroscopic (infra-red) signatures of the surface aluminol in aqueous media.⁷⁸ This stands in line with other studied on aluminum oxides.^{61?}

Within the diversity of complex oxides and interfaces, the evolution of the understanding of γ -Al₂O₃ surface structure has probably been among the most illustrious over the last decades.⁷⁹ Gaining from the concurrent advances in spectroscopy (Infra-Red, Nuclear Magnetic Resonance, X-Ray spectroscopies) and computer simulations, the model has always been enhanced over the years. Krokidis *et al.*⁸⁰ first proposed a model of bulk γ -Al₂O₃. Shortly after, a model of the surface of one of the most popular support in heterogeneous catalysis was proposed and then refined over the years, carefully trying to model properly the level of hydroxylation of the surface (as a function of the pretreatment temperature) and the possible reconstruction of the surface.^{81?–86} This solid/gas interface model has successfully been used in collaboration with experiments to understand alcohol dehydration,^{87–89} metallic particle deposition,^{90–94} polyols adsorption,^{95,96} support effects on metal-catalyzed reactions,⁹⁷ *etc.* Recently, γ -Al₂O₃ has been experimentally shown to be usable as a support under hydrothermal conditions for biomass conversion, in spite of its expected total hydration to (oxo)hydroxides.^{96,98,99} It appears that organics intervene at the interface to stabilize the surface of γ -Al₂O₃. Here we propose an *Ab Initio* Molecular Dynamics study on the structuration of water and the modification of its dynamics at the interface with the predominant and hydrophilic (110) surface of γ -Al₂O₃. An analysis of the vibrational signature of the aluminols and chemisorbed water molecules is also proposed to computationally characterize the inter-

face. This study aims at establishing a starting point for the investigation of surface reactivity and decomposition under hydrothermal conditions.

Computational Details

To model the dynamical properties of the γ -Al₂O₃/H₂O(ℓ) interface we performed periodic *ab initio* molecular dynamics (AIMD) simulations within the framework of Density Functional Theory (DFT), using the system represented in Figure 7.1 and further detailed in this section.

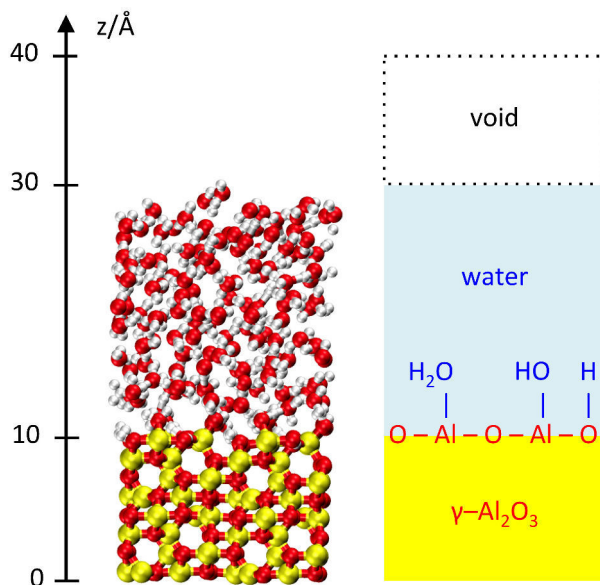


Figure 7.1: Snapshot of the simulation of the H₂O(ℓ)/ γ -Al₂O₃ (110) interface. Pink balls are aluminum atoms, white ones are hydrogens and red ones are oxygens.

The crystal structure of γ -Al₂O₃ used in the present study was reoptimized at the PBE-D3 level from the work of Krokidis *et al.*⁸⁰ (the cell parameters that we obtained are $a=7.83$ Å, $b=7.87$ Å, $c=8.02$ Å, $\alpha = \gamma = 90.00^\circ$ and $\beta = 90.59^\circ$, in close agreement with that of Krokidis *et al.*⁸⁰). We only considered the (110) surface of γ -Al₂O₃ as described by Digne *et al.*^{81,83?} and took into account the Al reconstruction evidenced by Wischert *et al.*^{85,86} upon surface hydration. From the most hydrated surface of the latter work, two extra molecules of water were added (see the two dark blue water molecules in Figure 7.2) on the remaining free Lewis acid sites in order to reach the previously reported[?] optimal water coverage under vacuum conditions. The size of the slab was doubled in

the two directions parallel to the surface to generate a bigger simulation box. A water film of 145 molecules was finally added on the surface (TIP3P box) ending up with a Al₁₂₈O₁₉₂(H₂O)₁₆₅ system with 145 free water molecules and 20 – partially dissociated – chemisorbed water molecules (see the snapshot in Figure 7.1).

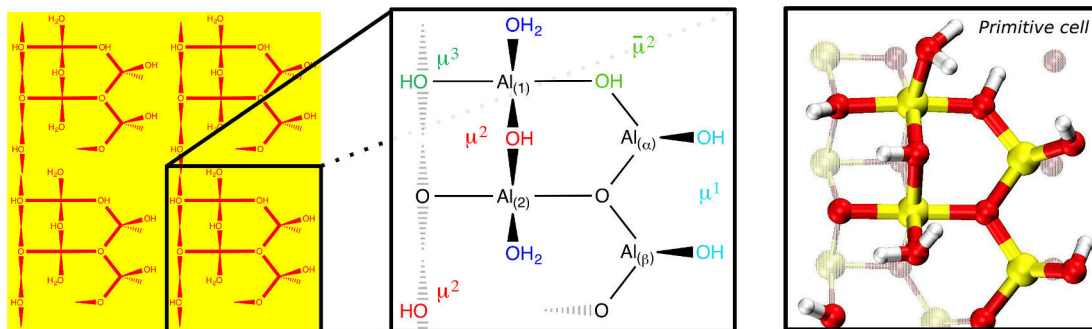


Figure 7.2: Skeletal representation of the γ -Al₂O₃ (110) primitive surface model used in this work. The unit cell consists of four of those. Aluminum atoms are not represented for simplicity but are found at each intersect between at least two bonds.

The core electrons were treated using the Goedecker-Teter-Hütter (GTH) pseudo-potentials (with 3 explicit electrons for Al)^{100–102} and the valence electrons were treated using the Gaussian¹⁰³ and Plane Waves (GPW) combined approach¹⁰⁴ as implemented in CP2K/Quickstep.^{105,106} The atomic wavefunctions were expanded on a double- ζ DZVP basis set and the auxiliary plane wave basis set for the electron density was truncated at a cutoff of 400 Ry. The electronic interactions were described using the Perdew-Burke-Ernzerhof (PBE)¹⁰⁷ exchange and correlation functional with a Grimme D3 correction¹⁰⁸ to account for dispersion. Justified by the size of the simulation box, the evaluation of energy was performed at the Γ -point, using the orbital transformation scheme,¹⁰⁹ with a strict criterion on the self-consistent field (SCF) algorithm of $5 \cdot 10^{-6}$ Ha. The always stable predictor corrector of order 3 was used as an extrapolation strategy for the wavefunction during MD.¹¹⁰ The nuclei were treated within the Born Oppenheimer approximation with a time step of 0.5 fs keeping the down most 160 atoms of the slab fixed at their bulk position. Using the Canonical Sampling through Velocity Rescaling (CSVR) thermostat¹¹¹ with a time constant of 100 fs, the temperature was fixed at 330 K. Using these parameters, the total energy drift was less than $3 \cdot 10^{-9}$ Ha/ps per atom over the whole simulation.

The simulation was equilibrated for 35 ps and most part of the results presented here

are based on the further 27.5 ps of simulation. Another further 11.5 ps simulation was performed printing the Wannier centers every fifth step (*ie* 2.5 fs) in order to calculate electrostatic dipole-based properties (dipole moments orientation, infrared spectrum). The generation of molecular dipole moments was partly performed using the molecular dynamics analyzer Travis.¹¹²

Results and Discussion

Concentration profiles and definition of structurally different layers

From the simulations, we extracted the concentration profiles (see Figure 7.3) of both water oxygens and water hydrogens - referred to as $[O]_{(z)}$ and $[H]_{(z)}$ respectively - as well as the $[O]:[H]$ ratio to characterize stoichiometry as a function of the height (the zero corresponds to the bottom of the solid slab *ie.* the first 10 Å are occupied by the solid). The oxygen concentration profile shows a very narrow peak at 11.3 Å. Integrating for 20 oxygens, it indeed corresponds to the 20 initial chemisorbed water molecules that remain on the surface during the whole simulation (with no exchange observed). The second peak at 13.3 Å also roughly integrates for 20 oxygens, and hence as many water molecules, but is much broader. This denotes the presence of a layer of water molecules that is more mobile than the first layer, but is still localized close to the surface. This second layer of water molecules will be referred to as the physisorbed layer. After these two peaks, the concentration of water oxygens shows only subtle fluctuations around the water bulk value of about 0.033 \AA^{-3} (corresponding to a mass density of $1 \text{ cm}^3/\text{g}$ as expected). Although the peaks in the hydrogen concentration profile overlap, the aforementioned strong structuration of water between 10 and 14 Å revealed by the analysis of the oxygen concentration profile is confirmed but seems to be marked even beyond 14 Å. The local stoichiometry of water is indeed strongly impacted and converges to $\frac{1}{2}$ only above 20 Å. To have a better characterization of water stoichiometry, one can consider that it is composed of two *fragments* namely O and H \cdots H in order to refer to stoichiometry as a 1:1 ratio. Similarly to diastereoisomeric or enantiomeric excesses defined in organic chemistry, one can now define a atomic excess *ae* that gives the relative deviation to stoichiometry locally:

$$ae(z) = \frac{[O]_{(z)} - [H \cdots H]_{(z)}}{[O]_{(z)} + [H \cdots H]_{(z)}} \quad (7.1)$$

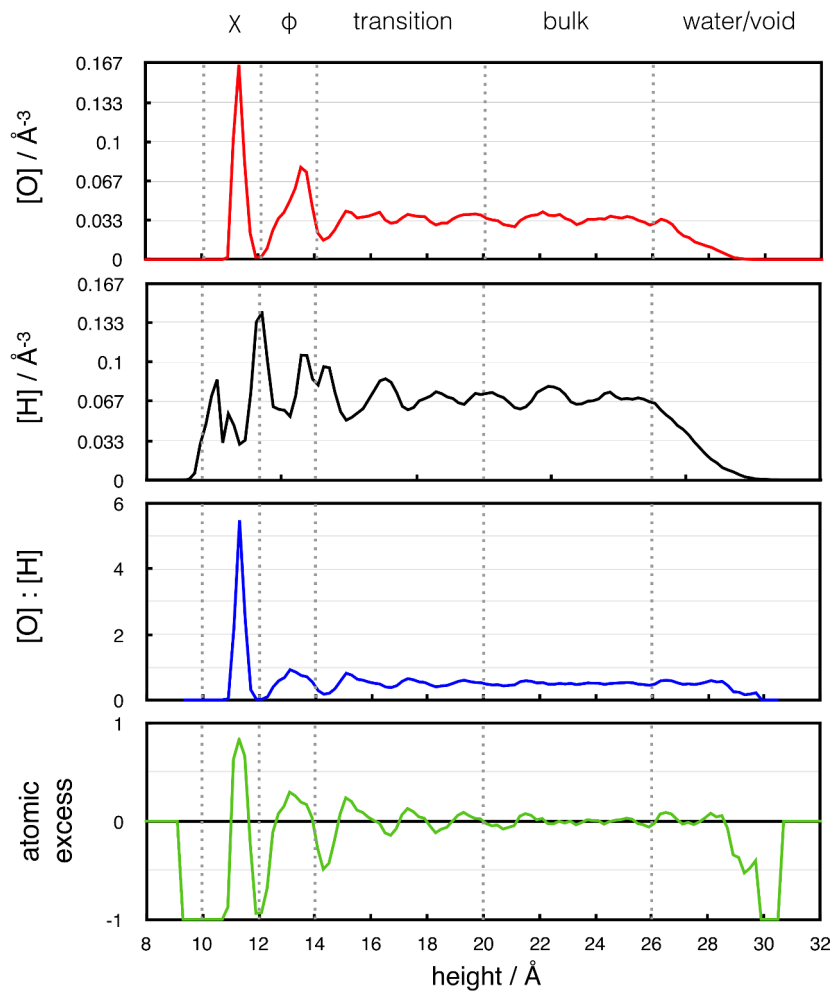


Figure 7.3: Concentration based characteristics of water as a function of height (the scale starts from the bottom of the alumina slab).

$$ae(z) = \frac{[O]_{(z)} - \frac{1}{2}[H]_{(z)}}{[O]_{(z)} + \frac{1}{2}[H]_{(z)}} \quad (7.2)$$

$$ae(z) = \frac{2[O]_{(z)} - [H]_{(z)}}{2[O]_{(z)} + [H]_{(z)}} \quad (7.3)$$

In particular, a positive ae shows an excess of oxygen whereas a negative ae indicates an excess of hydrogen. Unlike the simple $[O]:[H]$ ratio that treats depletion and accumulation regions unequally ($[0 : \frac{1}{2}[$ and $]\frac{1}{2} : +\infty[$ respectively), ae enables an easier identification of these regions and their characteristics. Using ae indeed confirms that water is still very structured between 10 and 20 Å with well defined regions with oxygen accumulation and hydrogen depletion on the one hand and oxygen depletion and hydrogen accumulation on the other hand. Between 20 and 28 Å, the atomic excess ae is almost uniformly zero (like bulk water structure) but drops after 28 Å suggesting a hydrogen accumulation. Very close to the void interface, water molecules appear to be oriented with upward protons. Considering again oxygen and hydrogen concentration profiles, the influence of void on the water film already started at about 25 Å. Finally, we end up with four distinct layers: the chemisorbed layer between 10 and 12 Å, the physisorbed layer between 12 and 14 Å, the transition layer (or over-structured bulk water) between 14 and 20 Å, the layer consisting of bulk water between 20 and 25 Å and the void/water interface between 25 and about 30 Å. Interestingly enough, the stoichiometry of water is well defined in this layer before the Gibbs dividing surface at 27.3 Å and shows an accumulation of protons above it.

Molecular self-diffusion of water

Within each layer, we can now evaluate the impact of the structuration on the mobility of water. To this end, we determined the average mean square displacements (MSD) of all the water molecules as a function of time. Assigning to each molecule the layer in which it initially was, we have obtained the MSD given in Figure 7.4. Using Einstein relationship given in Equation 7.4, one can determine the self diffusivity of water molecules in each layer. The results are given in Table 7.1.

$$D = \lim_{\tau \rightarrow +\infty} \frac{\text{MSD}(\tau)}{6\tau} \quad (7.4)$$

From our simulations at 330 K we can estimate the self-diffusivity of water in the bulk

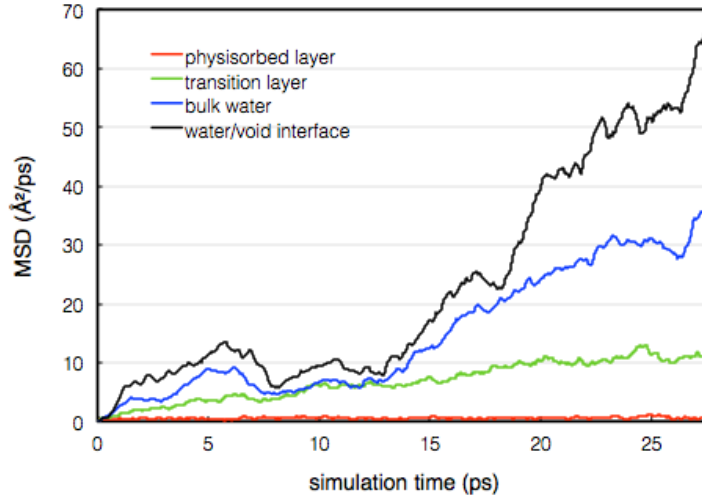


Figure 7.4: Mean square displacements (MSD) of the oxygen of the water molecules that initially were in the layers defined above. MSDs are normalized for the number of water molecules.

layer at $2 \cdot 10^{-1} \text{ \AA}^2/\text{ps}$. This is about 50% lower than expected experimentally (see Table 7.1).¹¹³ This is expected considering the tendency of DFT to over-bind water. In spite of that, we still obtain a good order of magnitude that actually corresponds to liquid water at 273 K. Beyond the absolute determination of diffusivities, our simulation shows that water diffusivity drastically drops at the contact with γ -Al₂O₃ to reach $5 \cdot 10^{-3} \text{ \AA}^2/\text{ps}$ in the physisorbed layer – namely two orders of magnitude less than in bulk water. The ordering of water at the interface therefore happens to have a strong influence on the dynamics of the water molecules. Conversely, the diffusivity of water increases at the interfaces with void : this can be attributed to the decrease of the density of the liquid (see Figure 7.3) in this layer.

Dipole orientation distribution

Besides the translational mobility of the water molecules in each layer, the structuration of water can be characterized using the distribution of their dipole orientation. Using the orientation angle θ defined in Figure 7.5, we have determined the distribution of angles in each layer and compared to the uniform distribution $\frac{1}{2} \sin \theta$. The latter corresponds to the probability of find a point on a sphere with azimuthal angles between θ and $\theta + d\theta$ and is therefore characteristic for a statistically well mixed system.

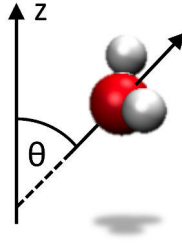


Figure 7.5: Definition of the dipole orientation angle θ . The z -axis is the normal to the γ -Al₂O₃ surface.

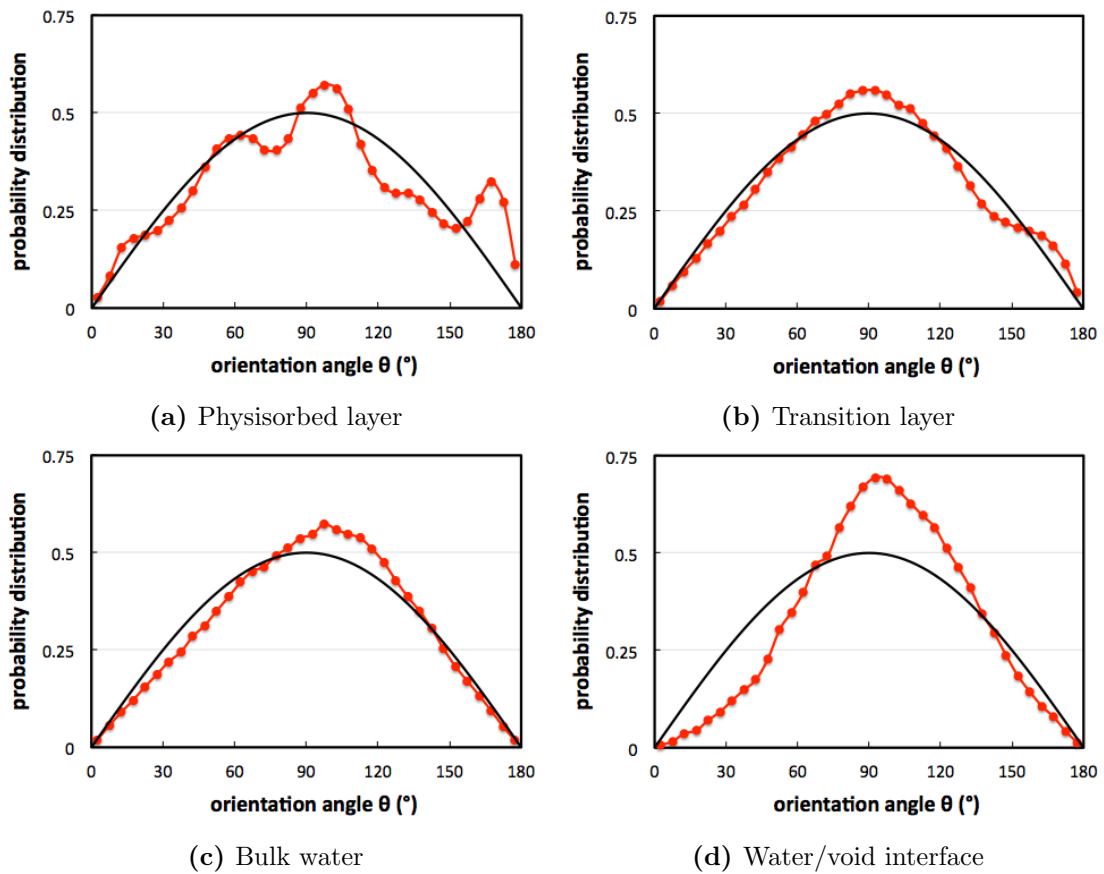


Figure 7.6: Dipole orientation distributions in (a) the physisorbed layer, (b) the transition layer, (c) bulk water, and (d) the interface with void. The black plain curve is the uniform distribution $\frac{1}{2} \sin \theta$ and the red dotted curves are the distributions obtained from the simulation.

layer	D ($\text{\AA}^2/\text{ps}$)
physisorbed layer	$5 \cdot 10^{-3}$
transition layer	$8 \cdot 10^{-2}$
bulk	$2 \cdot 10^{-1}$
tail	$3 \cdot 10^{-1}$
exp. at 273 K	$2.023 \cdot 10^{-1}$
exp. at 330 K	$4.497 \cdot 10^{-1}$

Table 7.1: Self-diffusivity of water in the different layers. For comparison, experimental data¹¹³ are reported.

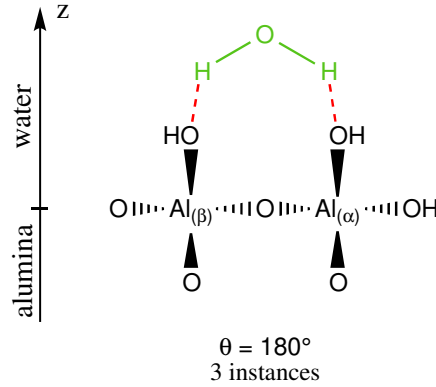


Figure 7.7: Favored orientation of water at the interface with γ -Al₂O₃.

As shown in Figures 7.6b and 7.6c, the distributions in both the transition and bulk layers is very close to be uniform. The small deviation might arise from the limited simulation time and the 2D periodicity of the water film. More interestingly, the water/void interface shows bigger deviations. The small angle orientations ($< 70^\circ$) are depopulated for the benefit of medium angle orientations ($70^\circ < \theta < 140^\circ$). Above 140° the distribution becomes more uniform. More strikingly, the orientation distribution in the physisorbed layer is not only deformed but also shows a substructure that is characteristic for frozen orientations. Their exact nature remains to be determined. However, the simulation indeed shows a couple of structures (see Figure 7.7), the orientation of which only slightly changes over the whole run.

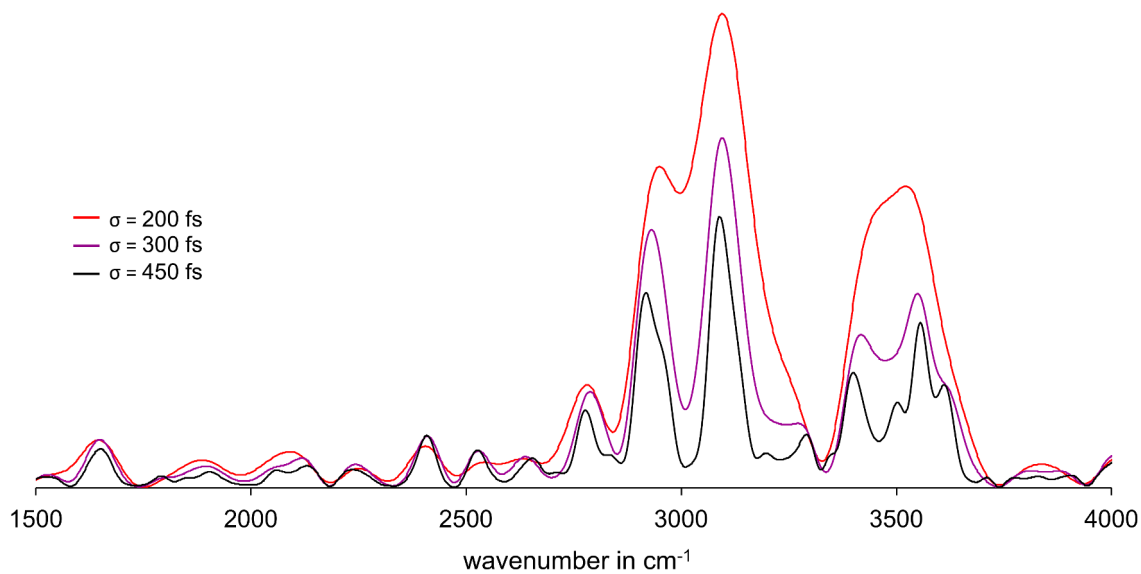


Figure 7.8: Infrared spectrum in the 1500-4500 cm^{-1} region. σ is the standard deviation of the convoluting gaussian used to get rid of the noise.

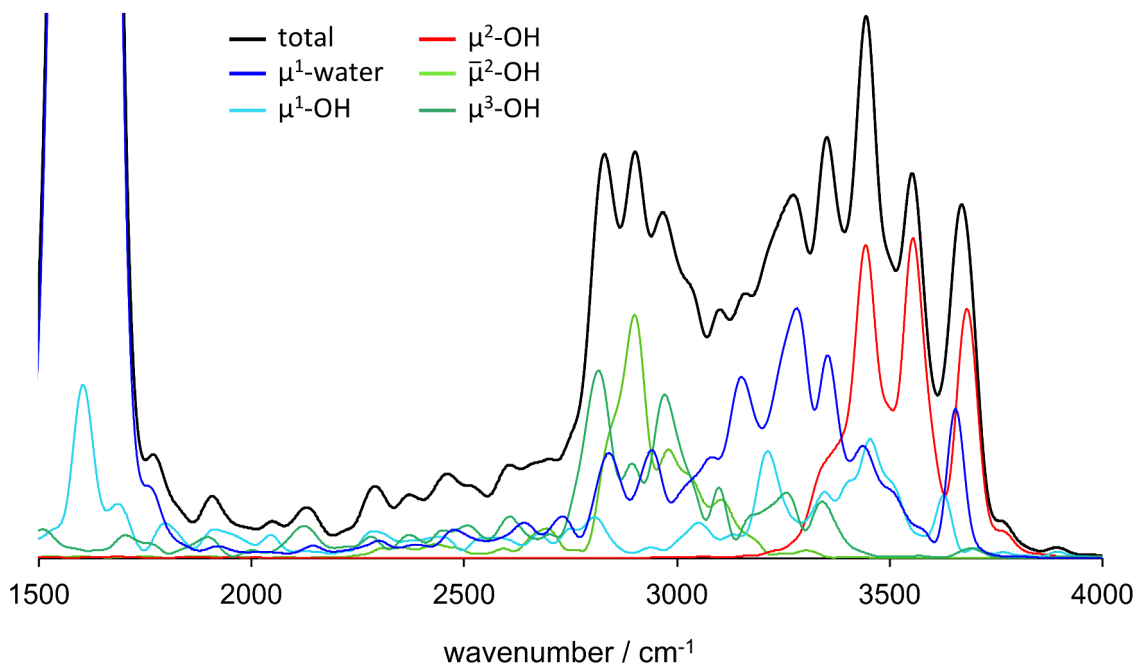


Figure 7.9: Decomposition of the Vibrational Density of States (VDOS) on the internal coordinates of OH groups on γ -Al₂O₃ (110) surface.

Infrared spectroscopy of the chemisorbed water molecules

With the Wannier centres printed as a function of time, we can also compute the auto-correlation function $\langle \dot{M}(t)\dot{M}(0) \rangle$ of the time derivative of the dipole moment $\dot{M}(t)$, the Fourier Transform of which gives the infra-red spectrum $I(\omega)$.¹¹⁴ To get rid of the noise, the signal can be convoluted with a gaussian $g(t)$ with a standard deviation σ (see Equation 7.5).

$$I(\omega) \propto \int e^{i\omega t} \langle \dot{M}(t)\dot{M}(0) \rangle g(t) dt \quad (7.5)$$

Only considering the slab and the chemisorbed water molecules (part of them being dissociated) we have obtained the spectrum given in Figure 7.8. It clearly shows two bands in the OH stretching region: one around 3500 cm⁻¹ and another one the maximum of which peaks at about 3200 cm⁻¹. A similar behavior has already been reported in the literature for many other interfaces with water including CaF₂ and α -Al₂O₃. The higher energy band is usually referred to as the *liquid-like* band in opposition to the *ice-like* band at lower energies. Beyond simple analogies with ice and liquid water infrared spectra, these two bands are indeed indicative of the environment of the OH groups. The denser, more ordered hydrogen bond network in ice is indeed responsible for the red-shift of the OH stretching. To assign these bands to characteristic groups on the γ -Al₂O₃ surface (see Figure 7.2 for a graphical definition), we have projected the total Vibrational Density of States on the mass-weighted internal coordinates of the surface OH groups, , as represented in Figure 7.9. It appears that the stretching mode of the $\bar{\mu}^2$ and μ^3 mainly vibrate around 2900 cm⁻¹ (light and dark green in Figures 7.9 and 7.2). They must therefore be involved in strong hydrogen bonds that weaken the aluminol OH bond. The μ^1 water molecules (dark blue in Figures 7.9 and 7.2) and hydroxy (hell blue in Figures 7.9 and 7.2) mainly contribute between 3250 and 3450 cm⁻¹. Strikingly, the μ^2 OH (red in Figures 7.9 and 7.2) vibrations really stand out from the mass : they contribute the most to the *liquid-like* band above 3400 cm⁻¹. They must be involved in weak hydrogen bonds.

Conclusion

In order to get insights on the interface between γ -Al₂O₃ and liquid water, we have performed AIMD simulations focusing on the preponderant (110) surface. Using the newly introduced *atomic excess* descriptor, we have showed that γ -Al₂O₃ has a strong influence

on water over about 10 Å. Within this interface, the translational and rotational mobilities of water is highly impacted, in particular in the chemisorbed and physisorbed layers. This seems to arise from a strong interaction between physisorbed and chemisorbed water molecules and has been further evidenced simulating the infra-red spectrum in the OH stretching region. It appears however that this strong interaction favors some aluminols over others. This has to be further investigated studying, for example, the hydrogen bond network (donor and acceptor) between the chemisorbed and physisorbed layers.

Bibliography

- [1] Zaera, F. *Chem. Rev.* **2012**, *112*, 2920–2986.
- [2] McGuire, J. A.; Shen, Y. R. *Science (80-.)*. **2006**, *313*, 1945–1948.
- [3] Shen, Y. R.; Ostroverkhov, V. *Chem. Rev.* **2006**, *106*, 1140–1154.
- [4] Zhang, L.; Tian, C.; Waychunas, G. A.; Shen, Y. R. *J. Am. Chem. Soc.* **2008**, *130*, 7686–7694.
- [5] Fitts, J. P.; Machesky, M. L.; Wesolowski, D. J.; Shang, X.; Kubicki, J. D.; Flynn, G. W.; Heinz, T. F.; Eienthal, K. B. *Chem. Phys. Lett.* **2005**, *411*, 399–403.
- [6] Christoforou, S. C.; Efthimiadis, E. A.; Vasalos, I. A. *Ind. Eng. Chem. Res.* **2002**, *41*, 2090–2095.
- [7] Boudesocque, S.; Dargaud, O.; Stievano, L.; Méthivier, C.; Lambert, J.-F.; Coradin, T.; Pradier, C.-M. *Surf. Interface Anal.* **2010**, *42*, 466–470.
- [8] Jena, K. C.; Hore, D. K. *Phys. Chem. Chem. Phys.* **2010**, *12*, 14383.
- [9] Lee, A. F.; Gawthrope, D. E.; Hart, N. J.; Wilson, K. *Surf. Sci.* **2004**, *548*, 200–208.
- [10] Rossini, A. J.; Zagdoun, A.; Lelli, M.; Lesage, A.; Copéret, C.; Emsley, L. *Acc. Chem. Res.* **2013**, *46*, 1942–1951.
- [11] Berruyer, P.; Lelli, M.; Conley, M. P.; Silverio, D. L.; Widdifield, C. M.; Siddiqi, G.; Gajan, D.; Lesage, A.; Copéret, C.; Emsley, L. *J. Am. Chem. Soc.* **2017**, *139*, 849–855.

-
- [12] Spohr, E.; Heinzinger, K. *Chem. Phys. Lett.* **1986**, *123*, 218–221.
- [13] Spohr, E. *Chem. Phys. Lett.* **1993**, *207*, 214–219.
- [14] Hautman, J.; Halley, J. W.; Rhee, Y.-J. *J. Chem. Phys.* **1989**, *91*, 467–472.
- [15] Raghavan, K.; Foster, K.; Motakabbir, K.; Berkowitz, M. *J. Chem. Phys.* **1991**, *94*, 2110–2117.
- [16] Xia, X.; Berkowitz, M. L. *Phys. Rev. Lett.* **1995**, *74*, 3193–3196.
- [17] Hartnig, C.; Spohr, E. *Chem. Phys.* **2005**, *319*, 185–191.
- [18] Schravendijk, P.; van der Vegt, N.; Delle Site, L.; Kremer, K. *ChemPhysChem* **2005**, *6*, 1866–1871.
- [19] Duan, S.; Xu, X.; Luo, Y.; Hermansson, K.; Tian, Z.-Q. *Phys. Chem. Chem. Phys.* **2013**, *15*, 13619.
- [20] Li, R.; Wang, L.; Yue, Q.; Li, H.; Xu, S.; Liu, J. *New J. Chem.* **2014**, *38*, 683–692.
- [21] Bodenschatz, C. J.; Sarupria, S.; Getman, R. B. *J. Phys. Chem. C* **2015**, *119*, 13642–13651.
- [22] Ramos-Alvarado, B.; Kumar, S.; Peterson, G. P. *J. Phys. Chem. Lett.* **2016**, *7*, 3497–3501.
- [23] Videla, P. E.; Ansourian, L.; Laria, D. *J. Phys. Chem. C* **2016**, *120*, 27276–27284.
- [24] Argyris, D.; Tummala, N. R.; Striolo, A.; Cole, D. R. *J. Phys. Chem. C* **2008**, *112*, 13587–13599.
- [25] Argyris, D.; Cole, D. R.; Striolo, A. *J. Phys. Chem. C* **2009**, *113*, 19591–19600.
- [26] Argyris, D.; Ho, T.; Cole, D. R.; Striolo, A. *J. Phys. Chem. C* **2011**, *115*, 2038–2046.
- [27] Butenuth, A.; Moras, G.; Schneider, J.; Koleini, M.; Köppen, S.; Meißner, R.; Wright, L. B.; Walsh, T. R.; Ciacchi, L. C. *Phys. Status Solidi B* **2012**, *249*, 292–305.

BIBLIOGRAPHY

- [28] Cole, D. J.; Payne, M. C.; Csányi, G.; Mark Spearing, S.; Colombi Ciacchi, L. *J. Chem. Phys.* **2007**, *127*, 204704.
- [29] Criscenti, L. J.; Cygan, R. T.; Kooser, A. S.; Moffat, H. K. *Chem. Mater.* **2008**, *20*, 4682–4693.
- [30] de Leeuw, N. H.; Parker, S. C. *Phys. Rev. B* **1998**, *58*, 13901–13908.
- [31] Floess, J. K.; Murad, S. *Chem. Phys. Lett.* **2011**, *516*, 216–219.
- [32] Fogarty, J. C.; Aktulga, H. M.; Grama, A. Y.; van Duin, A. C. T.; Pandit, S. A. *J. Chem. Phys.* **2010**, *132*, 174704.
- [33] Kerisit, S.; Ilton, E. S.; Parker, S. C. *J. Phys. Chem. B* **2006**, *110*, 20491–20501.
- [34] Machesky, M. L.; Predota, M.; Wesolowski, D. J.; Vlcek, L.; Cummings, P. T.; Rosenqvist, J.; Ridley, M. K.; Kubicki, J. D.; Bandura, A. V.; Kumar, N.; Sofo, J. O. *Langmuir* **2008**, *24*, 12331–12339.
- [35] Mahadevan, T. S.; Garofalini, S. H. *J. Phys. Chem. C* **2008**, *112*, 1507–1515.
- [36] Predota, M.; Machesky, M. L.; Wesolowski, D. J. *Langmuir* **2016**, *32*, 10189–10198.
- [37] Predota, M.; Cummings, P. T.; Wesolowski, D. J. *J. Phys. Chem. C* **2007**, *111*, 3071–3079.
- [38] Predota, M.; Machesky, M. L.; Wesolowski, D. J.; Cummings, P. T. *J. Phys. Chem. C* **2013**, *117*, 22852–22866.
- [39] Predota, M.; Zhang, Z.; Fenter, P.; Wesolowski, D. J.; Cummings, P. T. *J. Phys. Chem. B* **2004**, *108*, 12061–12072.
- [40] Panagiotou, G. D.; Petsi, T.; Bourikas, K.; Garoufalis, C. S.; Tsevis, A.; Spanos, N.; Kordulis, C.; Lycourghiotis, A. *Adv. Colloid Interface Sci.* **2008**, *142*, 20–42.
- [41] Rosenqvist, J.; Machesky, M. L.; Vlcek, L.; Cummings, P. T.; Wesolowski, D. J. *Langmuir* **2009**, *25*, 10852–10862.
- [42] Wang, H.-W.; DelloStritto, M. J.; Kumar, N.; Kolesnikov, A. I.; Kent, P. R. C.; Kubicki, J. D.; Wesolowski, D. J.; Sofo, J. O. *J. Phys. Chem. C* **2014**, *118*, 10805–10813.

- [43] Yue, J.; Jiang, X.; Yu, A. *Solid State Sci.* **2011**, *13*, 263–270.
- [44] Zarzycki, P.; Kerisit, S.; Rosso, K. M. *J. Phys. Chem. C* **2015**, *119*, 3111–3123.
- [45] Takae, K.; Onuki, A. *J. Phys. Chem. B* **2015**, *119*, 9377–9390.
- [46] de Leeuw, N. H.; Parker, S. C.; Catlow, C. R. A.; Price, G. D. *Phys. Chem. Miner.* **2000**, *27*, 332–341.
- [47] Leng, Y.; Cummings, P. T. *Phys. Rev. Lett.* **2005**, *94*, 026101.
- [48] Wang, J.; Kalinichev, A. G.; Kirkpatrick, R. J.; Cygan, R. T. *J. Phys. Chem. B* **2005**, *109*, 15893–15905.
- [49] Kalinichev, A. G.; Wang, J.; Kirkpatrick, R. J. *Cem. Concr. Res.* **2007**, *37*, 337–347.
- [50] Kerisit, S.; Liu, C.; Ilton, E. S. *Geochim. Cosmochim. Acta* **2008**, *72*, 1481–1497.
- [51] Rotenberg, B.; Marry, V.; Vuilleumier, R.; Malikova, N.; Simon, C.; Turq, P. *Geochim. Cosmochim. Acta* **2007**, *71*, 5089–5101.
- [52] Stack, A. G.; Raiteri, P.; Gale, J. D. *J. Am. Chem. Soc.* **2012**, *134*, 11–14.
- [53] Stack, A. G.; Borreguero, J. M.; Prisk, T. R.; Mamontov, E.; Wang, H.-W.; Vlcek, L.; Wesolowski, D. J. *Phys. Chem. Chem. Phys.* **2016**, *18*, 28819–28828.
- [54] Zhou, Q.; Zhu, R.; Parker, S. C.; Zhu, J.; He, H.; Molinari, M. *RSC Adv.* **2015**, *5*, 47022–47030.
- [55] Nadler, R.; Sanz, J. F. *J. Chem. Phys.* **2012**, *137*, 114709.
- [56] Liu, J.; Cao, X.-M.; Hu, P. *Phys. Chem. Chem. Phys.* **2014**, *16*, 4176.
- [57] Hansen, M. H.; Rossmeisl, J. *J. Phys. Chem. C* **2016**, *120*, 29135–29143.
- [58] Lin, X.; Evers, F.; Groß, A. *Beilstein J. Nanotechnol.* **2016**, *7*, 533–543.
- [59] Herron, J. A.; Morikawa, Y.; Mavrikakis, M. *Proc. Natl. Acad. Sci.* **2016**, *113*, E4937–E4945.
- [60] Bellarosa, L.; García-Muelas, R.; Revilla-López, G.; López, N. *ACS Cent. Sci.* **2016**, *2*, 109–116.

BIBLIOGRAPHY

- [61] Gaigeot, M.-P.; Sprik, M.; Sulpizi, M. *J. Phys. Condens. Matter* **2012**, *24*, 124106.
- [62] Cimas, Á.; Tielens, F.; Sulpizi, M.; Gaigeot, M.-P.; Costa, D. *J. Phys. Condens. Matter* **2014**, *26*, 244106.
- [63] Pfeiffer-Laplaud, M.; Gaigeot, M.-P.; Sulpizi, M. *J. Phys. Chem. Lett.* **2016**, *7*, 3229–3234.
- [64] Pfeiffer-Laplaud, M.; Gaigeot, M.-P. *J. Phys. Chem. C* **2016**, *120*, 14034–14047.
- [65] Pfeiffer-Laplaud, M.; Costa, D.; Tielens, F.; Gaigeot, M.-P.; Sulpizi, M. *J. Phys. Chem. C* **2015**, *119*, 27354–27362.
- [66] Machesky, M. L.; Predota, M.; Wesolowski, D. J.; Vlcek, L.; Cummings, P. T.; Rosenqvist, J.; Ridley, M. K.; Kubicki, J. D.; Bandura, A. V.; Kumar, N.; Sofo, J. O. *Langmuir* **2008**, *24*, 12331–12339.
- [67] Mattioli, G.; Filippone, F.; Caminiti, R.; Bonapasta, A. A. *J. Phys. Chem. C* **2008**, *112*, 13579–13586.
- [68] Tilocca, A.; Selloni, A. *J. Phys. Chem. C* **2012**, *116*, 9114–9121.
- [69] Khatib, R.; Backus, E. H. G.; Bonn, M.; Perez-Haro, M.-J.; Gaigeot, M.-P.; Sulpizi, M. *Sci. Rep.* **2016**, *6*, 24287.
- [70] Lee, M.-S.; Peter McGrail, B.; Rousseau, R.; Glezakou, V.-A. *Sci. Rep.* **2015**, *5*, 14857.
- [71] Liu, L.-M.; Krack, M.; Michaelides, A. *J. Chem. Phys.* **2009**, *130*, 234702.
- [72] Presti, D.; Pedone, A.; Mancini, G.; Duce, C.; Tiné, M. R.; Barone, V. *Phys. Chem. Chem. Phys.* **2016**, *18*, 2164–2174.
- [73] Holmström, E.; Spijker, P.; Foster, A. S. *Proc. R. Soc. A Math. Phys. Eng. Sci.* **2016**, *472*, 20160293.
- [74] Parvaneh, L. S.; Donadio, D.; Sulpizi, M. *J. Phys. Chem. C* **2016**, *120*, 4410–4417.
- [75] Tazi, S.; Rotenberg, B.; Salanne, M.; Sprik, M.; Sulpizi, M. *Geochim. Cosmochim. Acta* **2012**, *94*, 1–11.

- [76] Hass, K. C.; Schneider, W. F.; Curioni, A.; Andreoni, W. *Science (80-.)*. **1998**, *282*, 265–268.
- [77] Hass, K. C.; Schneider, W. F.; Curioni, A.; Andreoni, W. *J. Phys. Chem. B* **2000**, *104*, 5527–5540.
- [78] Ma, S.-Y.; Liu, L.-M.; Wang, S.-Q. *J. Phys. Chem. C* **2016**, *120*, 5398–5409.
- [79] Raybaud, P.; Chizallet, C.; Mager-Maury, C.; Digne, M.; Toulhoat, H.; Sautet, P. *J. Catal.* **2013**, *308*, 328–340.
- [80] Krokidis, X.; Raybaud, P.; Gobichon, A.-E.; Rebours, B.; Euzen, P.; Toulhoat, H. *J. Phys. Chem. B* **2001**, *105*, 5121–5130.
- [81] Digne, M.; Raybaud, P.; Sautet, P.; Guillaume, D.; Toulhoat, H. *Phys. Chem. Chem. Phys.* **2007**, *9*, 2577–2582.
- [82] Joubert, J.; Fleurat-Lessard, P.; Delbecq, F.; Sautet, P. *J. Phys. Chem. B* **2006**, *110*, 7392–7395.
- [83] Digne, M.; Raybaud, P.; Sautet, P.; Rebours, B.; Toulhoat, H. *J. Phys. Chem. B* **2006**, *110*, 20719–20720.
- [84] Joubert, J.; Salameh, A.; Krakoviack, V.; Delbecq, F.; Sautet, P.; Copéret, C.; Basset, J. M. *J. Phys. Chem. B* **2006**, *110*, 23944–50.
- [85] Wischert, R.; Copéret, C.; Delbecq, F.; Sautet, P. *Angew. Chemie Int. Ed.* **2011**, *50*, 3202–3205.
- [86] Wischert, R.; Laurent, P.; Copéret, C.; Delbecq, F.; Sautet, P. *J. Am. Chem. Soc.* **2012**, *134*, 14430–14449.
- [87] Christiansen, M. A.; Mpourmpakis, G.; Vlachos, D. G. *J. Catal.* **2015**, *323*, 121–131.
- [88] Larmier, K.; Chizallet, C.; Cadran, N.; Maury, S.; Abboud, J.; Lamic-Humblot, A.-F.; Marceau, E.; Lauron-Pernot, H. *ACS Catal.* **2015**, *5*, 4423–4437.
- [89] Larmier, K.; Nicolle, A.; Chizallet, C.; Cadran, N.; Maury, S.; Lamic-Humblot, A.-F.; Marceau, E.; Lauron-Pernot, H. *ACS Catal.* **2016**, *6*, 1905–1920.

BIBLIOGRAPHY

- [90] Wang, Y.; Su, Y.; Kang, L. *Phys. Lett. A* **2016**, *380*, 718–725.
- [91] Hu, C. H.; Chizallet, C.; Mager-Maury, C.; Corral-Valero, M.; Sautet, P.; Toulhoat, H.; Raybaud, P. *J. Catal.* **2010**, *274*, 99–110.
- [92] Mager-Maury, C.; Bonnard, G.; Chizallet, C.; Sautet, P.; Raybaud, P. *ChemCatChem* **2011**, *3*, 200–207.
- [93] Mager-Maury, C.; Chizallet, C.; Sautet, P.; Raybaud, P. *ACS Catal.* **2012**, *2*, 1346–1357.
- [94] Gorczyca, A.; Moizan, V.; Chizallet, C.; Proux, O.; Del Net, W.; Lahera, E.; Hazemann, J.-L.; Raybaud, P.; Joly, Y. *Angew. Chemie Int. Ed.* **2014**, *53*, 12426–12429.
- [95] Copeland, J. R.; Shi, X.-R.; Sholl, D. S.; Sievers, C. *Langmuir* **2013**, *29*, 581–593.
- [96] Copeland, J. R.; Santillan, I. A.; Schimming, S. M.; Ewbank, J. L.; Sievers, C. *J. Phys. Chem. C* **2013**, *117*, 21413–21425.
- [97] Silaghi, M.-C.; Comas-Vives, A.; Copéret, C. *ACS Catal.* **2016**, *6*, 4501–4505.
- [98] Ravenelle, R. M.; Copeland, J. R.; Van Pelt, A. H.; Crittenden, J. C.; Sievers, C. *Top. Catal.* **2012**, *55*, 162–174.
- [99] Jongerius, A. L.; Copeland, J. R.; Foo, G. S.; Hofmann, J. P.; Bruijninx, P. C. A.; Sievers, C.; Weckhuysen, B. M. *ACS Catal.* **2013**, *3*, 464–473.
- [100] Goedecker, S.; Teter, M.; Hutter, J. *Phys. Rev. B* **1996**, *54*, 1703–1710.
- [101] Hartwigsen, C.; Goedecker, S.; Hutter, J. *Phys. Rev. B* **1998**, *58*, 3641–3662.
- [102] Krack, M. *Theor. Chem. Acc.* **2005**, *114*, 145–152.
- [103] VandeVondele, J.; Hutter, J. *J. Chem. Phys.* **2007**, *127*, 114105.
- [104] Lippert, G.; Hutter, J.; Parrinello, M. *Mol. Phys.* **1997**, *92*, 477–487.
- [105] VandeVondele, J.; Krack, M.; Mohamed, F.; Parrinello, M.; Chassaing, T.; Hutter, J. *Comput. Phys. Commun.* **2005**, *167*, 103–128.
- [106] Hutter, J.; Iannuzzi, M.; Schiffmann, F.; VandeVondele, J. *Wiley Interdiscip. Rev. Comput. Mol. Sci.* **2014**, *4*, 15–25.

- [107] Perdew, J. P.; Burke, K.; Ernzerhof, M. *Phys. Rev. Lett.* **1996**, *77*, 3865–3868.
- [108] Grimme, S.; Antony, J.; Ehrlich, S.; Krieg, H. *J. Chem. Phys.* **2010**, *132*, 154104.
- [109] VandeVondele, J.; Hutter, J. *J. Chem. Phys.* **2003**, *118*, 4365–4369.
- [110] Kolafa, J. *J. Comput. Chem.* **2004**, *25*, 335–342.
- [111] Bussi, G.; Donadio, D.; Parrinello, M. *J. Chem. Phys.* **2007**, *126*, 014101.
- [112] Brehm, M.; Kirchner, B. *J. Chem. Inf. Model.* **2011**, *51*, 2007–2023.
- [113] Holz, M.; Heil, S. R.; Sacco, A. *Phys. Chem. Chem. Phys.* **2000**, *2*, 4740–4742.
- [114] Thomas, M.; Brehm, M.; Fligg, R.; Vöhringer, P.; Kirchner, B. *Phys. Chem. Chem. Phys.* **2013**, *15*, 6608.

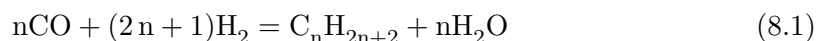
BIBLIOGRAPHY

Chapter 8

Insights from *Ab Initio* Molecular Dynamics on the Early Stage Mechanism of γ -Al₂O₃ decomposition in neutral liquid water

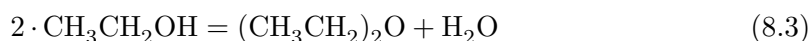
Introduction

With its physical (thermal stability, specific surface area, etc.) and its chemical (Lewis and Brønsted acidities) properties, γ -Al₂O₃ is one of the most popular oxides in heterogeneous catalysis.¹ It is a broadly used support for many processes ranging from biomass conversion to automotive and petroleum industries. One reaction of such relevance is the Fischer-Tropsch process that can be catalyzed with the Co/ γ -Al₂O₃ catalyst (see Equation 8.1).^{2,3}



Beyond a simple and innocent support, its inherent chemistry has been shown to intervene in catalytic cycles of metal catalyzed reactions. It is, for example, responsible for the trans-methylation of lignin-like aromatics in hydrodeoxygenation reactions.^{4,5} It also plays a key role in the CH₃ReO₃/ γ -Al₂O₃ catalyzed olefin metathesis⁶ and in the

Ni/ γ -Al₂O₃ catalyzed CO₂ activation⁷ with its tricoordinated aluminum atoms. Alone, it even catalyzes reactions such as alcohol dehydration and alcohol condensation (see overall reactions involving ethanol in Equations 8.2 and 8.3).^{8,9}



However it is no coincidence that γ -Al₂O₃ catalyzes dehydration reactions: it indeed has a strong affinity with H₂O.^{10,11} The molecular or dissociative adsorption of water onto γ -Al₂O₃ has been reported to have an important impact on the chemical nature of the surface in terms of OH surface density and superficial Al migrations.^{10–13} In aqueous media, this chemical degradation (also called *weathering*) can even spread to the bulk with the formation of new phases including hydroxides Al(OH)₃ (in particular bayerite, nordstrandite and gibbsite) and/or γ -AlOOH (boehmite), an oxohydroxide.^{14–17} These new phases have been shown to detrimentally make the adsorbed metallic particles sinter and completely change the physical and chemical properties of the support.¹⁵ Even if the formation of hydroxides and oxohydroxides is thermodynamically favored in presence of water,¹¹ the *weathering* of γ -Al₂O₃ is thermally activated and needs hours to weeks to proceed. This transformation is moreover highly affected by pH¹⁴ and by the adsorption of metallic particles, inorganics and organics.^{15–19}

Notwithstanding little is known about the exact mechanism of alumina hydration, even if two scenarii have been proposed in literature.^{3,14} The first one, which we refer to as *migration* mechanism, corresponds to the direct and superficial hydrolysis of the Al–O and/or Al–O–Al bonds. That would be followed by a proper migration of aluminum atoms in order to form the (oxo)hydroxide phases. The alternative mechanism, which we refer to as *dissolution/nucleation* mechanism, is thought to initiate with the partial dissolution of γ -Al₂O₃ into soluble hydroxides in water. From there, the hydroxides could nucleate on what remains of the γ -Al₂O₃ surface. This latter scenario has received strong experimental supports recently.^{17,20} Carrier *and co-workers* have indeed been able to detect the presence of soluble Al³⁺ species and follow their concentration as a function of time. Moreover they have shown that the capping of the free Al–OH groups efficiently inhibits the hydration process of γ -Al₂O₃.^{17,20} This seems to indicate that the free Al–OH groups are involved in the *dissolution/nucleation* mechanism. In

spite of this important breakthrough, the exact role of the Al–OH free groups is still to be determined to allow the rational design of hydration inhibitors and optimize the utilization of γ -Al₂O₃ as a support or a catalyst.

With the development of advanced methods for molecular dynamics simulations, the description of the dissolution and/or nucleation processes at the atomic level is now possible using computational chemistry.^{21,22} For instance metadynamics, which can describe the intrinsic fluctuations of a liquid and force a reaction to proceed along a given reaction coordinate, has been performed for such systems ranging from molecular solids (like aspirin,²³ methane,²⁴ ice,²⁵ and urea^{26,27}) and ionic solids (like barite,²⁸ calcite^{29,30}) to even more complex systems involving a metal surface, surfactants and calcium carbonates.³¹ Such studies inform on the role of the solvent, the geometry of approach of the solute and the chemistry of the interface. Here we propose a first principles study of the hydration process of γ -Al₂O₃ using metadynamics. The two scenarii are considered and the role of the Al–OH free groups is also investigated.

Computational Details

We performed *Ab Initio* Molecular Dynamics (AIMD) simulations with the same thermalized Al₁₂₈O₁₉₂(H₂O)₁₆₅ system as that described in **Chapter 7** on the γ -Al₂O₃/H₂O(ℓ) interface and built from previous first principles studies.^{12,13,32?–35} The same computational set-up was also used.

To make the system follow a given reaction coordinate and have a reaction proceed within the time of the simulation (tens of ps), we performed metadynamics simulations.^{22,36} The reaction coordinate was described with a combination of collective variables (CVs) consisting of coordination numbers (CNs). These latter count the number of first neighbors with the help of a switching function $s(r_{ij})$ between atoms i and j separated by a distance r_{ij} (see Equation 8.4).

$$\text{CN} = \sum_i \sum_j s(r_{ij}) \quad (8.4)$$

The most common form for the switching function depends on two exponents n and p and two length parameters r_0 and d_0 (see Equation 8.5), as implemented in Plumed.³⁷ Only the latter can equal zero. Along these coordinates, repulsive gaussians of width σ and height h are added every 2.5 fs (*i.e.* 5 MD step). Details on the choice of all the

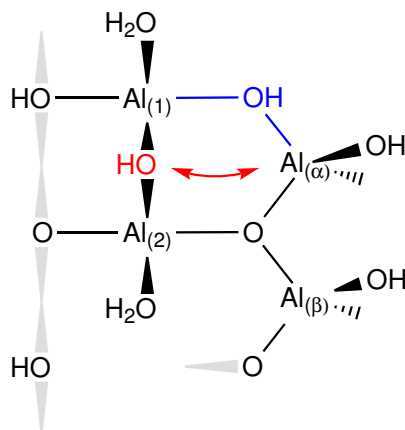


Figure 8.1: Skeletal representation of the **s5** primitive cell surface of γ -Al₂O₃ (110). The bonds in blue are associated with the two CVs of metadynamics #1, namely CN(Al₍₁₎,OH_(1 α)) and CN(Al_(α),OH_(1 α)). The red double arrow stands for CN(Al_(α),OH₍₁₂₎) used in metadynamics #2 along with CN(Al_(α),O).

parameters are given in the Results and Discussion section.

$$s(r_{ij}) = \frac{1 - \left(\frac{r_{ij} - d_0}{r_0}\right)^n}{1 - \left(\frac{r_{ij} - d_0}{r_0}\right)^p} \quad (8.5)$$

Results and Discussion

This part reports ongoing research and some aspects are still under investigation. However the simulations reported here provide a rich exploration of the system regarding to its hydration and offers perspectives for short-term enhancements of the simulations. The first part focuses on *migration* mechanisms and the second part proposes a more general approach that treats hydration regardless of any presupposed mechanism. The surface aluminum atoms are labelled as in Figure 8.1 using greek letters for tetrahedral aluminum atoms (Al_(α) and Al_(β)) and arabic numbers for octahedral aluminum atoms (Al₍₁₎ and Al₍₂₎). The hydroxy and chemisorbed water units are referred to, whenever needed, using the labels of the aluminum atoms they are bound to (for instance HO_(1 α), HO₍₁₂₎ or H₂O_(α)). When referring to coordination numbers CN(X,O), CN(X,O_{*a*}) and CN(X,O_{*w*}), O, O_{*a*} and O_{*w*} stand for the set of all oxygen atoms, the set of alumina oxygens and the set of water oxygens respectively.

Migration mechanisms

In the first metadynamics simulation, we have chosen the coordination numbers of OH_(1 α) to both the tetrahedral Al_(α) and the octahedral Al₍₁₎ (see blue bonds in Figure 8.1 and Table 8.1 for further numerical details). This allows to test the hydrolysis mechanism, through which one of bonds of the Al₍₁₎–OH_(1 α)–Al_(α) moiety is likely to get cleaved.

parameters	switching function				gaussian	
	r_0 (Å)	d_0 (Å)	n	p	h (kJ/mol)	σ
metadynamics #1						
CN(Al _(α) ,OH _(1α))	2.8	0.0	3	6	2.1	0.03
CN(Al ₍₁₎ ,OH _(1α))	2.8	0.0	3	6	2.1	0.03
metadynamics #2						
CN(Al _(α) ,OH ₍₁₂₎)	2.8	0.0	3	6	2.1	0.03
CN(Al _(α) ,O)	2.8	0.0	3	6	2.1	0.06

Table 8.1: Parameters concerning the switching function and the gaussian bias potential used for the simulation of the Al *migration* mechanism.

Starting from the basin centered around (0.8 ; 0.8) in Figure 8.2, we can notice that, with the help of the bias potential, the system gets pushed away from the initial position and visits a phase space that is almost three times as big in the CN(Al_(α),OH_(1 α)) direction as in the CN(Al₍₁₎,OH_(1 α)) direction. It seems to indicate that the tetrahedral Al_(α) atom is prompter to a modification of its coordination sphere than the octahedral Al₍₁₎. With the accumulation of gaussians, the system finally reaches a saddle-point of the free energy potential at around (0.2 ; 0.5) and flees towards the second basin centered around (0.05 ; 0.05). It means that the OH_(1 α) is neither bound to the tetrahedral Al_(α) nor the octahedral Al₍₁₎ anymore.

A careful analysis of the simulation shows that an extra water molecule (green in Figure 8.3) is actually involved in this mechanism, which appears to be a hydrolysis of the Al₍₁₎–OH_(1 α)–Al_(α) bond as shown in Figure 8.3. As the variations of the CVs suggest, the mechanism is extremely asynchronous. CN(OH_{1 α} ,Al₍₁₎) first decreases from 0.8 to 0.3 keeping CN(OH_{1 α} ,Al_(α)) constant. It is only then that CN(OH_{1 α} ,Al_(α)) decreases. As represented in Figure 8.3, the hydrolysis also involves the OH₍₁₂₎ (red in Figure 8.3) that replaces the OH_(1 α) (blue in Figure 8.3). The main issue of this simulation lies in the choice of the CV. Singling out one oxygen in particular in such a mechanism where this

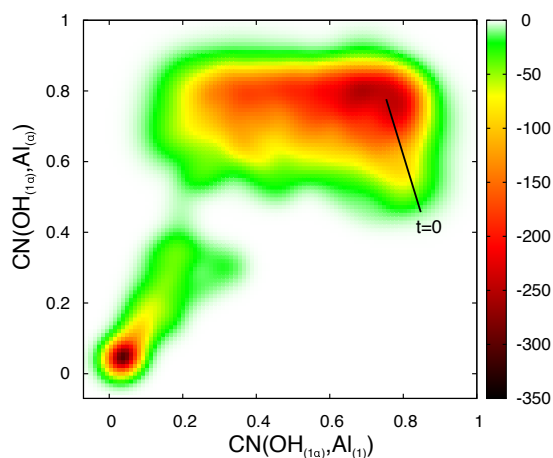


Figure 8.2: Reconstructed Free Energy profile in the dimensions of the two CVs used for metadynamics #1. The color scale is given in kJ/mol.

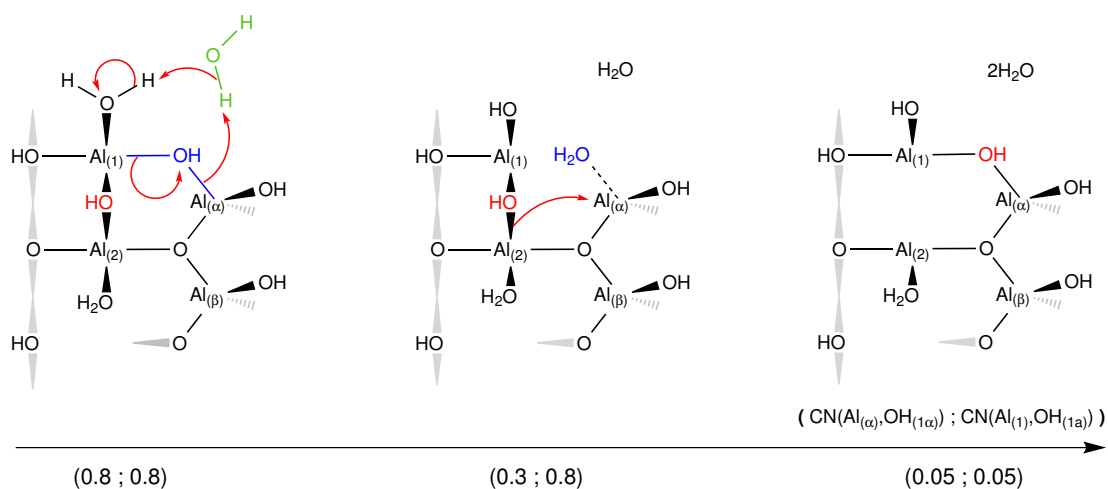


Figure 8.3: Skeletal representation of the hydrolysis of the $Al_{(1)}-OH_{(1\alpha)}-Al_{(\alpha)}$ bond along the reaction coordinate described by $CN(Al_{(\alpha)}, OH_{(1\alpha)})$ and $CN(Al_{(1)}, OH_{(1\alpha)})$. The initially bridging OH group is colored in red to facilitate its tracking along the process. The extra physisorbed water molecule involved in the proton transfer is colored in green.

very oxygen flees away in the liquid makes the entire process completely irreversible. As soon as the system is in the second basin at (0.05 ; 0.05) it indeed cannot come back and a very large number (if finite) of gaussians is added in this basin. Even if the phase space cannot be sampled properly with this simulation, it still gives an order of magnitude of the free energy barrier, which is here computed at 256 kJ/mol.

Since an extra water molecule, as well as the OH₍₁₂₎ group, have appeared to be involved in the mechanism, we have performed a second metadynamics using CN(Al_{(α),OH₍₁₂₎) and CN(Al_{(α),O) as CVs (see Table 8.1 for the choice of the parameters). However we have not been able to locate any particular products. Worse, the CN(Al_{(α),O) appears to be ill-defined since the expected coordination number of the tetrahedral Al_{(α) should equal 4 and not a value between 4.5 and 6 as suggested by the Free Energy Surface given in Figure 8.4. The main issue comes from the choice of the switching function in the definition of CN(Al_{(α),O). With the exponents $n = 3$ and $p = 6$ the switching function is too soft and counts contributions, albeit very small, for all the very numerous oxygen atoms (357 atoms). This ill-defined CV drastically slows the simulation down since a lot of time is spent adding gaussians along this direction while nothing particular happens. We therefore need a better definition of the CN.}}}}}

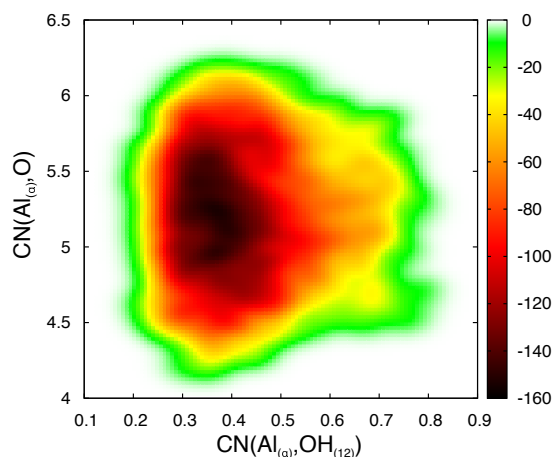


Figure 8.4: Reconstructed Free Energy profile in the dimensions of the two CVs used for metadynamics #2. The color scale is given in kJ/mol.

A more general approach to hydration

Since the coordination numbers to one particular oxygen atom does not seem to be relevant to study the hydration of alumina as metadynamics #1 has proved, we have decided to keep looking at general coordination numbers (of one particular Al to all the oxygen atoms) and optimized the parameters involved in Equation 8.5 using non-zero d_0 . We performed three different metadynamics simulations with $n = 6$, $p = 12$, $r_0 = 0.8 \text{ \AA}$, $d_0 = 1.85 \text{ \AA}$ for the definition of CNs, and $h = 5 \text{ kJ/mol}$ and $\sigma = 0.07$ for the gaussian bias potential.

In metadynamics #3 we have first examined the coordination number of each tetrahedral aluminum atom ($\text{Al}_{(\alpha)}$ and $\text{Al}_{(\beta)}$) to all the oxygen atoms of both alumina and water. The reconstructed Free Energy Surface is given in Figure 8.5. Starting from a point near (4.2 ; 4.2) as expected for two tetrahedral aluminum atoms, the system explores, over the simulation run, very well defined coordination spheres, as the square pattern that appears suggests. The most stable structures are associated with the increase of $\text{CN}(\text{Al}_{(\beta)}, \text{O})$ keeping $\text{CN}(\text{Al}_{(\alpha)}, \text{O})$ around 4. Although the new choice of the CVs seems to identify well-defined coordination spheres, we need to go further and sample the phase-space distinguishing between water oxygens O_w and alumina oxygens O_a . Only in this way can we describe properly the intrusion of water and its impact on the bonding of Al centers to alumina.

Metadynamics #4, which focuses on $\text{Al}_{(\alpha)}$, provides an example of such a CV choice. The reconstructed free energy profile as a function of $\text{CN}(\text{Al}_{(\alpha)}, \text{O}_a)$ and $\text{CN}(\text{Al}_{(\alpha)}, \text{O}_w)$ as CVs is given in Figure 8.6. Starting at (3.5 ; 1) – $\text{Al}_{(\alpha)}$ is indeed bound to three alumina oxygens and to one chemisorbed water OH group – the system seems to evolve towards the decrease of $\text{CN}(\text{Al}_{(\alpha)}, \text{O}_w)$ and the increase of $\text{CN}(\text{Al}_{(\alpha)}, \text{O}_s)$ to 6: $\text{Al}_{(\alpha)}$ rather dehydrates to dive into the bulk and acquires an octahedral coordination sphere. The hydration process is therefore unlikely to involve $\text{Al}_{(\alpha)}$, at least, directly.

Following the same strategy, we have then focused on $\text{Al}_{(\beta)}$ in metadynamics #5 using $\text{CN}(\text{Al}_{(\beta)}, \text{O}_a)$ and $\text{CN}(\text{Al}_{(\beta)}, \text{O}_w)$ as CVs. The reconstructed free energy profile and the time evolution of the CVs are given in Figures 8.7a and 8.7b, respectively. The simulation starts at a point near (3 ; 1) labeled **A**, which corresponds to the actual initial structure of $\text{Al}_{(\beta)}$ bound to the surface with 3 oxygens and with a free OH group that originates from water. As shown in Figure 8.7a, the total coordination number of $\text{Al}_{(\beta)}$ to all oxygen always remains above 4 in the phase-space sampled by metadynamics #5.

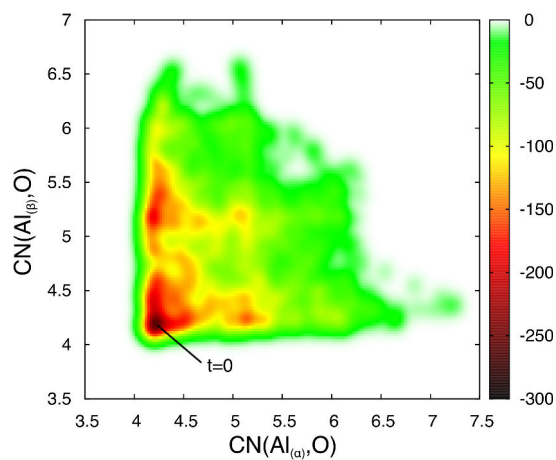


Figure 8.5: Reconstructed Free Energy profile in the dimensions of the two CVs used for metadynamics #3. The color scale is given in kJ/mol.

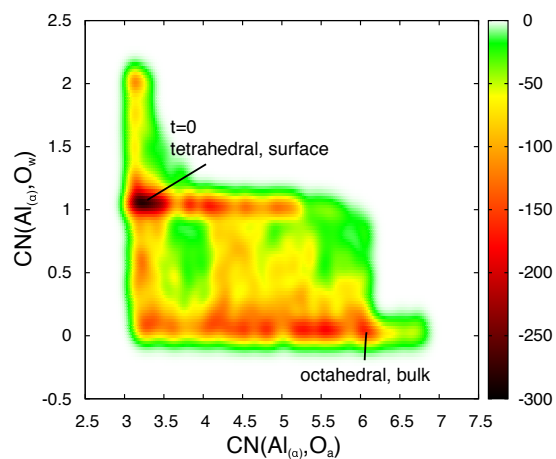


Figure 8.6: Reconstructed Free Energy profile in the dimensions of the two CVs used for metadynamics #4. The color scale is given in kJ/mol.

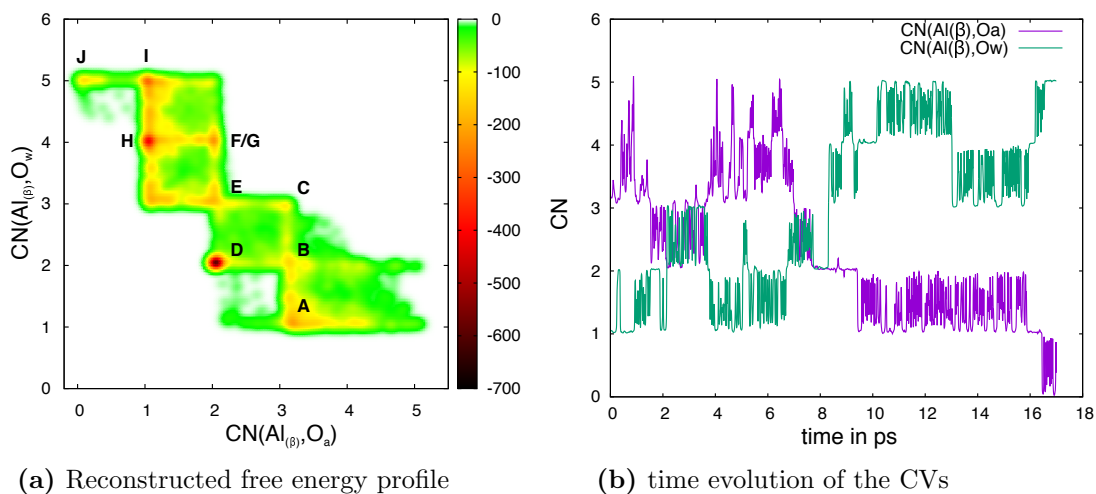


Figure 8.7: Free energy profile and time evolution of the CVs for metadynamics #5.

Even if $\text{Al}_{(\beta)}$ has tried to hook an oxygen of γ -Al₂O₃ (regions where $\text{CN}(\text{Al}_{(\beta)}, \text{O}_a) \geq 4$), it more preferably detaches from the surface (decrease of $\text{CN}(\text{Al}_{(\beta)}, \text{O}_a)$) while catching water molecules (increase of $\text{CN}(\text{Al}_{(\beta)}, \text{O}_w)$).

The corresponding mechanism is represented in Figure 8.8. Starting from state **A**, $\text{Al}_{(\beta)}$ acquires an octahedral geometry by capturing the chemisorbed water molecule at $\text{Al}_{(2)}$ (**A** → **B**) and an extra physisorbed water molecule (**B** → **C**). This is followed by a reorganization of the whole coordination sphere of $\text{Al}_{(\beta)}$ that is pushed away from the average plane of the surface and attains a tetrahedral geometry. Its coordination number to surface oxygens $\text{CN}(\text{Al}_{(\beta)}, \text{O}_a)$ diminishes from 3 to 2, yielding to state **D**. This very same strategy that involves, first a chemisorbed water molecule, second a physisorbed water molecule and third a O_a - $\text{Al}_{(\beta)}$ bond cleavage occurs for the second detachment from the surface (steps **D** → **H**). However, an extra step inserts just after the physisorbed water molecule enters the coordination sphere, namely a proton transfer (**F** → **G**). This proton transfer is important since it likely increases the nucleophilicity of the hydroxyl at $\text{Al}_{(1)}$, involved in the formation of state **I**. The last step corresponds to the cleavage of the last $\text{Al}_{(\beta)}$ - O_a bond, leaving a surface hydroxyl behind. The associated structure **J** corresponds to an Al^{3+} cation bound to chemisorbed water molecules.

From a Free Energy point of view, it appears that the formation of intermediate **E** is rather difficult. Points near (2 ; 2.5) and (2.5 ; 3) in Figure 8.7a indeed have a high free energy. However, metadynamics #5 is not converged, and such conclusions must be taken with care. Moreover, the simulation seems to show instances of *hill surfing*:

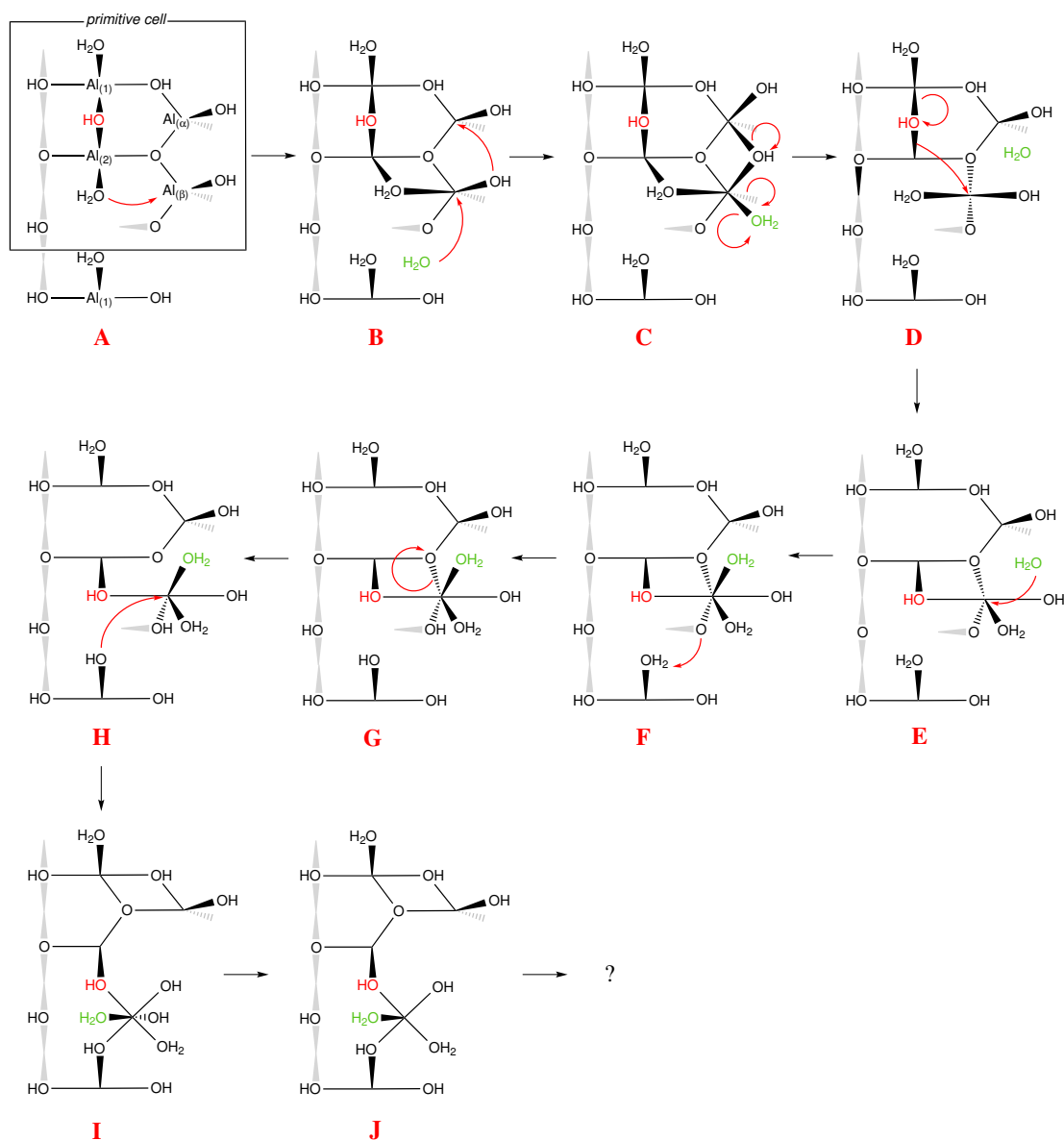


Figure 8.8: Schematic mechanism associated with metadynamics #5 using the skeletal representation for the alumina surface. For simplicity, aluminum atoms are explicitly represented only for structure A. Green H_2O does not represent any specific water molecule.

during the process of adding gaussians at a given frequency, the system does not have time to relax and gaussians start being added one upon another (see plateaus in like the one around 8 ps in Figure 8.7b, which gives the time evolution of the CV during the simulation). This creates the equivalent of locally higher temperatures and can induce a skewed sampling of the phase space and a wrong evaluation of the free energy. To solve such a problem, one can use smaller gaussians (like the ones used in metadynamics #1, the volume of which being about 10 times smaller) in order to perturb the system in a gentler manner, or go to more advanced metadynamics methods as mentioned in Part 1 of this manuscript.

Conclusion and Perspectives

In this work we have performed several metadynamics simulations to try to model the hydration mechanism of γ -Al₂O₃ on the (110) facet at the interface with liquid water.

We have tried several sets of CVs to describe the early stages of γ -Al₂O₃ decomposition in liquid water. The couple of CVs involving the coordination number of aluminum centers to water oxygen atoms on the one hand and γ -Al₂O₃ oxygen atoms on the other hand has appeared to be a good choice to describe the different structures produced upon hydration. It allows a step by step monitoring of the detachment of aluminum cations along with the gradual increase of their coordination sphere.

This study seems to point out the particular role played by the tetrahedral Al_(β) atom that holds a free OH group. This atom was already shown to migrate upon hydration by Wischert *et al.*¹³ Its mobility and reactivity towards water seem to corroborate with recent experimental studies that have showed the significance of free OH groups. To a lesser extent, chemisorbed water molecules and hydroxyl adsorbed on the octahedral Al₍₁₎ and Al₍₂₎ also happen to play a role in the process of hydration. That could explain why the adsorption of polyols on these octahedral Al₍₁₎ and Al₍₂₎ centers can inhibit the hydration process.

In spite of all these nice conclusions, it is necessary to rerun the simulations (in particular the promising metadynamics #5 and probably the similar metadynamics #4) with a less violent perturbation. Well-tempered metadynamic simulations are also considered to have well converged data and prevent from *hill surfing* issues.

Bibliography

- [1] Euzen, P.; Raybaud, P.; Krokidis, X.; Toulhoat, H.; Le Loarer, J.-L.; Jolivet, J.-P.; Froidefond, C. *Handb. Porous Solids*; 2002; Vol. 3; pp 1591–1677.
- [2] Khodakov, A. Y.; Chu, W.; Fongarland, P. *Am. Chem. Soc.* **2007**, *107*, 1692–1744.
- [3] Trueba, M.; Trasatti, S. P. *Eur. J. Inorg. Chem.* **2005**, 3393–3403.
- [4] Bui, V. N.; Laurenti, D.; Delichère, P.; Geantet, C. *Appl. Catal. B Environ.* **2011**, *101*, 246–255.
- [5] Wang, H.; Feng, M.; Yang, B. *Green Chem.* **2017**,
- [6] Valla, M.; Wischert, R.; Comas-Vives, A.; Conley, M. P.; Verel, R.; Copéret, C.; Sautet, P. *J. Am. Chem. Soc.* **2016**, *138*, 6774–6785.
- [7] Silaghi, M.-C.; Comas-Vives, A.; Copéret, C. *ACS Catal.* **2016**, *6*, 4501–4505.
- [8] Larmier, K.; Chizallet, C.; Cadran, N.; Maury, S.; Abboud, J.; Lamic-Humblot, A.-F.; Marceau, E.; Lauron-Pernot, H. *ACS Catal.* **2015**, *5*, 4423–4437.
- [9] Larmier, K.; Nicolle, A.; Chizallet, C.; Cadran, N.; Maury, S.; Lamic-Humblot, A.-F.; Marceau, E.; Lauron-Pernot, H. *ACS Catal.* **2016**, *6*, 1905–1920.
- [10] Digne, M.; Sautet, P.; Raybaud, P.; Euzen, P.; Toulhoat, H. *J. Catal.* **2002**, *211*, 1–5.
- [11] Lefevre, G.; Duc, M.; Lepeut, P.; Caplain, R.; Fédoroff, M. *Langmuir* **2002**, *18*, 7530–7537.
- [12] Wischert, R.; Copéret, C.; Delbecq, F.; Sautet, P. *Angew. Chemie Int. Ed.* **2011**, *50*, 3202–3205.
- [13] Wischert, R.; Laurent, P.; Copéret, C.; Delbecq, F.; Sautet, P. *J. Am. Chem. Soc.* **2012**, *134*, 14430–14449.
- [14] Carrier, X.; Marceau, E.; Lambert, J. F.; Che, M. *J. Colloid Interface Sci.* **2007**, *308*, 429–437.

BIBLIOGRAPHY

- [15] Ravenelle, R. M.; Copeland, J. R.; Kim, W.-G.; Crittenden, J. C.; Sievers, C. *Am. Chem. Soc. Catal.* **2011**, *1*, 552–561.
- [16] Ravenelle, R. M.; Copeland, J. R.; Van Pelt, A. H.; Crittenden, J. C.; Sievers, C. *Top. Catal.* **2012**, *55*, 162–174.
- [17] Abi Aad, J.; Courty, P.; Decottignies, D.; Michau, M.; Diehl, F.; Carrier, X.; Marceau, E. *ChemCatChem* **2017**, *9*, 2106–2117.
- [18] Ravenelle, R. M.; Diallo, F. Z.; Crittenden, J. C.; Sievers, C. *ChemCatChem* **2012**, *4*, 492–494.
- [19] Jongerius, A. L.; Copeland, J. R.; Foo, G. S.; Hofmann, J. P.; Bruijninx, P. C. A.; Sievers, C.; Weckhuysen, B. M. *ACS Catal.* **2013**, *3*, 464–473.
- [20] Abi Aad, J.; Casale, S.; Michau, M.; Courty, P.; Diehl, F.; Marceau, E.; Carrier, X. *ChemCatChem* **2017**, *9*, 2186–2194.
- [21] Angioletti-Uberti, S.; Ceriotti, M.; Lee, P. D.; Finnis, M. W. *Phys. Rev. B* **2010**, *81*, 125416.
- [22] Giberti, F.; Salvalaglio, M.; Parrinello, M. *IUCrJ* **2015**, *2*, 256–266.
- [23] Schneider, J.; Reuter, K. *J. Phys. Chem. Lett.* **2014**, *5*, 3859–3862.
- [24] Lauricella, M.; Meloni, S.; English, N. J.; Peters, B.; Ciccotti, G. *J. Phys. Chem. C* **2014**, *118*, 22847–22857.
- [25] Quigley, D.; Rodger, P. M. *J. Chem. Phys.* **2008**, *128*, 154518.
- [26] Salvalaglio, M.; Vetter, T.; Giberti, F.; Mazzotti, M.; Parrinello, M. *J. Am. Chem. Soc.* **2012**, *134*, 17221–17233.
- [27] Salvalaglio, M.; Perego, C.; Giberti, F.; Mazzotti, M.; Parrinello, M. *Proc. Natl. Acad. Sci.* **2015**, *112*, E6–E14.
- [28] Stack, A. G.; Raiteri, P.; Gale, J. D. *J. Am. Chem. Soc.* **2012**, *134*, 11–14.
- [29] Quigley, D.; Freeman, C. L.; Harding, J. H.; Rodger, P. M. *J. Chem. Phys.* **2011**, *134*.

- [30] Freeman, C. L.; Harding, J. H.; Duffy, D. M. *Langmuir* **2008**, *24*, 9607–9615.
- [31] Côté, A. S.; Darkins, R.; Duffy, D. M. *J. Phys. Chem. C* **2014**, *118*, 19188–19193.
- [32] Digne, M.; Raybaud, P.; Sautet, P.; Rebours, B.; Toulhoat, H. *J. Phys. Chem. B* **2006**, *110*, 20719–20720.
- [33] Digne, M.; Raybaud, P.; Sautet, P.; Guillaume, D.; Toulhoat, H. *Phys. Chem. Chem. Phys.* **2007**, *9*, 2577–2582.
- [34] Joubert, J.; Salameh, A.; Krakoviack, V.; Delbecq, F.; Sautet, P.; Copéret, C.; Basset, J. M. *J. Phys. Chem. B* **2006**, *110*, 23944–50.
- [35] Joubert, J.; Fleurat-Lessard, P.; Delbecq, F.; Sautet, P. *J. Phys. Chem. B* **2006**, *110*, 7392–7395.
- [36] Laio, A.; Parrinello, M. *Proc. Natl. Acad. Sci.* **2002**, *99*, 12562–12566.
- [37] Tribello, G. A.; Bonomi, M.; Branduardi, D.; Camilloni, C.; Bussi, G. *Comput. Phys. Commun.* **2014**, *185*, 604–613.

BIBLIOGRAPHY

Chapter 9

Adsorption of Ethanol and Propane-1,3-diol on γ -Al₂O₃ at the Interface with Water

Introduction

Within the context presented in the last two chapters, we have decided to examine the adsorption of alcohols on γ -Al₂O₃ at the interface with water. Alcohols, and in particular polyols, have indeed been shown to inhibit the decomposition of γ -Al₂O₃, in spite of the presence of water. Many DFT studies have reported the adsorption and reactivity of alcohols on the (100) facet.^{1,2} This surface indeed shows a good compromise between adsorption and bond activation for the heterogeneous alcohol dehydration to olefins and condensation to ethers. However its affinity to water is not comparable to that of the predominant (110) facet,[?] which is thought to be where the detrimental hydration of γ -Al₂O₃ takes place.^{3,4} Combining spectroscopy and theory, Sievers and coworkers studied in particular the adsorption of glycerol on γ -Al₂O₃,³ which was reported to have an inhibiting effect on γ -Al₂O₃ hydration.⁵ In absence of water, it adsorbs on the two octahedral Al centers of the (110) surface labelled Al₍₁₎ and Al₍₂₎ in Figure 9.1. These sites are normally occupied by two chemisorbed water molecules and one bridging OH group, each of them being involved, according to the preliminary results showed in the previous chapter, in the decomposition mechanism of γ -Al₂O₃. The replacement of these groups with an organic oxygenate therefore seems to stabilize the surface and

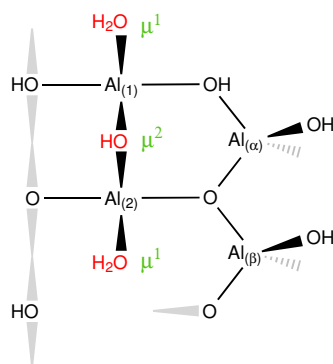


Figure 9.1: Skeletal representation of surface γ -Al₂O₃. In this work we considered the exchange of the functional groups represented in red (namely μ^1 water molecules and the bridging μ^2 hydroxyle group).

hinder the attack of water, like protecting groups in organic chemistry. However, it is not clear why the substitution of water by alcohol should induce such a stabilization since it corresponds to the change of one Al–O bond by another Al–O bond.

In order to assess the impact of alcohols adsorption on the interface and their possible inhibiting effect on γ -Al₂O₃ hydration, we have performed molecular dynamics simulations to characterize the changes induced by the adsorption of ethanol (EtOH) and 1,3-propanediol (1,3-PDO) on two different adsorption sites. Their relative stability has been partially investigated using constrained molecular dynamics.

Computational Details

Using the same computational set-up as that described in **Chapter 7** and **Chapter 8**, we performed *Ab Initio* Molecular Dynamics (AIMD) simulations on different systems. We considered EtOH and 1,3-PDO at two different adsorption sites each with molecular formula Al₁₂₈O₁₉₂(H₂O)₁₆₄[CH₃CH₂OH] and Al₁₂₈O₁₉₂(H₂O)₁₆₃[HO(CH₂)₃OH] respectively.

The different structures of the thermodynamic integration were first generated using the slow growth algorithm as implemented in CP2K, using the thermalized adsorbed structures as starting point. Selected geometries were used to perform constrained molecular dynamics (MD) simulations, using the height of the desorbing oxygen as a constraint. Each simulation had been run for 10 ps but only the last 5 ps were consid-

ered for the time average of the lagrangian multipliers.

Results and Discussion

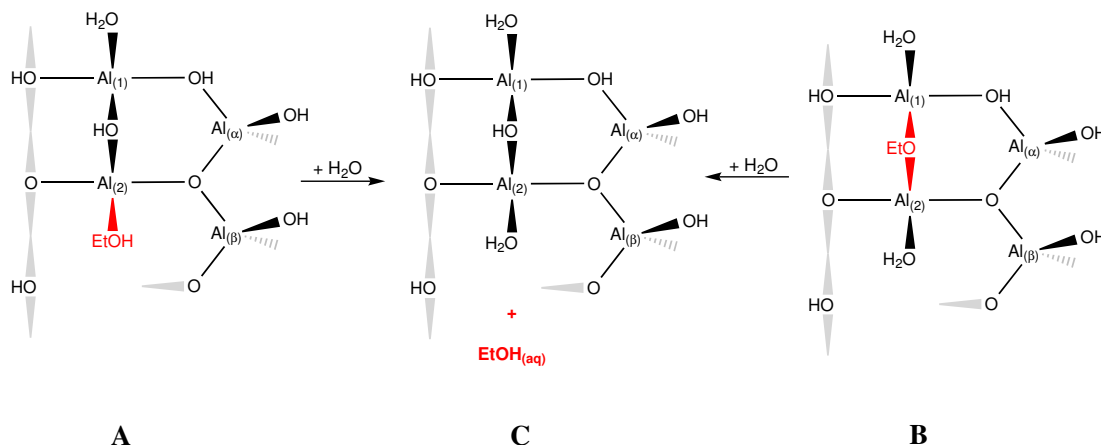


Figure 9.2: Ethanol desorption from states **A** and **B** to state **C**. This desorption process is actually an exchange of EtOH/EtO⁻ with water molecular since the simulation is performed in liquid water.

EtOH and 1,3-PDO can adsorb on different sites on γ -Al₂O₃ by replacing molecularly or dissociatively chemisorbed water molecules. In the line with the previous study reported in the literature,⁵ only the adsorption modes involving the octahedral Al₍₁₎ and Al₍₂₎ have been considered. Water molecules indeed interact the least with those sites and can therefore easily be replaced by alcohols. Three modes can be enumerated, namely μ^1 at Al₍₁₎, μ^2 between Al₍₁₎ and Al₍₂₎, and μ^1 at Al₍₂₎. Because of the strong similarities between the two μ^1 modes, we have only considered the μ^1 at Al₍₂₎ mode (state **A** in Figure 9.2) and the μ^2 between Al₍₁₎ and Al₍₂₎ mode (state **B** in Figure 9.2) for ethanol. To compare their relative stability, we simulated, performing a thermodynamic integration on the height of the coordinated oxygen atom, the whole desorption process from states **A** and **B** to state **C**, namely solvated EtOH in water separated from the fully hydrated γ -Al₂O₃. State **C** is used here as a free energy reference in order to align the obtained profiles given in Figure 9.3.

As shown in Figure 9.3, desorption from state **A** is thermodynamically easier ($\Delta_{des}F = 60$ kJ/mol) than that from state **B** ($\Delta_{des}F = 150$ kJ/mol). Moreover desorption from state **B** happens to be an activated process ($\Delta_{des}^\ddagger F = 175$ kJ/mol). This likely

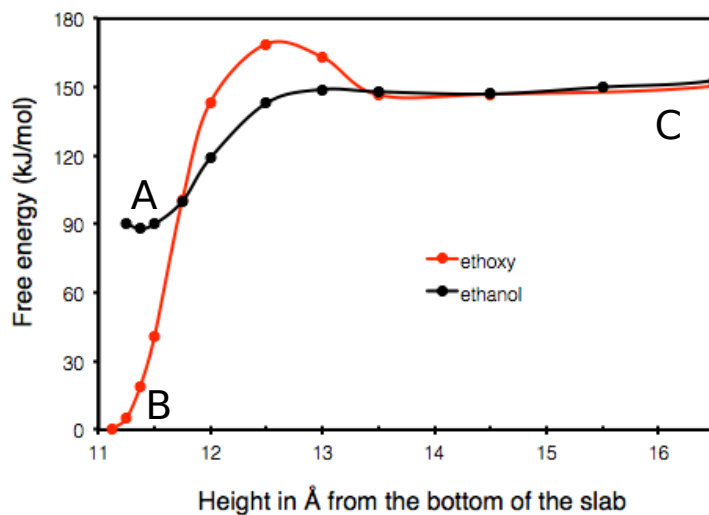


Figure 9.3: Free-energy profiles of EtOH/EtO⁻ desorption (including water exchange) associated with the states **A**, **B** and **C** as given in Figure 9.2.

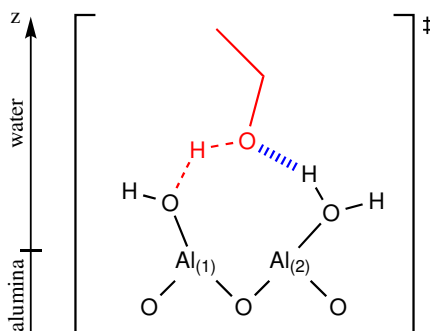


Figure 9.4: Transition state associated with the desorption of EtO⁻ from state **B** to state **C**. The proton of a neighboring chemisorbed water molecule is transferred to the ETO⁻ group, implying a displacement of the resulting hydroxyle group in a bridging position between Al₍₁₎ and Al₍₂₎.

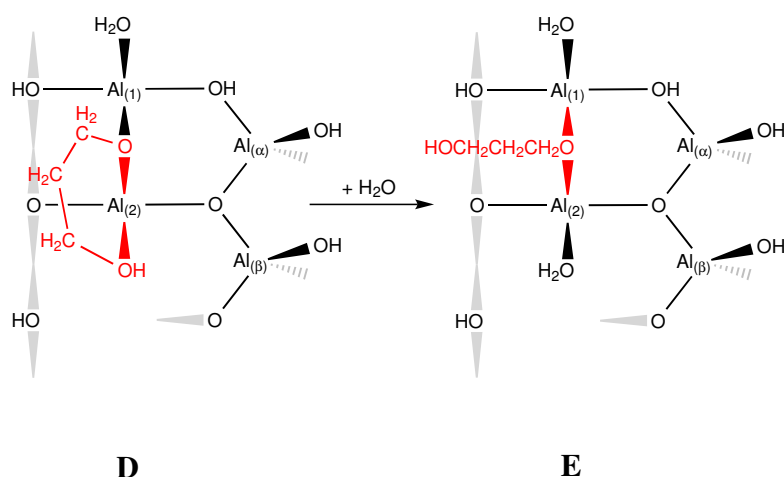


Figure 9.5: Partial desorption of bidentate 1,3-PDO on γ -Al₂O₃ (including exchange with water) from state **D** to state **E**.

results from the strong reorganization of the connectivity between atoms. Along with the cleavage of the ethoxy Al₍₁₎-O-Al₍₂₎ bonds, a vicinal chemisorbed water molecule transfers its proton to ethoxy to yield ethanol. The second chemisorbed water molecule stabilizes the transition state *via* a hydrogen bond. When ethanol goes further away from the surface, the hydroxyle group moves to the bridging position between Al₍₁₎ and Al₍₂₎. The newly formed Lewis basic site, in the course of the process, captures a water molecule from the physisorbed layer. Beyond all these mechanistic considerations bridging ethoxy (state **B**) happens to be more stable than ethanol (state **A**) on γ -Al₂O₃ with a free energy gain of 90 kJ/mol at 330 K.

Based on this result, we have then considered the adsorption of 1,3-PDO on γ -Al₂O₃. As a primary alcohol, it should indeed show a similar reactivity than EtOH. That is why we started studying 1,3-PDO at the μ^2 bridging site (state **E**) with a pending arm solvated by interfacial water. However, the second alcohol group can also chemically interact with γ -Al₂O₃ on Al₍₁₎ with an η^2 geometry (state **D**). From the results on EtOH, the latter is expected to be more stable. However, because of the possible extra energetic and entropic constraints on the η^2 geometry, we have decided to perform a second thermodynamic integration to model the transformation from state **D** to state **E**. The free energy profile is given in Figure 9.6. For comparison, the profile of ethanol desorption (**A** to **C**) is also reported. Strikingly the two profiles are overlaid from 1 to 3 Å. It indicates that the partial desorption of 1,3-PDO from states **D** to

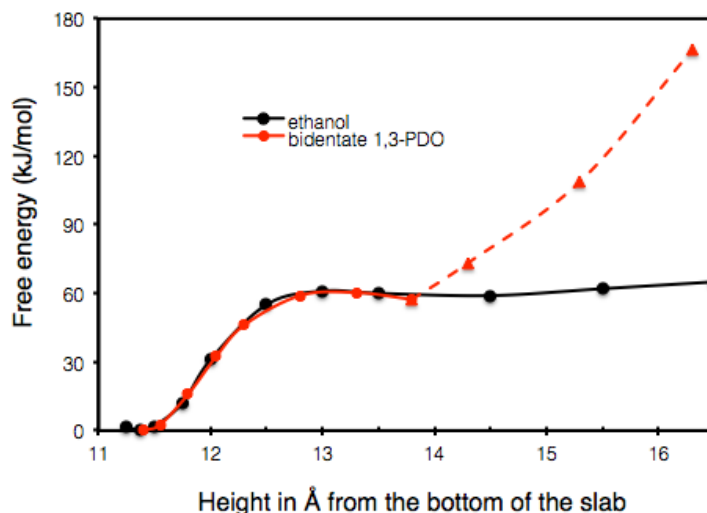


Figure 9.6: Free-energy profile of 1,3-PDO partial desorption (as described in Figure 9.5) compared to that of EtOH. The dotted line represents over-constrained points that are likely to be irrelevant.

state **E** does not show any particular extra constraint or, at least, that the energetic and entropic contributions compensate at 330 K. Above 3 Å, which roughly corresponds to the average height of the OH group determined from a standard AIMD simulation of about 10 ps on state **E**, the free energy profile takes off and deviates from that of ethanol. This likely results from a too important constraint on the height of the oxygen atom that induces an undesired deformation of the aliphatic chain. From this point, the height of the other oxygen should be used instead in order to model properly the whole desorption process, which has not been performed yet. However the simulation of ethoxy desorption (**B** to **C**) should give a rather good estimation of its free energy profile. The η^2 mode (state **D**) stands out to be more stable than the η^1 mode (state **E**) of about 60 kJ/mol. With the second detachment, the whole free energy barrier of desorption should reach roughly 235 kJ/mol (60+175 kJ/mol).

Conclusion

In the present work, we have performed several AIMD simulations to assess the relative stability of EtOH and 1,3-PDO with various adsorption modes and sites at the interface with liquid water. We have shown in particular that ethanol adsorbs dissociatively to

produce a bridging surface ethoxy between two octahedral aluminum atoms with a free energy gain of 150 kJ/mol. We have also shown that 1,3-PDO strongly interacts with the octahedral sites in an η^2 geometry and estimated the free energy barrier of desorption to about 235 kJ/mol.

Putting into perspective the results of **Chapter 2** and **Chapter 3** brings insights into the hydration mechanism of γ -Al₂O₃ on the (110) facet on the one hand and the inhibiting role of alcohols on the other hand. Upon adsorption, EtOH and 1,3-PDO indeed replace water molecules that are involved in the hydration mechanism proposed in **Chapter 2**. The only way to make hydration/decomposition possible requires the desorption of organics which is all the more difficult with the increasing number of anchoring alcohol groups. This is consistent with reported experimental data that shows an increasing protecting effect from glycerol to sorbitol (polymer) on γ -Al₂O₃.⁵

Bibliography

- [1] Larmier, K.; Chizallet, C.; Cadran, N.; Maury, S.; Abboud, J.; Lamic-Humblot, A.-F.; Marceau, E.; Lauron-Pernot, H. *ACS Catal.* **2015**, *5*, 4423–4437.
- [2] Larmier, K.; Nicolle, A.; Chizallet, C.; Cadran, N.; Maury, S.; Lamic-Humblot, A.-F.; Marceau, E.; Lauron-Pernot, H. *ACS Catal.* **2016**, *6*, 1905–1920.
- [3] Copeland, J. R.; Shi, X.-R.; Sholl, D. S.; Sievers, C. *Langmuir* **2013**, *29*, 581–593.
- [4] Abi Aad, J.; Casale, S.; Michau, M.; Courty, P.; Diehl, F.; Marceau, E.; Carrier, X. *ChemCatChem* **2017**, *9*, 2186–2194.
- [5] Ravenelle, R. M.; Copeland, J. R.; Van Pelt, A. H.; Crittenden, J. C.; Sievers, C. *Top. Catal.* **2012**, *55*, 162–174.

BIBLIOGRAPHY

Conclusion

Over the last three years, we have computationally studied the reactivity of various systems in the context of biomass conversion in heterogeneous catalysis. The complexity of their structure led us to perform a variety of different calculations and to strongly interact with experimentalists in order to improve our models and be guided in the exploration of reaction networks.

In the first part, we have considered systems involving a platinum catalyst and aromatic oxygenates (produced from the depolymerization of lignin biomass). We have shown that their adsorption can be rationalized using simple molecular descriptors. We have then scrutinized, in collaboration with surface science experimentalists, the large reaction networks of anisole and 2-phenoxyethanol deoxygenation on platinum. Our studies suggest that a minimal amount of hydrogen is needed under catalytic conditions to prevent the aromatics from their dehydrogenation and their subsequent breakdown. However hydrogen does not seem to be appropriate to deoxygenate aromatics on platinum. An extra reductant (in our case, carbonaceous species) happens to be necessary. This stands in the line with other studies that have recently reported the role of reductants in the deoxygenation reactions under both vacuum and catalytic conditions.

In the second part, we have considered the interface between water and γ -Al₂O₃. This system is particularly challenging in terms of both modeling and getting familiar with it. Its model structure is indeed very dependent on the conditions (and therefore varies importantly from one paper to another) and it has never been studied in liquid water computationally. However computational chemistry has proven to be here a promising tool to get an atomic-scale insight on the role of water in the detrimental decomposition of γ -Al₂O₃ as a support. *Ab Initio* molecular dynamics has allowed us to characterize

the interface with water. We have showed that water is strongly structured on a slice of about 10 Å thick and we have distinguished different vibrational signatures likely arising from a preferential solvation of certain aluminol groups. We have then studied the intrinsic reactivity of γ -Al₂O₃ with water and proposed a scheme for the investigation of its decomposition mechanism. The first results seem to indicate the particular role of both chemisorbed water and tetrahedral aluminum atoms. Although our results have to be refined, they could explain the very recent experimental observation published on the topic.^{1,2} We have finally considered the adsorption of alcohols on γ -Al₂O₃ and showed their strong affinity with the surface. The exact origin of the interaction is still unclear but might arise from the ability of surface water to better solvate organics than bulk water.

Beyond these scientific results, we have, through the present work, contributed to the investigation of the reactivity of always more complex and therefore more realistic systems. Concerning lignin, this effort has also been the target of other groups like Vlachos's or Heyden's.³⁻⁶ The community has probably reached a sufficient level of complexity in terms of substrate, but the recent results of Medlin's group indicate the necessity to tackle the problem of catalyst formulation.⁷ It appears that the metals needed for the adsorption of aromatic moieties are not the ones required for their deoxygenation. Concerning alumina, we have showed that metadynamics can be employed to elucidate γ -Al₂O₃ decomposition mechanism in water, even if further improvements of our simulations are still to be realized. The development of this *rare event* method, albeit widely used in the context of zeolite catalysis,⁸ could be, in a close future, of great support in the understanding of chemical reactions at the interface between a solid and a solvent.

Bibliography

- [1] Abi Aad, J.; Casale, S.; Michau, M.; Courty, P.; Diehl, F.; Marceau, E.; Carrier, X. *ChemCatChem* **2017**, *9*, 2186–2194.
- [2] Abi Aad, J.; Courty, P.; Decottignies, D.; Michau, M.; Diehl, F.; Carrier, X.; Marceau, E. *ChemCatChem* **2017**, *9*, 2106–2117.
- [3] Gao, D.; Xiao, Y.; Varma, A. *Ind. Eng. Chem. Res.* **2015**, *54*, 10638–10644.

- [4] Lu, J.; Heyden, A. *J. Catal.* **2015**, *321*, 39–50.
- [5] Lu, J.; Behtash, S.; Mamun, O.; Heyden, A. *ACS Catal.* **2015**, *5*, 2423–2435.
- [6] Lu, J.; Wang, M.; Zhang, X.; Heyden, A.; Wang, F. *ACS Catal.* **2016**, *6*, 5589–5598.
- [7] Robinson, A. M.; Mark, L.; Rasmussen, M. J.; Hensley, J. E.; Medlin, J. W. *J. Phys. Chem. C* **2016**, *120*, 26824–26833.
- [8] Van Speybroeck, V.; De Wispelaere, K.; Van der Mynsbrugge, J.; Vandichel, M.; Hemelsoet, K.; Waroquier, M. *Chem. Soc. Rev.* **2014**, *43*, 7326–7357.